THE ROLE OF LAND USE CHANGE AND LAND MANAGEMENT
IN THE GLOBAL CARBON CYCLE: SIMULATION AS A TEST
OF PROCESS UNDERSTANDING

by

Leonardo Calle

A dissertation submitted in partial fulfillment
of the requirements for the degree

of

Doctor of Philosophy

in

Ecology and Environmental Science

MONTANA STATE UNIVERSITY
Bozeman, Montana

April 2019

# DEDICATION

For Ingrid.

## ACKNOWLEDGEMENTS

Thanks to my partner, Ingrid, for her loving support through my journey and to my baby boy, Henry, for providing a daily perspective on life and work. Thanks to my family who have always been there for me, always believed in me, and always supported my passions. Thanks to my Japanese colleagues Masa Kondo, Kazu Ichii, Hisashi Sato and Tazu Saeki who made my stay in Japan result in longtime friends. Thanks to my graduate school colleagues for their laughter, comradery, adventures and honest conversation. Many thanks to Kristen Emmet, Katie Renwick, Ayodele Ogunkoya, Ben Tumolo, Eric Scholl, and Kurt Heim for their support and encouragement of my wild ideas.

Thanks to my advisor, Ben Poulter, for extending his network to me, for imprinting upon me the importance of advancing climate science this day in age. Thanks to Prabir Patra for his generosity and openness to discuss and pursue new ideas. Thanks to Dave Roberts and Tad Weaver for being good lab mates in my final years in Lewis Hall, for good conversations and a gratitude for their confidence in me as a scientist.

Thanks to the folks maintaining the Hyalite Computer Cluster, Pol Llovet and Erik Bryer, among many others. Without Hyalite, simulations in this research may still be running on my laptop without end in sight. Many thanks to all Ecology faculty, but specifically to Lindsey Albertson, Wyatt Cross, Andy Hansen, and Tom McMahon for their encouragement and thoughtful discussions. Thanks to Jim Barutha, Sarah Deaton, Meghan Heim, and Julie Geyer for their help in managing my finances and paperwork.

FUNDING ACKNOWLEDGEMENTS

Funding for research was provided by the National Science Foundation (NSF) and the Japan Society for Promotion of Science (JSPS) East Asia Pacific Summer Institutes (2015) and the National Aeronautics and Space Administration (NASA) Earth and Space Science Fellowship (ESSF) for 2016-2019 (GRANT# NNX16AP86H). Funding support to attend scientific workshops and conferences were provided by the Japan Agency for Marine Earth Science and Technology, the Mechanisms and Interactions of Climate Change in Mountain Regions Hemholtz Research School at the Karlsruhe Institute of Technology, the Montana Institute on Ecosystems at Montana State University, and the Ecological Society of America.

# TABLE OF CONTENTS

TABLE OF CONTENTS CONTINUED

TABLE OF CONTENTS CONTINUED

TABLE OF CONTENTS CONTINUED

## LIST OF TABLES

# LIST OF FIGURES

LIST OF FIGURES CONTINUED

# ABSTRACT

Humans have left their mark on Earth's ecosystems for centuries. Since 1900, the human population has grown more than 400%. Land conversion and land management have helped meet an ever-increasing demand for natural resources. Forests have been cleared for agriculture, grasslands have been used for grazing by farmed animals, and extensive logging activity has provided fuelwood for energy and raw materials for building. But a long history of land management has also led to a change in forest production, leaving century-old legacies of human activity on Earth's ecosystems.

As land is deforested, wood can be used for building or other products. Unused biomass can be burned for fuel or naturally broken down by microbes into soils, ultimately being converted to carbon dioxide. This phase conversion of carbon, from solid to gas, is a natural process but humans have sped up this process, leading to more carbon dioxide in the atmosphere than would otherwise occur naturally. Increasing levels of carbon dioxide in the atmosphere is a direct cause of increasing global temperatures and changes to regional climates.

For these reasons, the focus of research in this Dissertation has been to track each and every process during land use change and land management, to provide a better accounting of where and how much carbon gets transferred from solid to gas during land use activities, and to identify any alteration to the productivity of ecosystems long after timber harvest has removed wood for products or agricultural lands have been abandoned and the forest allowed to regrow.

The research papers in Chapter Two and Three have been published in peer-reviewed scientific journals, and Chapter Four is prepared for submission for publication. Each chapter focuses on a very specific problem, but the thread connecting all these works is carbon – How much carbon is transferred to a gas when natural lands are modified and resources extracted to meet human demand? Does deforestation leave a unique and long-lasting signal in the atmosphere? Land management creates more young, fast-growing forests, but can models represent forests of different ages at global scales?

# CHAPTER ONE

## INTRODUCTION

The foundation of this research rests on the premise that simulation models provide an evaluation of the scientific community's collective understanding of how the natural and human-modified *world* works – world being emphasized here because this research is indeed global. Simulation models of global ecosystems attempt to use first principles of biophysical and ecological theory to represent natural phenomena of soil hydrology, leaf-level photosynthesis, and vegetation dynamics, such as plant competition for light, space, and water. If simulation models can reproduce complex patterns observed in independent 'gold-standard' datasets, such as field inventories or remote-sensing, then we might say the models are good emulators of the natural world, and that the manner in which simulated processes are represented within the models are good approximations to the real phenomena. If models do a poor job of representing a particular process or phenomena, then such process is usually revised with up-to-date knowledge, drawing from fields as seemingly disparate as geophysics, pedology, plant biochemistry, ecology, or the atmospheric sciences.

Global ecosystem models of today are fine-tuned 2001 Toyota Corollas, with added improvements over time. Some simulated processes have been left unchanged since 1996, such as a tried and true method for representing the biochemical process of leaf-level photosynthesis (Farqhuar et al. 1980, Haxeltine and Prentice 1996). But as rollup windows became electric, global ecosystem models were improved too, especially among processes that were considered more uncertain.

Land use change had been determined to be one of the most uncertain processes in global models and had caused low confidence in model projections of the future (Pongratz et al. 2014, Arneth et al. 2017). Historic land use change was considered pretty straightforward when first implemented in models; there were natural lands and managed lands. It shortly become clear that every fraction of land – every field abandoned, every stand harvested, and every landscaped burned – required representation in models.

Land use change and land management modifies the structure and function of natural lands, even when human activity is abandoned and forests allowed to regrow. For example, biomass ‘residue’ is left on-site after timber harvest, a consequence of harvest inefficiencies or a higher market demand for the bole and less so for wood in branches, roots, and the biomass in leaves. Whereas primary production is the only plant process that converts carbon dioxide to solid biomass, these residues add to the detrital carbon cycle, which only increases carbon transfer to the atmosphere over time and leaves a legacy impact from past harvest on carbon balances of the future. The age of a forest is also modified during land management or when managed lands are abandoned and allowed to regrow. A young forest is unlike an old forest. Young forests are thickets of tree species competing for resources. Older forests have many fewer trees by comparison, although each remaining tree could be quite large and retain the same amount of carbon in woody tissue as a thousand saplings. Land use change and land management is not simply natural and managed lands, but involves many component processes which make up the whole.

Simulation models were subsequently improved to represent a wider array of land management, from tilling and nitrogen fertilization on agricultural lands, to shifting cultivation and timber harvest. This added detail in accounting of carbon led to one conclusion – simulations models are underestimating the sink capacity, or rather the productivity of natural lands, when these additional losses of carbon from land use activity were considered in models. Some models pointed to the 'green' revolution led by agricultural production in the late 20$^{th}$ century as an explanatory cause (Gray et al. 2014, Zeng et al. 2014), or that afforestation (Chen et al. 2019) and ecosystem demography (forest age dynamics; Pan et al. 2011, Kondo et al. 2018, Pugh et al. 2019) has led to a more productive Earth. In any case, there was increasing recognition that simulation models that lacked detailed representations of land use change, land management, and ecosystem demography could not provide state-of-the-art guidance to the scientific community about the projections of a future Earth because critical processes were lacking (Pugh et al. 2016, Arneth et al. 2017, Fisher et al. 2018).

This dissertation presents three research studies that demonstrate the complex problem of detailed accounting of carbon during land use change and land management (Chapter Two), benchmarking simulation models to atmospheric data and detecting signals of deforestation in the atmosphere (Chapter Three), and simulating the effects of land use change and land management on forest age structure in a global ecosystem model (Chapter Four). This research advances the field of ecosystem modeling one step forward and improves the scientific understanding of the role of land use change and land management in ecosystem dynamics and the global carbon cycle.

**Literature Cited**

1. Arneth, A., Sitch, S., J. Pongratz, Stocker, B. D., Ciais, P., Poulter, B., Bayer, A. D., Bondeau, A., Calle, L., Chini, L. P., Gasser, T., Fader, M., Friedlingstein, P., Kato, E., Li, W., Lindeskog, M., Nabel, J. E. M. S., Pugh, T. A. M., Robertson, E., Viovy, N., Yue, C., & Zaehle, S.: Historical carbon dioxide emissions caused by land-use changes are possibly larger than assumed. Nature Geoscience, 10. doi:10.1038/NGEO2882, 2017.

2. Chen, C., Park, T., Wang, X., Piao, S., Xu, B., Chaturvedi, R. K., Fuchs, R., Brovkin, V., Ciais, P., Fensholt, R., Tømmervik, H., Bala, G., Zhu, Z., Nemani, R. R., and Myneni, R. B.: China and India lead in greening of the world through land-use management. *Nature Sustainability*, 2, 122-129, 2019.

3. Farquhar, G. D., von Caemmerer, S., and Berry, J. A.: A biochemical model of photosynthetic $CO_2$ assimilation in leaves of $C_3$ plants. *Planta*, 149, 78-90, 1980.

4. Fisher, R. A., Koven, C. D., Anderegg, W. R. L., Christoffserson, B. O., Dietze, M. C., Farrior, C. E., Holm, J. A., Hurtt, G. C., Knox, R. G., Lawrence, P. J., Lichstein, J. W., Longo, M., Matheny, A. M., Medvigy, D., Muller-Landau, H. C., Powell, T. L., Serbin, S. P., Sato, H., Shuman, J. K., Smith, B., Trugman, A. T., Viskari, T., Verbeeck, H., Weng, E., Xu, C., Xu, X., Zhang, T., and Moorcroft, P. R.: Vegetation demographics in Earth System Models: A review of progress and priorities. *Global Change Biology*, 24, 35-54, doi:10.111/gcb.13910, 2018.

5. Gray, J. M., Frolking, S., Kort, E. A., Ray, D. K., Kucharik, C. J., Ramankutty, N., and Friedl, M. A.: Direct human influence on atmospheric CO2 seasonality from increased cropland productivity. *Nature*, 515, 398-401, doi:10.1038/nature13957, 2014.

6. Haxeltine, A., and Prentice, I. C.: A general model for the light-use efficiency of primary production. *Functional Ecology*, 10, 551-561, 1996.

7. Kondo, M., Ichii, K., Patra, P. K., Poulter, B., Calle, L., Koven, C., Pugh, T. A. M., Kato, E., Harper, A., Zaehle, S., and Wiltshire, A.: Plant regrowth as a driver of recent enhancement of terrestrial CO2 uptake. *Geophysical Research Letters*, 45,

4820-4830, doi:10.1029/2018GL077633, 2018.

8. Pan, Y., R. A. Birdsey, J. Fang, R. Houghton, P. E. Kauppi, W. A. Kurz, O. L. Phillips, A. Shvidenko, S. L. Lewis, J. G. Canadell, P. Ciais, R. B. Jackson, S. W. Pacala, A. D. McGuire, S. Piao, A. Rautiainen, S. Sitch, and D. Hayes. 2011. A large and persistent carbon sink in the world's forests. *Science* 333:988–993.

9. Pongratz, J., Reick, C. H., Houghton, R. A., and House, J. I.: Terminology as a key uncertainty in net land use and land cover change carbon flux estimates. *Earth System Dynamics*, 5, 177–195, 2014.

10. Pugh, T. A. M., Müller, C., Arneth, A., Haverd, V., and Smith, B.: Key knowledge and data gaps in modelling the influence of $CO_2$ concentration on the terrestrial carbon sink. *Journal of Plant Physiology*, 203, 3-15, 2016.

11. Pugh, T. A. M., Lineskog, M., Smith, B., Poulter, B., Arneth, A., Haverd, V., and Calle, L.: Role of forest regrowth in global carbon sink dynamics. *Proceedings of the National Academies of Science of the United States of America*, doi:10.1073/pnas.1810512116, 2019.

12. Zeng, N., Zhao, F., Collatz, G. J., Kalnay, E., Salawitch, R. J., West, T. O., and Guanter, L.: Agricultural green revolution as a driver of inreasing atmospheric CO2 seasonal amplitude. *Nature*, 515, 394-397, doi:10.1038/nature13893, 2014.

# CHAPTER TWO

# REGIONAL CARBON FLUXES FROM LAND USE AND LAND COVER CHANGE IN ASIA, 1980-2009

## Contribution of Authors and Co-Authors

Manuscript in Chapter Two

Author: Leonardo Calle

Contributions: wrote manuscript, processed data, performed analysis, interpreted results, generated tables and figures

Co-Author: Josep G. Canandell

Contributions: contributed to writing of manuscript, interpretation of results, and suggested figures and analysis methods

Co-Author: Prabir K. Patra

Contributions: contributed to writing of manuscript, interpretation of results, and suggested figures and analysis methods

Co-Author: Philippe Ciais

Contributions: contributed to writing of manuscript, interpretation of results, and suggested figures and analysis methods

Co-Author: Kazuhito Ichii

Contributions: contributed to writing of manuscript, interpretation of results

Co-Author: Hanqin Tian

Contributions: contributed to writing of manuscript, interpretation of results, and provided datasets for analysis

Co-Author: Masayuki Kondo

Contributions: contributed to writing of manuscript, interpretation of results

Co-Author: Shilong Piao

Contributions: contributed to writing of manuscript, interpretation of results

Co-Author: Almut Arneth

Contributions: contributed to writing of manuscript, interpretation of results, and provided datasets for analysis

Co-Author: Anna B. Harper

Contributions: contributed to writing of manuscript, interpretation of results, and provided datasets for analysis

Co-Author: Akihiko Ito

Contributions: contributed to writing of manuscript, interpretation of results, and provided datasets for analysis

Co-Author: Etsushi Kato

Contributions: contributed to writing of manuscript, interpretation of results, and provided datasets for analysis

Co-Author: Charlie Koven

Contributions: contributed to writing of manuscript, interpretation of results, and provided datasets for analysis

Co-Author: Stephen Sitch

Contributions: contributed to writing of manuscript, interpretation of results, and provided datasets for analysis

Co-Author: Benjamin D. Stocker

Contributions: contributed to writing of manuscript, interpretation of results, and provided datasets for analysis

Co-Author: Nicolas Viovy

Contributions: contributed to writing of manuscript, interpretation of results, and provided datasets for analysis

Co-Author: Andy Wiltshire

Contributions: contributed to writing of manuscript, interpretation of results, and provided datasets for analysis

Co-Author: Sönke Zaehle

Contributions: contributed to writing of manuscript, interpretation of results, and provided datasets for analysis

Co-Author: Benjamin Poulter

Contributions: contributed to writing of manuscript, interpretation of results, provided datasets for analysis, and suggested figures and analysis methods

Manuscript Information

Leonardo Calle, Josep G Canadell, Prabir Patra, Philippe Ciais, Kazuhito Ichii, Hanqin Tian, Masayuki Kondo, Shilong Piao, Almut Arneth, Anna B Harper, Akihiko Ito, Etsushi Kato, Charlie Koven, Stephen Sitch, Benjamin D Stocker, Nicolas Vivoy, Andy Wiltshire, Sönke Zaehle and Benjamin Poulter

Environmental Research Letters

Status of Manuscript:
____ Prepared for submission to a peer-reviewed journal
____ Officially submitted to a peer-reviewed journal
____ Accepted by a peer-reviewed journal
_X__ Published in a peer-reviewed journal

IOP Publishing
Issue 11, doi:10.1088/1748-9326/11/7/074011

# REGIONAL CARBON FLUXES FROM LAND USE AND LAND COVER CHANGE IN ASIA, 1980-2009

Leonardo Calle[1], Josep G. Canadell[2], Prabir Patra[3], Philippe Ciais[4], Kazuhito Ichii[3, 5], Hanqin Tian[7], Masayuki Kondo[3], Shilong Piao[4, 8], Almut Arneth[9], Anna B. Harper[10], Akihiko Ito[5], Etsushi Kato[6], Charlie Koven[11], Stephen Sitch[12], Benjamin D. Stocker[13,14], Nicolas Vivoy[4], Andy Wiltshire[15], Sönke Zaehle[16], and Benjamin Poulter[1]

[1]Department of Ecology and Institute on Ecosystems, Montana State University, Bozeman, MT, USA, 59717
[2]Global Carbon Project, CSIRO Oceans and Atmospheric Research, GPO Box 3023, Canberra, ACT 2601, Australia
[3]Department of Environmental Geochemical Cycle Research/Japan Agency for Marine-Earth Science and Technology (JAMSTEC), 3173-25 Showa-machi, Kanawaza-ku Yokohama, 2360001, Japan
[4]Laboratoire des Sciences du Climat et de l'Environnement (LSCE CEA-CNRS-UVSQ), Gif-sur-Yvette, France
[5] Center for Global Environmental Research, National Institute for Environmental Studies, Japan, Onogawa, Tsukuba, 305-0053, Japan
[6] The Institute of Applied Energy (IAE), Minato, Tokyo 105-0003, Japan
[7]International Center for Climate and Global Change Research and School of Forestry and Wildlife Sciences, Auburn University, Auburn, AL 36849, USA
[8]Laboratoire de Glaciologie et Géophysique de l'Environnement, CNRS and Université Grenoble Alpes, Grenoble 38041, France
[9]Institute of Meteorology and Climate Research, Atmospheric Environmental Research, Karlsruhe Institute of Technology, 82467 Garmisch-Partenkirchen, Germany
[10]College of Engineering, Mathematics, and Physical Sciences, University of Exeter, Exeter, UK
[11]Earth Sciences Division, Lawrence Berkeley National Lab, Berkeley, CA, USA
[12]Department of Geography, University of Exeter, Exeter EX4 4QF, UK
[13]Imperial College London, Life Science Department, Silwood Park, Ascot, Berkshire SL5 7PY, UK
[14] Climate and Environmental Physics, and Oeschger Centre for Climate Change Research, University of Bern, Bern, Switzerland
[15]Met Office Hadley Centre, Exeter EX1 3PB, United Kingdom
[16]Biogeochemical Integration Department, Max Planck Institute for Biogeochemistry, Hans-Knoll-Str. 10, D-07745 Jena, Germany

**Abstract**

We present a synthesis of the land-atmosphere carbon flux from land use and land cover change (LULCC) in Asia using multiple data sources and paying particular attention to deforestation and forest regrowth fluxes. The data sources are quasi-independent and include the U.N. Food and Agriculture Organization-Forest Resource Assessment (FAO-FRA 2015; country-level inventory estimates), the Emission Database for Global Atmospheric Research (EDGARv4.3), the 'Houghton' bookkeeping model that incorporates FAO-FRA data, an ensemble of 8 state-of-the-art Dynamic Global Vegetation Models (DGVM), and 2 recently published independent studies using primarily remote sensing techniques. The estimates are aggregated spatially to Southeast, East, and South Asia and temporally for three decades, 1980-1989, 1990-1999 and 2000-2009. Since 1980, net carbon emissions from LULCC in Asia were responsible for 20-40% of global LULCC emissions, with emissions from Southeast Asia alone accounting for 15-25% of global LULCC emissions during the same period. In the 2000s and for all Asia, three estimates (FAO-FRA, DGVM, Houghton) were in agreement of a net source of carbon to the atmosphere, with mean estimates ranging between 0.24 to 0.41 Pg C $yr^{-1}$, whereas EDGARv4.3 suggested a net carbon sink of -0.17 Pg C $yr^{-1}$. Three of 4 estimates suggest that LULCC carbon emissions declined by at least 34% in the preceding decade (1990-2000). Spread in the estimates is due to the inclusion of different flux components and their treatments, showing the importance to include emissions from carbon rich peatlands and land management, such as shifting cultivation and wood harvesting, which appear to be consistently underreported.

## 1. Introduction

Unprecedented growth in energy consumption and rapid land use change in Asia has led to a major reshaping of the regional distribution and magnitude of greenhouse gas (GHG) sources and sinks. Although the combustion of fossil fuels accounts for the largest fraction of anthropogenic carbon emissions in Asia (Liu, Z. et al. 2015), land transformation in this region has some of the fastest rates of change in the world and high spatial contrast with deforestation in tropical Asia and reforestation in East Asia (Hansen et al. 2013, FAO-FRA 2015). Globally, net carbon emissions from Land Use and Land Cover Change (LULCC) are estimated at about $1.0 \pm 0.8$ Pg C yr $^{-1}$(Ciais et al. 2013, Le Quéré 2015). Asia is responsible for a growing fraction of the global LULCC flux, partly because of the slowdown of deforestation in South America (Hansen et al. 2013, Kim et al. 2015, Federici et al. 2015). However, the contributing gross fluxes of the net LULCC flux, in Asia and globally, are among the most uncertain quantities of the anthropogenic global carbon budget (Harris et al. 2012a, Pongratz et al. 2014).

The magnitude of LULCC net $CO_2$ flux depends on the size of the carbon pools immediately combusted or respired biomass (wood, leaves, roots), the fate of on-site slash materials, subsequent land-management practices and effects on soil carbon (e.g., slash and burn, shifting cultivation, permanent agriculture) and the fate of off-site harvested wood products, e.g., wood harvested for paper, fuel, pulp, and building material (Hurtt et al. 2006, 2011; Earles et al. 2012). The Intergovernmental Panel on

Climate Change Assessment Report 5 (IPCC AR5; Ciais et al. 2013) reports a 50-100% likelihood that global LULCC carbon emissions decreased between the 1990's (1.5 ± 0.8 Pg C $yr^{-1}$) and the 2000's (1.0 ± 0.8 Pg C $yr^{-1}$). However, large uncertainties are associated with the magnitude of change and with the regional attribution of carbon fluxes (Foley et al. 2005, Friedlingstein et al. 2010, Hansen et al. 2013, Ciais et al. 2013, Kim et al. 2015). Carbon emissions from deforestation and forest degradation are uncertain in Asia, and particularly in Southeast Asia (Hansen et al. 2013, Achard et al. 2014). A full and updated quantification of Asia's LULCC fluxes and their sources of uncertainty are necessary to constrain the perturbation of the global carbon budget, and to help understand the role of terrestrial ecosystems in Asia in contributing to, and mitigating increases of, GHG concentrations.

Here we present a comprehensive synthesis of the regional net carbon flux from LULCC in Asia using multiple data sources and models, and paying particular attention to its contributing fluxes. Estimates of LULCC fluxes are analyzed from a variety of quasi-independent data sources, including the FAO-FRA, the Emission Database for Global Atmospheric Research (EDGARv4.3), a bookkeeping model by Houghton et al. (2012), an ensemble of 8 state-of-the-art Dynamic Global Vegetation Models (DGVM) (Table 2.S1 in Supplementary Material). These analyses are supplemented with estimates taken from two remote-sensing studies. The estimates are aggregated spatially to Southeast Asia, East Asia, and South Asia (Figure 2.1; countries listed in Table 2.S2), and provided for three decades, 1980-1989, 1990-1999 and 2000-2009.

## 2. Methods

### 2.1 Datasets on Emissions from Land Use and Land Cover Change

Three data sources were analyzed for this study, representing the major approaches frequently used in LULCC assessments (Ciais et al. 2013). These data sources vary by the methods used to estimate LULCC fluxes, particularly with regards to the use of different sources for LULCC, carbon stocks, and methods to account for forest regrowth and legacy emissions (Table 2.1). Here, we categorize the data sources by their general methodologies: (i) bookkeeping model (Houghton et al. 2012) and inventory accounting (EDGARv3.1, FAO-FRA 2015), (ii) eight carbon-cycle models (DGVMs), and (iii) literature estimates from remote-sensing studies (Achard et al. 2014, Harris et al. 2012b).

For all data sources, carbon fluxes (sources and sinks) from natural lands (including forests) were considered, but only some datasets included emissions from agricultural lands (Table 2.2). All datasets included fluxes from aboveground and belowground biomass, whereas only a few datasets included emissions from litter, soil, fire, or land management. Secondary forest regrowth contributes to carbon uptake, but it was not included consistently across the data sources (Table 2.2). The DGVM carbon-cycle models and the bookkeeping model differed from the other approaches based on their inclusion of *instantaneous* (e.g., the immediate combustion of fuel wood) as well as *legacy* (or delayed) emissions (Pongratz et al. 2014), e.g., from slash left on-site or delayed decomposition of wood products used in furniture or homes. The importance of the distinction is that emissions associated with legacy fluxes are partly realized and included in present and future emission estimates, and can amount to as much as instantaneous emissions themselves (Houghton et al. 2012). We summarize the data sources in detail below, but refer to the *Supplementary Material (Section S1)* for a more detailed description of the datasets and their methods.

### *2.1.1 Bookkeeping and Inventory Approaches*

The bookkeeping model (Houghton et al. 2012) tracks all carbon pools (i.e., wood, roots, leaves, soil, litter) within a hectare, updating carbon pools over time based on ecosystem-specific growth and decay equations; the size of the carbon pools are initialized based on inventories. In contrast, standard inventory approaches, including the FAO-FRA and EDGAR used here, use similar accounting to track carbon over time, but typically they do not track carbon losses from soils and litter and use country-level estimates for carbon aboveground vegetation. A common underlying source for the change in forest area used in the bookkeeping and inventory approaches (FAO-FRA, EDGARv3.1) comes from country-level FAO-FRA reporting. The inventory approaches utilize IPCC (2006) Tier 1 methods (Ruesch et al. 2008) to estimate LULCC emissions at the country level by the difference in carbon gained from biomass growth and carbon lost from deforestation. The bookkeeping model and EDGARv4.3 both include carbon emissions from peatland fires. We compare the inventory estimates analyzed in this study with a similar approach adopted by Pan et al. (2011). Pan et al. (2011) utilized a variety of national-level forest inventories other than FAO-FRA to estimate forest area, changes in forest area, and carbon stocks, but they utilized the Houghton et al. (2003) bookkeeping model to estimate forest regrowth and legacy fluxes from soil carbon after land use change.

### *2.1.2 Carbon-cycle Models*

As part of the TRENDY model inter-comparison project, version 3 (Sitch et al. 2015), the eight DGVMs in this study were used to estimate carbon stocks and fluxes using process-based approaches and to predict global vegetation distribution based on impacts of climate, atmospheric $CO_2$ concentrations, and land cover change. Some models include an interactive nitrogen cycle (such as CLMv4.5, LPX, OCN), which often result in smaller forest regrowth than models without C-N coupling (Yang et al. 2010). The DGVM models (Sitch et al. 2015) utilized alternate versions of land cover from the HistorY Database of the global Environment, HYDE version 3 (Goldewijk et al. 2001) (Table 2.1) to determine land use change. DGVM estimates of LULCC fluxes are obtained by difference of the net land-atmosphere $CO_2$ flux between one simulation (S3) with land use change, transient $CO_2$ concentrations and variable climate and an alternate simulation (S2) with only transient $CO_2$, variable climate, and pre-industrial land cover in

1860 (Sitch et al. 2015). Only the CLMv4.5, LPX and VISIT models accounted for gross land cover transitions (e.g. parallel abandonment to and from agricultural land within a grid cell), and only CLMv4.5 and VISIT accounted for carbon fluxes from wood and crop harvest. Finally, we compare the DGVM estimates with the estimates from a regionally-parametrized carbon-cycle model by Tao et al. (2013), which included fluxes from crop harvest, irrigation and nitrogen fertilization.

### *2.1.3 Remote-sensing Studies*

We use literature estimates from two remote-sensing-based studies (Achard et al. 2014, Harris et al. 2012b) estimated forest area, changes in forest area, and carbon stocks from independent sources of satellite data for both land cover and biomass. Their emission estimates do not include emissions from the decay of litter, soils, including peatlands, or the effects of forest degradation and land management.

## **2.2 Analyses**

### *2.2.1 Changes in Forest Area*

Changes in forest area and carbon stocks are two major determinants of LULCC emissions (Houghton et al. 2012). Therefore, we provide estimates of changes in forest area from FRA 2015 and the HYDE data product, supplemented with observed changes reported in recent literature. Different carbon-cycle modeling groups were responsible for determining rules for land cover transitions (e.g. primary forest -> agriculture, or secondary forest -> agriculture), and therefore make different assumptions about how to specify land-use transitions prescribed by HYDE. One approach assumes an equivalent loss of forest area for an increase in either cropland or pasture (*Section S4.1; Figure* 2.*S1*). The differences in approaches were not quantified, but can introduce carbon fluxes that are included in some, but not all DGVMs. The changes in forest area, by region and decade, are provided in the *Supplementary Material* (*Section S4.1; Figure* 2.*S1*).

### *2.2.2 Carbon in Biomass & DGVM Performance Ranking*

In this study, biomass estimates based on remote-sensing studies from Baccini et al. (2012), and Liu, Y. et al. (2015) are used as benchmarks to filter-out DGVMs with unreasonably high carbon stock in vegetation, and therefore, biased carbon fluxes from LULCC (Supplementary Materials Section 3). Based on the biomass benchmarks, the CLMv4.5, OCN, and ORCHIDEE models were filtered-out from DGVM emission estimates from Southeast Asia, and the CLMv4.5, JULES, and OCN models were filtered-out from DGVM emission estimates from East Asia; no models were filtered-out for South Asia.  We also provide IPCC 2006 Tier 1, country-level, estimates of aboveground biomass from the FRA 2010 report. We provide summary estimates of carbon in total and aboveground biomass by region, and country (*Supplementary Material* Section S4.1; Figures 2.S2 and 2.S3).

*2.2.3 Carbon Emissions from LULCC: Statistical Summaries by Geographic Regions*

The LULCC emissions were summarized with mean and standard deviations for each decade and region. Emission estimates reported by the DGVM ensemble have been summarized by taking the mean of decadal-mean estimates from individual DGVMs in the ensemble, after omitting individual models with unrealistic biomass (*see* Section 2.2.2); the range of estimates among the models is provided as a measure of uncertainty. We use an approach similar to the one of IPCC AR5 (Ciais et al. 2013) and from Kirschke et al. (2013) to assign a level of confidence in the sign of the emissions estimate and to the direction of change in emissions between decades by indicating the level of agreement (low, medium, high) among studies and the robustness of evidence (number of studies). In addition, we present a weighted-mean estimate of the mean decadal estimates from each approach (Table 2.3), which helps to address the inclusion of different component fluxes among estimates. First, we convert Table 2.2 into a binary table and we focus only on fluxes from carbon stocks, fire, and forest regrowth (e.g., if a particular estimate includes fire flux, then it is scored 1, otherwise 0). We give each of these component fluxes equal weight, but we refrain from scoring legacy fluxes, fluxes from climate response, and fluxes from land management because we cannot quantify their contribution relative to the other fluxes. The relative weight for each approach (Table 2.2) reflects the maximum number of component fluxes in any single approach. The weighted-mean of mean decadal estimates is presented in Table 2.4, along with the qualitative assessment of confidence in the magnitude and change among decades.

## 3. Results: Carbon Emissions from LULCC

### *3.1 Southeast Asia*

There was high agreement among all estimates in the magnitude of carbon emissions from LULCC during the 1980s in Southeast Asia (Tables 2.3, 2.4; Figure 2.2), ranging from 0.22 to 0.29 Pg C $yr^{-1}$. In the 1990s, there was also high agreement and high confidence that the emissions were at *least* 0.21 Pg C $yr^{-1}$, but this value was not well constrained with a range of [0.21, 0.66] Pg C $yr^{-1}$. Between the 1980s and 1990s there was moderate agreement for increasing emissions, although the magnitude of the increase was uncertain. In comparison, Tao et al. (2013) reported emission estimates that overlapped between the two time periods, suggesting little to no change in emissions. During the 2000s, there was high agreement among data sources and high confidence indicating that emission estimates were *at least* 0.11 Pg C $yr^{-1}$. Although the range of the estimates ([0.11, 0.46] Pg C $yr^{-1}$) was smaller than in the previous decade, the weighted-mean estimate in the 2000s (0.363 ± 0.131 Pg C $yr^{-1}$) was larger than weighted-mean estimate for the 1990s (0.255 ± 0.019 Pg C $yr^{-1}$). Among all estimates, there was low agreement in the change of emissions between the 1990s and the 2000s. The bookkeeping model and Pan et al. (2011), both of which utilized similar data sources from FAO-FRA, suggested a 30-53% reduction in emissions, respectively, between the 1990s and 2000s. The DGVMs and Achard et al. (2012) suggested a smaller reduction of less than 10% or no change in emissions, respectively, between the 1990s and the 2000s. By contrast, the

FAO-FRA suggested an increase in emissions (24%+) between the 1990s and 2000s (Table 2.3), but it is unclear how the absence of legacy and regrowth fluxes (Table 2.2) may have influenced their estimates. Similarly, the inclusion of emissions from harvested wood products in the estimates by the bookkeeping model and Pan et al. (2011) resulted in higher emissions than those from other data sources that did not include these important fluxes, although its inclusion would not have impacted an assessment of change in emissions between decades because wood harvest volumes did not change appreciably among decades according to the FRA (2015).

Overall, the carbon emissions from LULCC in Southeast Asia, taken as the weighted-mean estimate among all data sources, is estimated to be 0.363 ± 0.131 Pg C $yr^{-1}$ in the 1990s and +0.271 ± 0.116 Pg C $yr^{-1}$ in the 2000s (Table 2.4), or 20 to 30% of global LULCC emissions, respectively, using global LULCC estimates based on the bookkeeping model. The increasing fraction of carbon emissions from LULCC in Southeast Asia, relative to global LULCC emissions, is partly due to near constant emissions during the 1990s and 2000s, and at the same time, declining global emissions from LULCC (Figure 2.3).

*3.2 East Asia*

In East Asia, there was low agreement in the estimate of net fluxes from LULCC in the 1980s between the bookkeeping model and the DGVMs (Table 2.3, 2.4). The DGVMs also simulated higher emissions during the 1990s that were of similar magnitude as LULCC emissions in Southeast Asia during the 2000s (Table 2.3). By contrast in the 1990s, there was moderate agreement among data sources and medium confidence indicating a small forest regrowth sink (Table 2.3, 2.4). In the 2000s, there was also moderate agreement in the deforestation and regrowth trends, and high agreement in the strengthening of a carbon sink compared to fluxes from the 1990s; only the magnitude of the change between decades differed among the data sources (Table 2.4). The DGVMs generally estimated much higher emissions in the 1980s and 1990s, but there was a strong decline in emissions during the 2000s from previous decades, and a regrowth sink was evident in a few of the models (Figure 2.S5, 2.S8).

DGVMs do not quantify explicitly how the legacy emissions from past land use change contribute to higher emission estimates, but it is clear that emissions from LULCC in East Asia have declined substantially (Fig. S8), to less than 10% of the global emissions from LULCC in the 2000's (Figure 2.3). The decreasing fraction of emissions from LULCC in East Asia, according to DGVMs, can be attributed to a stronger decline in emissions from this region than the decline in LULCC emissions observed at the global scale; this pattern is driven largely by a strong decline in LULCC emissions and an intensification of the land sink in China, due to reforestation and forest regrowth according to some estimates (Fang et al. 2001, Piao et al. 2009, Li et al. 2015).

*3.3 South Asia*

In South Asia, there was low agreement among LULCC net flux estimates during the 1980s, with the bookkeeping model estimating a carbon sink, and the DGVMs a carbon source (Table 2.3). In the 1990s, there was moderate agreement in the sign and magnitude of the LULCC flux being a net source of carbon as estimated by the DGVMs and FAO-FRA (less than 33% difference), whereas the bookkeeping model continued to estimate a carbon sink (Table 2.3). There was also low agreement about the direction of change in emissions (increasing or decreasing) between the 1980s and 1990s, with the DGVMs suggesting that carbon emissions doubled between the two time periods, and the bookkeeping model suggesting the opposite, that the strength of the regrowth sink increased during the 1990s relative to 1980s levels (Table 2.3). In the 2000s, there was high agreement among data sources and medium confidence in decreasing emissions compared to estimates from the 1990s, along with moderate agreement in a regrowth sink (Tables 2.3 and 2.4, and Fig. S9). Although the emissions estimated by the DGVMs were mostly positive (Figure 2.S6), it is clear that modeled carbon in biomass was not a factor because there was little bias between individual DGVMs and the biomass benchmarks (Figure 2.S2, 2.S3). Therefore, it is possible that factors related to climate could have influenced the emission estimates in the DGVMs, but which would not have been included in the other estimates (Table 2.2). Overall, emissions from LULCC in South Asia are estimated to be less than 5% of global LULCC emissions (Figure 2.3), the bulk of these carbon emissions are from India alone, and the decline in emissions between 1990s and 2000s is shown in most estimates (Figure 2.S9).

## 4. Discussion

### 4.1 Regional Emissions

The goal of this article was to present the carbon emissions from LULCC as estimated by a range of approaches and for these estimates to serve as a baseline for future studies. The problems associated with having multiple estimates of the net carbon flux of LULCC based on different contributing fluxes have been discussed at length before (Pongratz et al. 2014, Rosa et al. 2014), as well as adding unwarranted controversy with regards to the magnitude of the carbon flux (Harris et al. 2012a). We provided a weighted-means approach to account for the inclusion of component fluxes in some, but not in all estimates, and we treated each component flux with similar weight. The weighted-mean estimates provide some satisfaction for an ensemble-mean estimate of the LULCC flux, but it does have its own inherent biases. For example, some component fluxes will be important in some regions, but not in others (e.g. peat flux), and therefore the relative contribution of the component flux to the overall LULCC flux will be greater (or less). The accuracy of the weighted-means approach can therefore be improved if we can ascribe some value [0, 1] to the relative influence of each component flux to the overall net carbon flux estimate. For example, if the wood harvest flux can be quantified and is known to be 90% of the LULCC flux in a particular region or time period, then those methods that include a wood harvest flux would be weighted higher than those methods that do not include wood harvest, and a more accurate ensemble estimate would prevail; until the relative contribution of the component fluxes can be quantified the weighted-mean ensemble estimates should be used with discretion. Below, we discuss the major patterns in emissions among regions as evidenced by this study, and we review the magnitude and contribution of each component flux to the total net LULCC flux from a review of the literature.

The bookkeeping model and DGVMs both suggest that total Asian emissions have declined by at least 34% between 1990s and 2000s, driven largely from an increasing carbon sink in China, with the carbon sink of South Asia playing a smaller role. However, the inventory data (FAO-FRA) suggests that emissions grew by 17% across Asia between 1990s and 2000s, but it was more due to larger increases in carbon emissions from Southeast Asia than a smaller decreases in carbon emissions from East and South Asia regions, which is consistent with the bookkeeping model and DGVMs. For Southeast Asia, most methods suggest similar carbon fluxes between 1990s and 2000s (Fig. S7), and at most, a decline in carbon fluxes between the 1990s than in the 2000s, which suggests that the missing fluxes of a tier-1 approach such as the FAO-FRA has important effects on the net flux; alternatively, carbon stocks at the country-level could be over-estimated which would also lead to higher emissions fluxes.

In Southeast Asia, there is general agreement among the bookkeeping model, the FAO-FRA, and DGVMs showing that net carbon emissions from LULCC in Southeast Asia is responsible for 75-88% of Asian LULCC fluxes in the 2000s. Recent remote-sensing studies of deforestation activity in Southeast Asia showed that forest loss has been constant or increasing during the past two decades (Hansen et al. 2013, Achard et al. 2014, Margano et al. 2014, Stibig et al. 2014, Kim et al. 2015), suggesting that LULCC emissions should be constant or increasing as well, consistent with the changes in carbon emissions between decades reported in this study. As a caveat, Loarie et al. (2009) and Song et al. (2015) reported that, independent of gross losses to forest areas, carbon emissions from LULCC can be largely driven by spatial heterogeneity in carbon density. It is therefore plausible that decreasing trends in carbon emissions from LULCC in Southeast Asia between 1990s and 2000s, from the bookkeeping model as reported by Pan et al. (2011), occurred as a result of the use of carbon stock datasets that were derived from country-level statistics, and were therefore biased too low (Figure 2.S2, 2.S3). Before progress can be made on reducing the uncertainty in LULCC emissions in this region, it may be prudent to first evaluate the relative impact on LULCC emissions from the uncertainties inherent in the spatial variability in carbon density and areal changes in forest cover.

In East Asia, an increase in forest regrowth is responsible for reversing a carbon source to carbon sink from LULCC in East Asia between the decades 1990s and 2000s, at the very latest, and this is mainly driven by China, confirming similar reports by Piao et al.

(2012). The inclusion of legacy emissions may be the cause of an apparent lag in the source-sink dynamics observed in the DGVM emission estimates in East Asia between the 1980s, 1990s (both carbon sources) and the 2000's, during which there is a noticeable decline in emissions from previous decades (Fig. 4) and a carbon sink estimated by a few models (Fig. S5). The inclusion, or omission, of legacy emissions may explain the differences in decadal estimates for East Asia made by the DGVMs and inventory methods. Even still, the high agreement among the data sources suggest high confidence in East Asia trending towards a stronger carbon sink than in past decades even while accounting for LULCC in the region (Fig. S8).

**4.2 Land Management**

Wood harvesting practices in Borneo and Indonesia are particularly relevant drivers of emissions, as widespread practice of selective logging and clear-cutting results in considerable loss of biomass and carbon uptake capacity (Carlson et al. 2012, Gaveau et al. 2014, Kemen-Austin et al. 2015). Wood harvest practices result in forest-degradation and deforestation and can also create increasingly fragmented forests, but the effects of fragmentation, which are largely ignored, can amount to carbon emissions of 0.12 – 0.24 Pg C $yr^{-1}$ across all tropical forests (Pütz et al. 2014). In their carbon-cycle model, Tao et al. (2013) also prescribed cropping rotations, irrigation and fertilization amounts from FAO country-level statistics. However, it is unclear to what degree these practices impact carbon fluxes because Tao et al. (2013)'s emission estimates were roughly inline with other data sources reported here, which did not include these land management practices. The following emissions from wood harvest practices are based on EDGARv4.3, and these were not used for the EDGARv4.3 total LULCC emissions presented in Table 2.3, to allow adequate comparison to other estimates. Including emissions from wood harvest alone would increase emission estimates by 0.28 ± 0.01 Pg C $yr^{-1}$ in East Asia, by 0.48 ± 0.01 Pg C $yr^{-1}$ in South Asia, and 0.40 ± 0.01 Pg C $yr^{-1}$ in Southeast Asia, which would then switch East and South Asia regions to net carbon emitters from LULCC.

### 4.3 Peat and Soil Carbon Losses from Fire

Only the EDGARv4.3 emission estimates, which utilized the GFEDv3.1 dataset from van der Werf et al. (2006), include emissions from peat fires; although the DGVMs and the bookkeeping model did include carbon fluxes from soils, conditions promoting the carbon density of peat soils were not modeled explicitly. Further, none of the estimates in this study reported fluxes from the areal changes in peatlands (Miettinen et al. 2016) or the degradation and decomposition of peat soils, which are more carbon dense and result in higher fluxes than the typically represented organic soils (Hooijer et al. 2010). Emissions from peat fires are substantial fluxes in themselves and can be of the same order of magnitude as carbon emissions due to deforestation at the country-scale (van der Werf et al. 2006, Hooijer et al. 2010, Miettinen et al. 2011, Prentice et al. 2011). The carbon flux from peat fires in Southeast Asia are estimated to be at minimum 0.38 Pg C $yr^{-1}$ for 1997-2006 (Hooijer et al. 2006), and 0.08 - 0.18 Pg C $yr^{-1}$ for 2000-2006 (van der

Werf et al. 2008), but annual emissions from peat fires have ranged from 0.81 to 2.57 Pg C in fire intensive years like in 1997-98 (Page et al. 2002); however, the *maximum* emissions from fire anomalies in Asia may be closer to 1.3 Pg C, according to an inverse modeling study by Patra et al. (2005).

**4.4 Gross vs. Net Land Use Change**

Shifting cultivation is a method of rotational cropping that is commonly practiced in the Tropics; it is defined as the simultaneous clearing of forest for agriculture and abandonment of older agricultural land of equal area (Houghton et al. 2010). Shifting cultivation (i.e., gross changes in land use) can amount to a 30% increase in carbon emissions compared to emissions estimated by net changes in land use (Shevliakova et al. 2009, Stocker et al. 2014). In this study, only the bookkeeping model, CLMv4.5, LPX and VISIT models included emission estimates from gross changes in land use. Accounting for shifting cultivation is problematic for FAO-FRA emission estimates, and other inventory approaches, because net forest area may not change under shifting cultivation and may be under-reported. Remote-sensing surveys may be able to capture gross changes in forest cover, but will require more frequent surveys and correct attribution of young forest to the abandonment of managed land, as opposed to natural fires or disturbance. For an in depth review of the effects of gross versus net changes in land use, see (Shevliakova et al. 2009, Houghton et al. 2012, Stocker et al. 2014, Wilkenskjeld et al. 2014).

### 4.5 Forest Cover and Land Use Change

Consideration should be given to the use of gridded LULCC datasets that use detailed historical reconstructions from country-specific studies. For example, Tian et al. (2014) raised concerns about notable land use changes in India that were under-documented and missing in global LULCC datasets, such as HYDE. The discrepancies in the HYDE data model are apparent (Figure 2.S1), but ideally need to be checked against more reliable data sources, such as satellite imagery. A recent land-use study in China (Liu and Tian 2010) also suggested a different spatial distribution of cropland and pasture than the distribution predicted by the HYDE dataset, which could have influenced both the magnitude and change in emissions between decades in the DGVM estimates.

### 4.6 Carbon Stocks

In an analysis by Langner et al. (2014), biomass maps by Baccini et al. (2012) and Saatchi et al. (2011) were supported for REDD+ reporting, and one approach for their use as a discriminating filter for constraining emission estimates was presented in this study, for example by omitting DGVMs that simulated unrealistic biomass. The DGVMs and the remote-sensing studies account for spatial variability in carbon density, which is lacking in FAO-FRA and derivative emission estimates. This study used Baccini et al. (2012), and Liu, Y. et al. (2015) biomass maps as a benchmark to discriminate between DGVM models that were simulating unreasonably high carbon stocks.

## 5. Summary

In summary, the range in the magnitude of carbon fluxes from LULCC in each region was large among methods due to the inclusion of different component fluxes, but the direction of change in carbon fluxes between decades was internally consistent among methods (Figs. S7-S9). A weighted-means approach was used to derive an overall estimate for each region, with each estimate weighted by the number of component fluxes included, but the relative contribution of each component flux to the total estimate could be improved.

- In Southeast Asia, there is robust evidence that carbon emissions from LULCC (ignoring peat degradation) were at least 0.19 and 0.11 Pg C $yr^{-1}$ in the 1990s and 2000s, respectively. Southeast Asia is contributing a large fraction of the regional carbon emissions from LULCC, between 75-88% of regional LULCC emissions in the 2000s.
- There is robust evidence that East Asia switched from a carbon source to a carbon sink (median= -0.12 Pg C $yr^{-1}$, range= [+0.05, -0.25] Pg C $yr^{-1}$) from LULCC activities occurring between the 1990s and 2000s.
- In South Asia, there was low agreement in the sign of emissions, but moderate agreement in the presence of a carbon sink, and medium evidence of a change towards a carbon-sink between the 1990s and 2000s.
- To improve the accuracy of LULCC emissions, a reduction in uncertainty is needed in the estimates of carbon in biomass and soils, with particular attention to

peatlands, as well as increased focus on providing separate estimates, along with their uncertainties, for the component fluxes that make up the emissions from LULCC.

- Since 1980, carbons emissions from LULCC in Asia have comprised 20-40% of global LULCC emissions, with carbon emissions from LULCC in Southeast Asia accounting for 15-25% of global LULCC emissions during the same period.

## 6. Acknowledgements

This work was supported by the Asia Pacific Network for Global Change Research (ARCP2013-01CMY-Patra/Canadell). L. Calle was supported by the National Science Foundation East Asia Pacific Summer Institute (EAPSI) Fellowship. K. Ichii and P. Patra were supported by the Environment Research and Technology Development Funds (2-1401) from the Ministry of the Environment of Japan. J. G. Canadell thanks the support from the Australian Climate Change Science Program. A. Ito and E. Kato was supported by ERTDF (S-10) by the Ministry of the Environment, Japan. C. Koven is supported by DOE-BER through BGC-Feedbacks SFA and NGEE-Tropics. A. Wiltshire was supported by the Joint UK DECC/Defra Met Office Hadley Centre Climate Programme (GA01101) and EU FP7 Funding through project LUC4C (603542).

## 7. References

1. Achard, F., R. Beuchle, P. Mayaux, H.-J. Stibig, C. Bodart, A. Brink, S. Carboni, B. Desclée, F. Donnay, H. D. Eva, A. Lupi, R. Raši, R. Seliger, and D. Simonetti. 2014. Determination of tropical deforestation rates and related carbon losses from 1990 to 2010. *Global Change Biology* 20:2540–54.

2. Austin KG, P.S. Kasibhatla, D. L. Urban, F. Stolle, and J. Vincent. 2015. Reconciling Oil Palm Expansion and Climate Change Mitigation in Kalimantan, Indonesia. *PLoS ONE* 10(5): e0127963. doi:10.1371/journal.pone.0127963

3. Baccini, A., S. J. Goetz, W. S. Walker, N. T. Laporte, M. Sun, D. Sulla-Menashe, J. Hackler, P. S. a. Beck, R. Dubayah, M. a. Friedl, S. Samanta, and R. a. Houghton. 2012. Estimated carbon dioxide emissions from tropical deforestation improved by carbon-density maps. *Nature Climate Change* 2:182–185.

4. Carlson, K. M., L. M. Curran, D. Ratnasari, A. M. Pittman, B. S. Soares-Filho, G. P. Asner, S. N. Trigg, D. A. Gaveau, D. Lawrence, and H. O. Rodrigues. 2012. Committed carbon emissions, deforestation, and community land conversion from oil palm plantation expansion in West Kalimantan, Indonesia. *Proceedings of the National Academy of Sciences of the United States of America* 109(19):7559-7564.

5. Ciais, P., C. Sabine, G. Bala, L. Bopp, V. Brovkin, J. Canadell, A. Chhabra, R. DeFries, J. Galloway, M. Heimann, C. Jones, C. Le Quéré, R. B. Myneni, S. Piao, and P. Thornton. Carbon and other biogeochemical cycles, in: Climate Change 2013: The Physical Science Basis, edited by: Stocker, T. F., D. Qin, G. –K. Plattner, M. Tignore, S. K. Allen, J. Boschung, A. Nauels, Y. Xia, V. Bex, and P. M. Midgley. Cambridge University Press, Cambridge, 2013.

6. Earles, J. M., S. Yeh, and K. E. Skog. 2012. Timing of carbon emissions from global forest clearance. Nature Climate Change 2:682-685.

7. EDGARv4.3. Emission Database for Global Atmospheric Research (EDGAR), release version 4.3. European Commission, Joint Research Centre (JRC)/ Netherlands Environmental Assessment Agency (PBL): 2011. http://edgar.jrc.ec.europa.eu

8. Fang, J., A. Chen, C. Peng, S. Zhao, and L. Ci. 2001. Changes in forest biomass carbon storage in China between 1949 and 1998. *Science* 292:2320–2322.

9. FAO-FRA 2015. Global Forest Resource Assessment 2015. Food and Agriculture Organization of the United Nations.

10. Federici, S., F. N. Tubiello, M. Salvatore, H. Jacobs, and J. Schmidhuber. 2015. New estimates of CO2 forest emissions and removals: 1990-2015. *Forest Ecology and Management* 352:89–98.

11. Foley, J. A., R. Defries, G. P. Asner, C. Barford, G. Bonan, S. R. Carpenter, F. S. Chapin, M. T. Coe, G. C. Daily, H. K. Gibbs, J. H. Helkowski, T. Holloway, E. a Howard, C. J. Kucharik, C. Monfreda, J. a Patz, I. C. Prentice, N. Ramankutty, and P. K. Snyder. 2005. Global consequences of land use. *Science* 309:570–4.

12. Friedlingstein, P., R. A. Houghton, G. Marland, J. Hackler, T. A. Boden, T. J. Conway, J. G. Canadell, M. R. Raupach, P. Ciais, C. Le Quéré. 2010. Update on CO2 emissions. *Nature Geoscience*. 3:811-812. doi:10.1038/ngeo1022

13. Gaveau, D. L. A., S. Sloan, E. Molidena, H. Yaen, D. Sheil, N. K. Abram, M. Ancrenaz, R. Nasi, M. Quinones, N. Wielaard, and E. Meijaard. 2014. Four decades of forest persistence, clearance and logging on Borneo. *PLoS ONE* 9(7): e101654. doi:10.1371/journal.pone.0101654

14. Goldewijk, K. K. 2001. Estimating global land use change over the past 300 years: The HYDE Database. *Global Biogeochemical Cycles* 15:417–433.

15. Hansen, M. C., P. V Potapov, R. Moore, M. Hancher, S. a Turubanova, a Tyukavina, D. Thau, S. V Stehman, S. J. Goetz, T. R. Loveland, a Kommareddy, a Egorov, L. Chini, C. O. Justice, and J. R. G. Townshend. 2013. High-resolution global maps of 21st-century forest cover change. *Science* 342:850–3.

16. Harris, N., S. Brown, S. C. Hagen, A. Baccini, R. A. Houghton. 2012a. Progress toward a consensus on carbon emissions from tropical deforestation. *Policy Brief* for Winrock International, WHOI, and the Meridian Institute.

17. Harris, N. L., S. Brown, S. C. Hagen, S. S. Saatchi, S. Petrova, W. Salas, M. C. Hansen, P. V. Potapov, and A. Lotsch. 2012b. Baseline Map of Carbon Emissions from Deforestation in Tropical Regions. *Science* 336:1573. doi:10.1126/science.1217962

18. Hooijer, A., M. Silvius, H. Wösten, and S. Page. 2006. PEAT-CO2, Assessment of CO2 emissions from drained peatlands in SE Asia. *Delft Hydraulics report* Q3943/2006, 36p, http://peat-co2.deltares.nl.

19. Hooijer, A., S. Page, J. G. Canadell, M. Silvius, J. Kwadijk, H. Wösten, and J. Jauhiainen. 2010. Current and future CO2 emissions from drained peatlands in Southeast Asia. *Biogeosciences* 7:1505–1514.

20. Houghton, R. A. 2003. Revised estimates of the annual net flux of carbon to the atmosphere from changes in land use and land management 1850-2000. *Tellus* B: 378-390.

21. Houghton, R. A. 2010. How well do we know the flux of CO2 from land-use change? *Tellus* B: 337-351.

22. Houghton, R. A., J. I. House, J. Pongratz, G. R. Van Der Werf, R. S. Defries, M. C. Hansen, C. Le Quéré, and N. Ramankutty. 2012a. Carbon emissions from land use and land-cover change. *Biogeosciences* 9:5125–5142.

23. Hurtt, G. C., S. Frolking, M. G. Fearon, B. Moore, E. Shevliakova, S. Malyshev, S. W. Pacala, and R. a. Houghton. 2006. The underpinnings of land-use history: three centuries of global gridded land-use transitions, wood-harvest activity, and resulting secondary lands. *Global Change Biology* 12:1208–1229.

24. Hurtt, G. C., L. P. Chini, S. Frolking, R. A. Betts, J. Feddema, G. Fischer, J. P. Fisk, K. Hibbard, R. A. Houghton, A. Janetos, C. D. Jones, G. Kindermann, T. Kinoshita, K. Klein Goldewijk, K. Riahi, E. Shevliakova, S. Smith, E. Stehfest, A. Thomson, P. Thornton, D. P. van Vuuren, and Y. P. Wang. 2011. Harmonization of land-use scenarios for the period 1500-2100: 600 years of global gridded annual land-use transitions, wood harvest, and resulting secondary lands. *Climatic Change* 109:117–161.

*25.* Kim, D.H., J. O. Sexton, and J. R. Townshend. 2015. Accelerated Deforestation in the Humid Tropics from the 1990s to the 2000s. *Geophysical Research Letters* 42, 3495–3501. doi:*10.1002/2014GL062777*.

26. Kirschke, S., P. Bousquet, P. Ciais, M. Saunois, J. G. Canadell, E. J. Dlugokencky, P. Bergamaschi, D. Bergmann, D. R. Blake, L. Bruhwiler, P. Cameron-Smith, S. Castaldi, F. Chevallier, L. Feng, A. Fraser, M. Heimann, E. L. Hodson, S. Houweling, B. Josse, P. J. Fraser, P. B. Krummel, J.-F. Lamarque, R. L. Langenfelds, C. Le Quéré, V. Naik, S. O'Doherty, P. I. Palmer, I. Pison, D. Plummer, B. Poulter, R. G. Prinn, M. Rigby, B. Ringeval, M. Santini, M. Schmidt, D. T. Shindell, I. J. Simpson, R. Spahni, L. P. Steele, S. a. Strode, K. Sudo, S. Szopa, G. R. van der Werf, A. Voulgarakis, M. van Weele, R. F. Weiss, J. E. Williams, and G. Zeng. 2013. Three decades of global methane sources and sinks. *Nature Geoscience* 6:813–823.

27. Langner, A., F. Achard, and G. Grassi. 2014. Can recent pan-tropical biomass maps be used to derive alternative Tier 1 values for reporting REDD+ activities under UNFCCC? *Environmental Research Letters* 9:124008.

28. Le Quéré, C., R. Moriarty, R. M. Andrew, G. P. Peters, P. Ciais, P. Friedlingstein, S. Jones, S. Sitch, P. Tans, A. Arneth, T. A. Boden, L. Bopp, Y. Bozec, J. G. Canadell, L. P. Chini, F. Chevallier, C. E. Cosca, I. Harris, M. Hoppema, R. A. Houghton, J. I. House, A. K. Jain, T. Johannessen, E. Kato, R. F. Keeling, V. Kitidis, K. Goldewijk, C. Koven, C. S. Landa, P. Landschützer, A. Lenton, I. D. Lima, G. Marland, J. T. Mathis, N. Metzl, Y. Nojiri, A. Olsen, T. Ono, S. Peng, W. Peters, B. Pfeil, B. Poulter, M. R. Raupach, P. Regnier, C. Rödenbeck, S. Saito, J. E. Salisbury, U. Schuster, J. Schwinger, R. Séférian, J. Segschneider, T. Steinho, B. D., Stocker, A. J. Sutton, T. Takahashi, B. Tilbrook, G. R. van der Werf, N. Viovy, Y. –P. Wang, R. Wanninkhof, A. Wiltshire, and N. Zeng. 2015. Global carbon budget 2014. *Earth Syst. Sci. Data* 7, 47–85, doi:10.5194/essd-7-47-2015

29. Li, P., J. Zhu, H. Hu, Z. Guo, Y. Pan, R. Birdsey, and J. Fang. 2015. The relative contributions of forest growth and areal expansion to forest biomass carbon sinks in China. *Biogeosciences Discussions* 12:9587–9612.

30. Liu, M. and H. Q. Tian. 2010. China's land-cover and land-use change from 1700 to 2005: estimations from high-resolution satellite data and historical archives. *Global Biogeochemical Cycles* 24:GB3003. doi:10.1029/2009GB003687.

31. Liu, Y. Y., A. I. J. M. van Dijk, R. A. M. de Jeu, J. G. Canadell, M. F. McCabe, J. P. Evans, and G. Wang. 2015. Recent reversal in loss of global terrestrial biomass. *Nature Climate Change* 5:470–474.

32. Liu, Z., D. Guan, W. Wei, S. J. Davis, P. Ciais, J. Bai, S. Peng, Q. Zhang, K. Hubacek, G. Marland, and others. 2015. Reduced carbon emission estimates from fossil fuel combustion and cement production in China. *Nature* 524:335–338.

33. Loarie, S. R., G. P. Asner, and C. B. Field. 2009. Boosted carbon emissions from Amazon deforestation. *Geophysical Research Letters* 36:L14810

34. Margono, B. A., P. V. Potapov, S. Turubanova, F. Stolle, and M. C. Hansen. 2014. Primary forest cover loss in Indonesia over 2000-2012. *Nature Climate Change* 4:730-735.

35. Meittinen, J., C. Shi, and S. Chin Liew. 2011. Influence of peatland and land cover distribution on fire regimes in insular Southeast Asia. *Regional Environmental Change* 11:191-201.

36. Miettinen, J., C. Shi, and S. C. Liew. 2016. Land cover distribution in the peatlands of Peninsular Malaysia, Sumatra, and Borneo in 2015 with changes since 1990. *Global Ecology and Conservation* 6:67-78.

37. Pan, Y., R. A. Birdsey, J. Fang, R. Houghton, P. E. Kauppi, W. A. Kurz, O. L. Phillips, A. Shvidenko, S. L. Lewis, J. G. Canadell, P. Ciais, R. B. Jackson, S. W. Pacala, A. D. McGuire, S. Piao, A. Rautiainen, S. Sitch, and D. Hayes. 2011. A large and persistent carbon sink in the world's forests. *Science* 333:988–993.

38. Page, S. E., F. Siegert, J. O. Rieley, H.D. V. Boeheim, A. Jaya, and S. Limin. 2002. The amount of carbon released from peat and forest firest in Indonesia during 1997. *Nature* 420: 61-65.

39. Patra, P. K., M. Ishizawa, S. Maksyutov, T. Nakazawa, and G. Inoue. 2005. Role of biomass burning and climate anomalies for land-atmosphere carbon fluxes based on inverse modeling of atmospheric CO2. *Global Biogeochemical Cycles* 19:1–10.

40. Piao, S., J. Fang, P. Ciais, P. Peylin, Y. Huang, S. Sitch, and T. Wang. 2009. The carbon balance of terrestrial ecosystems in China. *Nature* 458:1009–1013.

41. Piao, S. L., A. Ito, S. G. Li, Y. Huang, P. Ciais, X. H. Wang, S. S. Peng, H. J. Nan, C. Zhao, A. Ahlström, R. J. Andres, F. Chevallier, J. Y. Fang, J. Hartmann, C. Huntingford, S. Jeong, S. Levis, P. E. Levy, J. S. Li, M. R. Lomas, J. F. Mao, E. Mayorga, A. Mohammat, H. Muraoka, C. H. Peng, P. Peylin, B. Poulter, Z. H. Shen, X. Shi, S. Sitch, S. Tao, H. Q. Tian, X. P. Wu, M. Xu, G. R. Yu, N. Viovy, S. Zaehle, N. Zeng, and B. Zhu. 2012. The carbon budget of terrestrial ecosystems in East Asia over the last two decades. *Biogeosciences* 9:3571–3586.

42. Pongratz, J., C. H. Reick, R. A. Houghton, and J. I. House. 2014. Terminology as a key uncertainty in net land use and land cover change carbon flux estimates. *Earth System Dynamics* 5:177–195.

43. Prentice, I. C., D. I. Kelley, P. N. Foster, P. Friedlingstein, S. P. Harrison, and P. J. Bartlein. 2011. Modeling fire and the terrestrial carbon balance. *Global Biogeochem Cycles* 25:GB3005–GB3005.

44. Pütz, S., J. Groeneveld, K. Henle, C. Knogge, A. C. Martensen, M. Metz, J. P. Metzger, M. C. Ribeiro, M. D. de Paula, and A. Huth. 2014. Long-term carbon loss in fragmented Neotropical forests. *Nature communications* 5:5037. doi:10.1038/ncomms6037

45. Rosa, I. M. D., S. E. Ahmed, and R. M. Ewers. 2014. The transparency, reliability and utility of tropical rainforest land-use and land-cover change models. *Global Change Biology* 20:1707-1722.

46. Ruesch, A., and H. K. Gibbs. 2008. New IPCC Tier-1 Global Biomass Carbon Map For the Year 2000. Available online from the Carbon Dioxide Information Analysis Center [http://cdiac.ornl.gov], Oak Ridge National Laboratory, Oak Ridge, Tennessee.

47. Saatchi, S. S., N. L. Harris, S. Brown, M. Lefsky, E. T. A. Mitchard, W. Salas, B. R. Zutta, W. Buermann, S. L. Lewis, S. Hagen, S. Petrova, L. White, M. Silman, and A. Morel. 2011. Benchmark map of forest carbon stocks in tropical regions across three continents. *Proceedings of the National Academy of Sciences of the United States of America* 108:9899–9904.

48. S. Sitch, P. Friedlingstein, N. Gruber, S. D. Jones, G. Murray-Tortarolo, A. Ahlström, S. C. Doney, H. Graven, C. Heinze, C. Huntingford, S. Levis, P. E. Levy, M. Lomas, B. Poulter, N. Viovy, S. Zaehle, N. Zeng, A. Arneth, G. Bonan, L. Bopp, J. G. Canadell, F. Chevallier, P. Ciais, R. Ellis, M. Gloor, P. Peylin, S. L. Piao, C. Le Quéré, B. Smith, Z. Zhu, and R. Myneni. 2015. Recent trends and drivers of regional sources and sinks of carbon dioxide. *Biogeosciences* 12:653-679.

49. Shevliakova, E., S. W. Pacala, S. Malyshev, G. C. Hurtt, P. C. D. Milly, J. P. Caspersen, L. T. Sentman, J. P. Fisk, C. Wirth, and C. Crevoisier. 2009. Carbon cycling under 300 years of land use change: importance of the secondary vegetation sink. *Global Biogeochemical Cycles* 23:GB2022.

50. Song, X.-P., C. Huang, S. S. Saatchi, M. C. Hansen, and J. R. Townshend. 2015. Annual Carbon Emissions from Deforestation in the Amazon Basin between 2000 and 2010. *PLoS ONE* 10(5): e0126754. doi:10.1371/journal.pone.0126754

51. Stibig, H.-J., F. Achard, S. Carboni, R. Raši, and J. Miettinen. 2014. Change in tropical forest cover of Southeast Asia from 1990 to 2010. *Biogeosciences*. 11:247-258.

52. Stocker B, F. Feissli, K. Strassmann (2014) Past and future carbon fluxes from land use change, shifting cultivation and wood harvest. *Tellus B* 66. doi:10.3402/tellusb.v66.23188

53. Tao, B., H. Tian, G. Chen, W. Ren, C. Lu, K.D. Alley, X. Xu, M. Liu, S. Pan, and H. Virji. 2013. Terrestrial carbon balance in tropical Asia: contribution from cropland expansion and land management. *Global and Planetary Change* 100:85-98. Doi:10.1016/j.gloplacha.2012.09.006.

54. Tian, H., K. Banger, B. Tao, V. K Dadhwal. 2014. History of land use in India during 1880-2010: Large-scale land transformation reconstructed from satellite data and historical achieves. *Global and Planetary Change* 121:76-88.

55. van der Werf, G. R., J. T. Randerson, L. Giglio, G. J. Collatz, P. S. Kasibhatla, and A. F. Arellano. 2006. Interannual variability of global biomass burning emissions from 1997 to 2004. *Atmospheric Chemistry and Physics* 6:3423–3441.

56. van der Werf, G. R., J. Dempewolf, S. N. Trigg, J. T. Randerson, P. S. Kasibhatla, L. Gigio, D. Murdiyarso, W. Peters, D. C. Morton, G. J. Collatz, A. J. Dolman, and R. S. DeFries. 2008. Climate regulation of fire emissions and deforestation in equatorial Asia. *Proceedings of the National Academy of Sciences of the United States of America* 105:20350–20355.

57. van der Werf, G. R., J. T. Randerson, L. Giglio, G. J. Collatz, M. Mu, P. S. Kasibhatla, D. C. Morton, R. S. DeFries, Y. Jin, *and* T. T. van Leeuwen. *2010.* Global fire emissions and the contribution of deforestation, savanna, forest, agricultural, and peat fires (1997–2009). *Atmospheric Chemistry and Physics* 10:11707–11735.

58. Wilkenskjeld, S., S. Kloster, J. Pongratz, T. Raddatz, and C. Reick. 2014. Comparing the influence of net and gross anthropogenic land use and land cover changes on the carbon cycle in the MPI-ESM. *Biogeosciences Discussions* 11:5443–5469.

59. Yang, X., T. K. Richardson, and A. K. Jain. 2010. Contributions of secondary forest and nitrogen dynamics to terrestrial carbon uptake. *Biogeosciences* 7:3041–3050.

**Table 2.1. Datasets and methods used for determining land use and land cover, carbon stocks, and forest regrowth. The HYDE data model version 3.0 (Goldewijk 2001) determines land use in the DGVMs, and an updated version of HYDEv3.1 is used in the Tao et al. (2013) study. The Global Land Cover 2000 (GLC 2000) and the FAO Global Ecological Zone map (FAO-GEZ) provide land use and land cover for the EDGARv4.3 dataset.**

| Dataset | Land Use and Land Cover | Carbon Stocks | Forest Regrowth |
|---|---|---|---|
| FAO-FRA | IPCC 2006 Tier1 methods<br>Country-level reporting | IPCC 2006 Tier1 methods<br>Carbon per hectare by Biome or Region | N/A |
| EDGARv4.3 | GLC 2000 and FAO-GEZ map for forest area<br>FAO-FRA for area change | IPCC 2006 Tier1 methods<br>Carbon per hectare by Biome | IPCC 2006 Tier1 methods<br>Biomass increment factors |
| DGVMs | HYDE | Process-based estimate | Process-based estimate $^{clim}$ |
| Achard et al. (2014) | Remote-sensing | Remote-sensing, allometric model | Implicit $^{clim}$ |
| Harris et al. (2012b) | Remote-sensing | Remote-sensing, allometric model | N/A |
| Houghton et al. (2012) | FAO-FRA | Bookkeeping model<br>Country-level statistics | Biomass Growth Equation |
| Pan et al. (2011) | FAO-FRA, Govt. reports | FAO-FRA, Houghton et al. (2012) | Houghton et al. (2012) |
| Tao et al. (2013) | HYDE 3.1 | Process-based estimate | Process-based estimate $^{clim}$ |

$^{clim}$ transient response to climate and $CO_2$ fertilization is included; implicit inclusion in Achard et al. (2014).

**Table 2.2. Component carbon emissions and factors affecting carbon stocks (IRR, FERT, Transient Response) included in each of the datasets in this study. Emissions from changes in aboveground and belowground live biomass (AGB and BGB, respectively) are included in all datasets. Emissions from fire may also be included as an emission source, and these may be independent of emissions from land use change. Forest regrowth can offset carbon emissions and the rate of regrowth can be modified by changes in climate (clim) or from $CO_2$ fertilization ($CO_2$), which is defined as a Transient Response; these effects are implicitly included in the remote sensing study by Achard et al. (2014). The carbon emissions from wood harvest products (WH) are reported separately for the EDGARv4.3 dataset; these emissions could not be separated from Houghton et al. (2012) or Pan et al. (2011). The relative weight score reflects the inclusion carbon fluxes from individual carbon stocks, fire and forest regrowth, relative to the dataset with the maximum number of component fluxes included in the estimate.**

| Dataset | Relative Weight | Emission Timescale | Land Types | Change in Carbon Stock | | | | | Fire | Land Management | | | | | Forest Regrowth | | |
|---|---|---|---|---|---|---|---|---|---|---|---|---|---|---|---|---|---|
| | | | | AGB | BGB | Litter | Soil | Peat | | SC | WH | CH | IRR | FERT | | Transient Response | |
| FAO-FRA | 0.67 | I, L* | N, Ag | ✔ | ✔ | | ✔ | | ✔□[Ŧ] | | | | | | | | |
| EDGARv4.3 | 1.00 | I | N | ✔ | ✔ | | ✔ □[θ] | ✔□[θ] | ✔□ | | | | | | ✔ | | |
| DGVMs | 1.00 | I, L | N, Ag | ✔ | ✔ | ✔ | ✔ | | ✔ | [1,2] | [1,2] | [1,2] | [1,2] | [1,2] | ✔ | clim | $CO_2$ |
| Achard et al. (2014) | 0.63 | I | N | ✔ | ✔ | | | | | | | | | | ✔ | clim | $CO_2$ |
| Harris et al. (2012b) | 0.50 | I | N | ✔ | ✔ | | | | | | | | | | | | |
| Houghton et al. (2012) | 1.00 | I, L | N, Ag | ✔ | ✔ | ✔ | ✔ | | ✔ | ✔ | ✔ | | | | ✔ | | |
| Pan et al. (2011) | 0.88 | I | N, Ag | ✔ | ✔ | ✔ | | | ✔ | | ✔ | | | | ✔ | | |
| Tao et al. (2013) | 0.88 | I, L | N, Ag | ✔ | ✔ | ✔ | ✔ | | | | | ✔ | ✔ | ✔ | ✔ | clim | $CO_2$ |

Emission Timescale: Immediate (I), Legacy (L)

Land Types: Natural (N), Agriculture (Ag)

Carbon Stock: Aboveground Biomass (AGB), Belowground biomass (BGB)

Land Management: Shifting cultivation (SC), Wood Harvest (WH), Crop Harvest (CH), Irrigation (IRR), Nitrogen Fertilization (FERT)

* Legacy emissions are only included for losses to organic soil carbon from Agricultural areas.

[Ŧ] Emissions from combustion of organic soils during biomass burning

[θ] Emissions from losses to organic and peat soils is derived from fire emissions in the GFEDv3.1 dataset (van der Werf et al. 2010)

[1] VISIT model included SC, WH, CH, IRR, and FERT

[2] CLMv4.5 included SC, WH, CH, IRR, and FERT

**Table 2.3. Regional carbon emissions from LULCC in Asia by decade (Petagram Carbon per year). Uncertainty is presented as mean ± standard deviation or as a range of maximum and minimum estimates.**

| Region | Ensemble/Study | 1980-1989 | 1990-1999 | 2000-2009 |
|---|---|---|---|---|
| Southeast Asia | DGVMs | 0.22 [0.15, 0.39] | 0.33 [0.16, 0.54] | 0.31 [0.18, 0.53] |
| | FAO-FRA | | 0.33 ± 0.06 | 0.41 ± 0.06 |
| | EDGAR v4.3 | | | 0.11 ± 0.13 |
| | Houghton et al. (2012) [Ŧ] | 0.29 ± 0.02 [Ŧ] | 0.66 ± 0.36 [Ŧ] | 0.46 ± 0.13 [Ŧ] |
| | Achard et al. (2014) | | [0.24, 0.35] | [0.24, 0.37] |
| | Harris et al. (2012b) [θ] | | | [0.17, 0.32] [θ] |
| | Pan et al. (2011) [Ŧ] | | 0.30 [Ŧ] | 0.14 [Ŧ] |
| | Tao et al. (2013) | [0.23, 0.26] | [0.21, 0.24] | |
| East Asia | DGVMs | 0.29 [0.16, 0.44] | 0.27 [0.12, 0.40] | 0.05 [-0.06, 0.16] |
| | FAO-FRA | | -0.11 ± 0.0003 | -0.12 ± 0.02 |
| | EDGAR v4.3 | | | -0.25 ± 0.02 |
| | Houghton et al. (2012) | -0.02 ± 0.006 | -0.03 ± 0.002 | -0.04 ± 0.005 |
| | Pan et al. (2011) [Ŧ] | | -0.21 [Ŧ] | -0.24 [Ŧ] |
| South Asia | DGVMs | 0.04 [0.01, 0.13] | 0.09 [0.03, 0.19] | 0.04 [0.001, 0.12] |
| | FAO-FRA | | 0.012 ± 0.00 | -0.018 ± 0.01 |
| | EDGAR v4.3 | | | -0.03 ± 0.01 |
| | Houghton et al. (2012) | -0.006 ± 0.002 | -0.014 ± 0.005 | -0.015 ± 0.005 |
| | Harris et al. (2012b)* | | | [0.014, 0.027] * |

[Ŧ] Includes carbon emissions from wood harvest, both instantaneous and legacy

[θ] Gross carbon emissions from deforestation only, for years between 2000-2005

**Table 2.4. Ranking of agreement and confidence among data sources for estimates of change and sign of emissions by region and decade. The weighted-mean of all mean decadal estimates is also listed by region and decade (mean Pg C per year ± SD of means). Triangle indicates a carbon source (up, red) or carbon sink (down, green), or an increasing (up, red) or deceasing (down, green) change from previous decade; a circle indicates that there is no change, given the stated uncertainties, between the decade considered and the previous one. Size of the triangle/circle indicates the number of independent estimates in agreement; small: 1 studies, medium: 2-3 studies, large: 4+ studies. Estimates with high agreement have only a single triangle, and high confidence is evident in estimates with the largest triangles.**

| Region | 1980-1989 | | 1990-1999 | | 2000-2009 | |
|---|---|---|---|---|---|---|
| | Source/Sink | Change | Source/Sink | Change | Source/Sink | Change |
| Southeast Asia | ▲ 0.255 ± 0.019 | | ▲ 0.363 ± 0.131 | ▲ ○ | ▲ 0.271 ± 0.116 | ▲ ▼ ○ |
| East Asia | ▲ ▼ 0.135 ± 0.083 | | ▲ ▼ 0.001 ± 0129 | ▲ ▼ | ▲ ▼ -0.077 ± 0.076 | ▼ |
| South Asia | ▲ ▼ 0.017 ± 0.013 | | ▲ ▼ 0.032 ± 0.029 | ▲ ▼ | ▲ ▼ -0.003 ± 0.021 | ▼ |

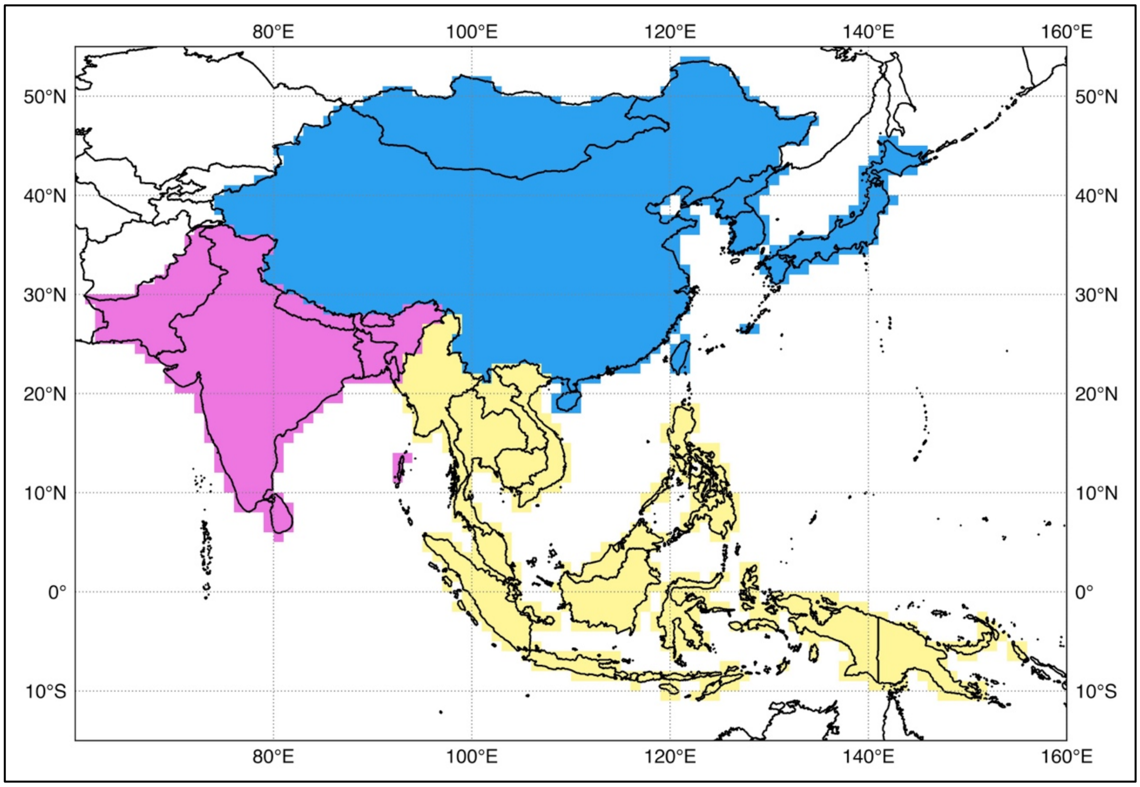


**Figure 2.1. Geographic areas were pre-defined for this study, corresponding to Southeast Asia (yellow), East Asia (blue), and South Asia (purple).**

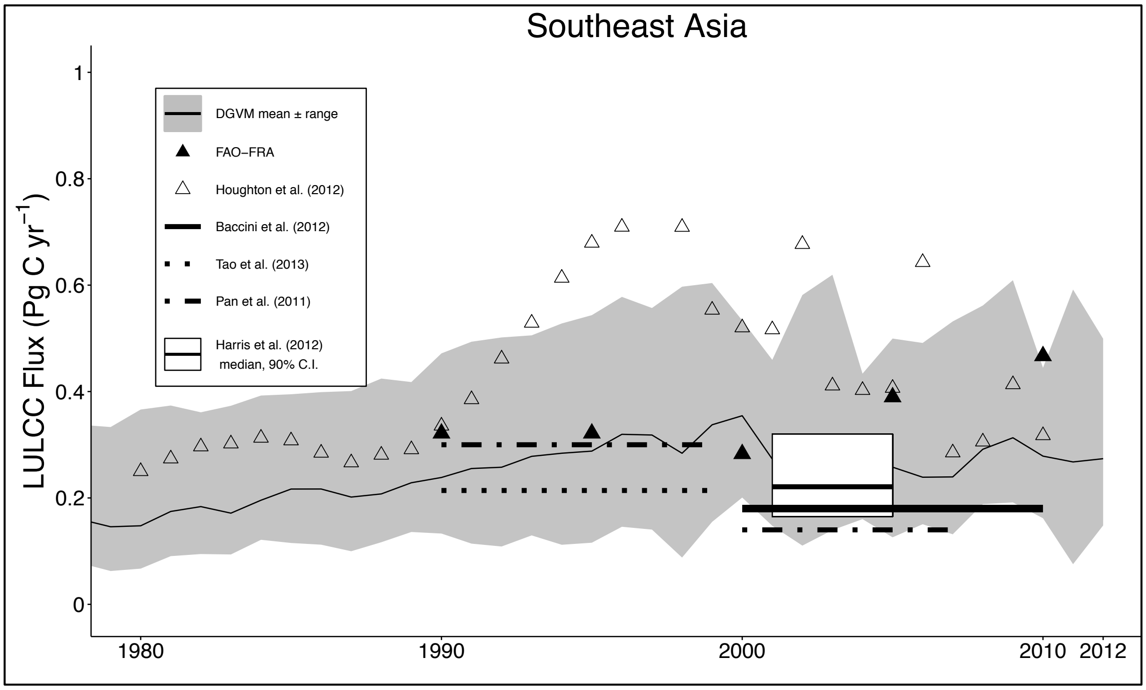


**Figure 2.2. Carbon emissions from Land Use and Land Cover Change (LULCC) in Southeast Asia between 1980 and 2012. Houghton et al. (2012) also reports an outlier emission estimate of 1.61 Pg C in 1997 (not shown), resulting from extensive peat fires in the region; these emissions were not included in the estimates of other studies reported here. The DGVM ensemble {JULES, LPJ, LPJ-GUESS, LPX, VISIT} mean estimate (thin solid line) is presented along with the range of annual estimates among the models (grey shaded area). Previously published estimates are provided as point and decadal (boxplot, and the horizontal dashed, dotted and solid lines) mean estimates.**

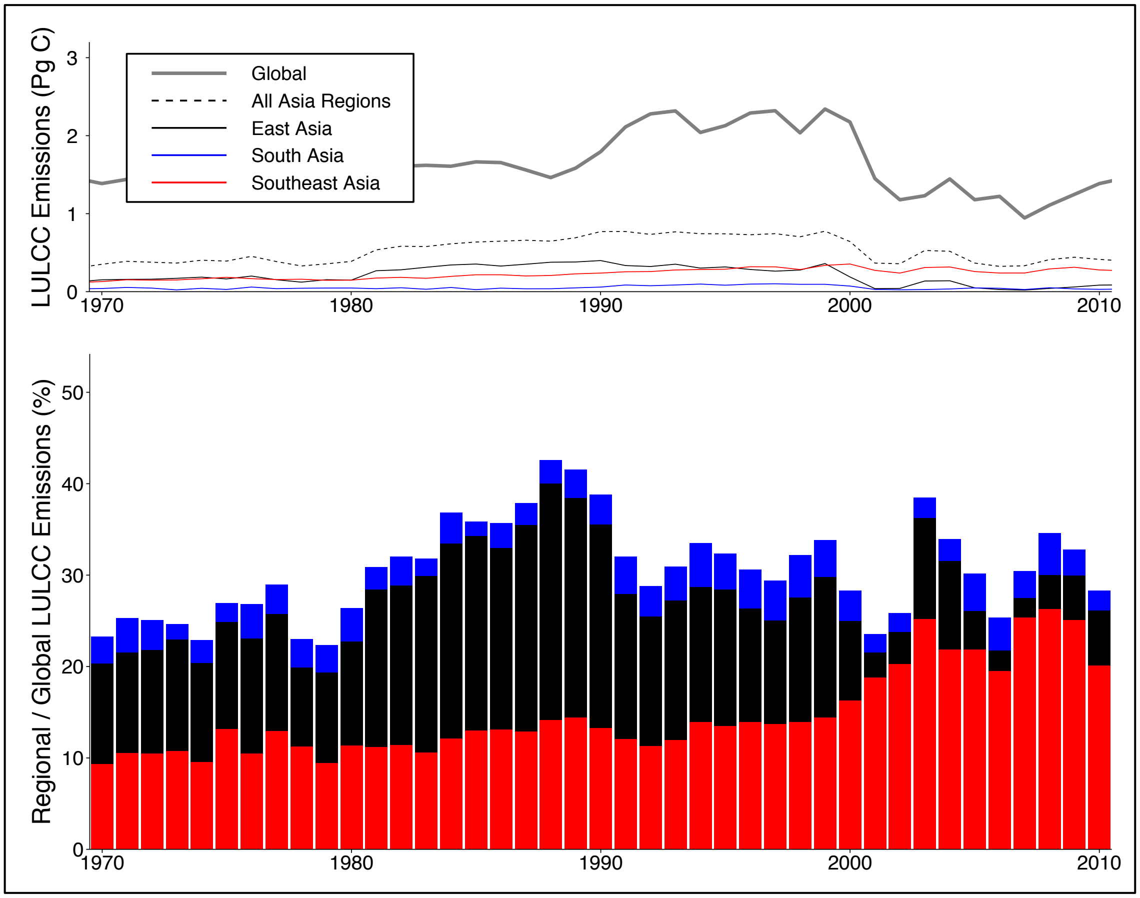


**Figure 2.3. Total emissions from land use and land cover change (LULCC) (top) and the contribution of LULCC emissions in Asia as a percent of Global LULCC emissions (bottom) for years 1901-2012. Estimates for Global and Asian LULCC fluxes are obtained from DGVM ensemble means (n=8). In the late 2000's, emissions from LULCC in Southeast Asia have accounted for 15 – 25 % of global LULCC emissions. Emissions from LULCC in East Asia peaked in the late 1980's at 25% of global LULCC emissions. A decline in the percent contribution of LULCC emissions in Asia to global LULCC emissions during the 1990's results mainly from an increase in Global LULCC emissions during the same time period.**

# CHAPTER THREE

# A SEGMENTATION ALGORITHM FOR CHARACTERIZING RISE AND FALL SEGMENTS IN SEASONAL CYCLES: AN APPLICATION TO $XCO_2$ TO ESTIMATE BENCHMARKS AND ASSESS MODEL BIAS

## Contribution of Authors and Co-Authors

Manuscript in Chapter Three

Author: Leonardo Calle

Contributions: wrote manuscript, performed simulations and processed data, developed methods and performed analyses, interpreted results, generated tables and figures

Co-Author: Prabir K. Patra

Contributions: contributed to writing of manuscript, performed simulations and processed data, interpretation of results, and suggested figures and analyses

Co-Author: Benjamin Poulter

Contributions: contributed to writing of manuscript, interpretation of results, and suggested figures and analyses

Manuscript Information

Leonardo Calle, Prabir Patra, and Benjamin Poulter

Atmospheric Measurement Techniques Discussions

Status of Manuscript:
____ Prepared for submission to a peer-reviewed journal
____ Officially submitted to a peer-reviewed journal
____ Accepted by a peer-reviewed journal
_X__ Published in a peer-reviewed journal

Published by the European Geoscience Union
doi:10.5194/amt-2018-296

# CHAPTER THREE

# A SEGMENTATION ALGORITHM FOR CHARACTERIZING RISE AND FALL SEGMENTS IN SEASONAL CYCLES: AN APPLICATION TO $XCO_2$ TO ESTIMATE BENCHMARKS AND ASSESS MODEL BIAS

Leonardo Calle[1], Benjamin Poulter[2], and Prabir K. Patra[3]

[1] Montana State University, Department of Ecology, Bozeman, Montana 59717, USA
[2] NASA Goddard Space Flight Center, Biospheric Science Laboratory, Greenbelt, Maryland 20771, USA
[3] Japan Agency for Marine-Earth Science and Technology (JAMSTEC), Yokohama, 236-0001, Japan

**Abstract.**

There is more useful information in the time series of satellite-derived column-averaged carbon dioxide ($XCO_2$) than is typically characterized. Often, the entire time series is treated at once without considering detailed features at shorter timescales, such as non-stationary changes in signal characteristics - amplitude, period, and phase. In many instances, signals are visually and analytically differentiable from other portions in a time series. Each *Rise* (increasing) and *Fall* (decreasing) *segment*, in the seasonal cycle is visually discernable in a graph of the time series. The Rise and Fall segments largely result from seasonal differences in terrestrial ecosystem production, which means that the segment's signal characteristics can be used to establish observational benchmarks because the signal characteristics are driven by similar underlying processes. We developed an analytical segmentation algorithm to characterize the Rise and Fall segments in $XCO_2$ seasonal cycles. We present the algorithm for general application of the segmentation analysis and emphasize here that the segmentation analysis is more generally applicable to cyclic time series.

We demonstrate the utility of the algorithm with specific results related to the comparison between satellite- and model-derived $XCO_2$ seasonal cycles (2009-2012) for large bioregions on the globe. We found a seasonal amplitude gradient of 0.74-0.77 ppm for every 10˚ degrees of latitude for the satellite data, with similar gradients for Rise and Fall segments. This translates to a south-north seasonal amplitude gradient of 8 ppm for $XCO_2$, about half the gradient in seasonal amplitude based on surface site in-situ $CO_2$ data (~19 ppm). The latitudinal gradients in period of the satellite-derived seasonal cycles

were of opposing sign and magnitude (-9 days/10˚ latitude for Fall segments, and 10 days/10˚ latitude for Rise segments), and suggests that a specific latitude (~ 2˚ N) exists which defines an inversion point for the period asymmetry. Before (after) the point of asymmetry inversion, the periods of Rise segments are less (greater) than the periods of Fall segments; only a single model could reproduce this emergent pattern. The asymmetry in amplitude and period between Rise and Fall segments introduces a novel pattern in seasonal cycle analyses, but while we show these emergent patterns exist in the data, we are still breaking ground in applying the information for science applications. Maybe the most useful application is that the segmentation analysis allowed us to decompose the model biases into their correlated parts of biases in amplitude, period, and phase, independently for Rise and Fall segments. We offer an extended discussion on how such information on model biases and the emergent patterns in satellite-derived seasonal cycles can be used to guide future inquiry and model development.

## 1. Introduction

Most of our understanding about atmospheric $CO_2$ dynamics has come from $CO_2$ sampled by in-situ flask samples or eddy-flux towers at Earth's surface (Ciais et al., 2014). While these data streams have proved incredibly useful, the transient dynamics of fluxes simulated by global-scale terrestrial models have only been compared to a relatively few locations on Earth. In contrast to surface $CO_2$ samples, which sample $CO_2$ concentrations in the planetary boundary layer, satellite observations of $CO_2$ are made by downward-looking Fourier spectrometers from the top of the atmosphere and represent an integrated estimate of $CO_2$ concentrations in a full column of atmosphere, hereafter '$XCO_2$' (Wunch et al., 2011; Crisp et al., 2012). Although fluxes from the surface have a large influence on the total column $CO_2$, the vertical and horizontal transport of air masses in higher atmospheric layers, each with different concentrations $CO_2$, also influences the $CO_2$ concentrations in the total column (Belikov et al., 2017), including that of the stratosphere (Saito et al., 2012).

The synoptic coverage and integrated nature of $XCO_2$ means that surface fluxes from around the globe impart information into the seasonal dynamics and inter-annual variability of regional seasonal cycles, which is both a confounding and useful property for evaluating large-scale models. The integrated nature of the data also means that even a few years of data will be sufficient to evaluate the simulated dynamics of global-scale models. We propose that if models can reasonably simulate the timing and magnitude of terrestrial surface fluxes in all bioregions, then we would expect that the simulated $XCO_2$ would match reasonably well with the seasonal dynamics from the benchmark satellite data. Such demonstrated ability could strengthen confidence in regional-to-global model simulations.

To gain insight into seasonal cycle dynamics of satellite $XCO_2$ and individual model behavior, we demonstrate a novel approach to extract more information from the seasonal cycle than is typically characterized. In evaluations of model performance, traditional performance statistics (root-mean-squared-error, correlation, standard deviation) are used to quantify bias in phase and amplitude of the seasonal cycle against a benchmark signal (Coupled Model Intercomparison Project (CMIP) Earth System Models *in* Glecker et al., 2008; DGVMs *in* Anav et al., 2015). In almost all applications, however, the entire time series is treated at once without considering detailed features at shorter timescales, such as non-stationary changes in amplitude, magnitude, period, or phase (Fig. 1). We suggest that traditional performance statistics be applied to categories of unique patterns in the seasonal cycle, and not to the entire time series, thereby characterizing the error structure in a manner that can relate temporal dynamics (amplitude, magnitude, phase) with unique underlying processes.

We extend and apply a time series segmentation method (Ehret and Zehe, 2011) to extract the Rise and Fall segments in seasonal cycles of satellite-derived and simulated $XCO_2$, based on a suite of terrestrial ecosystem models. The advantage of the segmentation approach is that it allows an error structure to be accurately characterized by separately calculating the errors in amplitude, period and phase for each segment type (Rise, Fall). For example, in a graph of a multi-year seasonal cycle of $XCO_2$ (Fig. 1), each *increasing* and *decreasing* segment is visually discernable and analytically differentiable from other portions in the seasonal cycle; hereafter, *Rise* refers to increasing segments and *Fall* refers to decreasing segments in a seasonal cycle. The Rise and Fall segments largely result from seasonal differences in the onset and cessation of terrestrial ecosystem production (Keeling et al., 1995), which means that a segment's signal characteristics (i.e., amplitude, period, phase) are likewise influenced by different stages of terrestrial ecosystem activity. By segmenting the time series into similar component signals, we can then test for differences in the signal characteristics of Rise and Fall patterns and provide insight into a model's ability to recreate these features of the seasonal cycle over multiple years.

Our first aim was to simply characterize the satellite-derived $XCO_2$ seasonal cycles in terms of Rise- and Fall-type segment variation. Secondly, we evaluated if signal characteristics and model biases differed or were correlated among Rise and Fall segments, which would help provide information in the missing parts of the satellite-based time-series (i.e., at high latitudes during boreal winter and in the Tropics during the wet-season), which we demonstrate is possible. We also evaluated if model biases between Rise and Fall segments differed enough to provide information about the underlying model representation of terrestrial dynamics, which we underscore as possible but discuss the limits for inference in this regard. Lastly, we explored how a single modeled process (land use and land cover change; LUC) manifests in the different signal characteristics and biases in Rise and Fall segments. We offer discussion on how the segment-based model biases and emergent patterns in satellite-derived seasonal cycles can be used to guide future inquiry and model development.

## 2. Methods

### 2.1 Satellite $XCO_2$ data

Satellite observations of $XCO_2$ were obtained from the Greenhouse gases Observing SATellite (GOSAT; version 7.3). Onboard the satellite, a Fourier-transform spectrometer measures the thermal and near-infrared absorption spectra of the constituent atmospheric gases within the footprint of observation (~10 km). Satellite data was freely obtained and analyzed only for 2009-2012 because it corresponded to the overlapping timeframe of available simulation data. The data were downloaded from NASA Goddard Earth Sciences (GES) Data and Information Services Center (DISC) online repository (<https://oco2.gesdisc.eosdis.nasa.gov/data/GOSAT_TANSO_Level2/ACOS_L2_Lite_FP.7.3/>; accessed 25 April 2018). We used the Level-2 *Lite* data products, which include only high-quality and bias-adjusted data points, based on the Atmospheric $CO_2$ Observations from Space (ACOS) retrieval algorithm version 7.3 (Crisp et al., 2012; O'Dell et al., 2012).

A note that satellite data have uncertainties of their own based on instrument noise, version of retrieval algorithm used to filter atmospheric effects, and averaging kernels (Yoshida et al., 2011; Lindqvist et al., 2015). We made the assumption that averaging kernel has a minimal effect on extracted seasonal cycles and we did not apply averaging kernels to the simulation data in this study. A full quantification of uncertainty in satellite-derived seasonal cycles is beyond the scope of this study, but such an analysis could be useful for benchmarking purposes as models continue to reduce large biases (>>

1.0 ppm). Nevertheless, we make the assumption that lower biases are generally indicative of better model performance.

### 2.2 Simulated Terrestrial Fluxes from DGVMs

The Net Biome Exchange (NBP) from land-to-atmosphere was simulated by six terrestrial ecosystem models (Table 3.1) that were part of the TRENDY model inter-comparison project version 2 (Sitch et al., 2015; dgvm.ceh.ac.uk). We use the atmospheric convention and make fluxes to the atmosphere positive, and fluxes to the land negative. We assumed that the primary modes of seasonal variability in terrestrial NBP at large scales is described by three terms, Net Ecosystem Production (Net Primary Production – Heterotrophic Respiration), fluxes from fire, and land use change (LUC). The protocol for the DGVM inter-comparison standardized the (i) forcing data: gridded (0.5°) climate (air temperature, short- and long-wave radiation, cloud cover, relative humidity and precipitation), global annual mean $CO_2$; and the (ii) initial conditions for time-varying simulations for the past century (1860-2012). We used simulated NBP for two sets of model simulations, one where land use (natural vegetation, crop, and pasture fractional cover) is fixed at values from the year 1860 (‘S2’ scenario described *in* Sitch et al., 2015), and another simulation where land use change is simulated according to the HistorY Database of the global Environment (HYDE v3.1; Goldewijk et al., 2011) (‘S3’ scenario as described *in* Sitch et al., 2015); both simulation types were forced with time-varying climate and $CO_2$.

### 2.3 Fossil Fuel and Ocean Fluxes

The modes of variability (trend, seasonality, intra- and inter-annual variability) in $XCO_2$ are also influenced by fluxes from oceanic exchange, fossil fuel consumption and cement production. We used a simplified model of oceanic $CO_2$ exchanges from Takahashi et al. (2009), and monthly-mean fossil fuel emissions from the European Commission's Emissions Database for Global Atmospheric Research (EDGAR v. 4.2), based on country-level reporting and emissions factors, and the Fossil Fuel Data Assimilation System (http://edgar.jrc.ec.europa.eu/).

### 2.4 Simulated $XCO_2$ using an Atmospheric Model

Simulations of atmospheric $CO_2$ were conducted for the period of 2009-2012 using the land, ocean, and fossil fuel fluxes. We used the Center for Climate Systems Research/National Institute for Environmental Studies/Frontier Research Center for Global Change (CCSR/NIES/FRCGC) AGCM-based chemistry transport model (ACTM) (Patra et al., 2009). The ACTM was run at a horizontal resolution of T106 (~1.125° X 1.125°), and 32 sigma-pressure vertical levels. The simulated $XCO_2$ values were obtained by taking the sum of the pressure-weighted $CO_2$ concentrations over all vertical layers, equivalent to the column-averaged observations. We then used 'co-location' sampling of the ACTM $XCO_2$ data to match the location and timeframe (13:00 hr local time) of observations, ± 5 days to account for (i.e., by averaging) sub-weekly transport errors (Guerlet et al., 2013). We obtained the simulated $XCO_2$ for each component flux (land, fossil fuel, ocean) and finally summed the components to get the $XCO_2$ used in bias evaluations.

**2.5 Extraction of $XCO_2$ Seasonal Cycles**

We first estimated the mean of daily $XCO_2$ values by averaging gridded values within each of the 11 TransCom region (Fig. 2), for both the observed and modeled $XCO_2$. This procedure was as straight forward as written above, and the accompanying computer code (software: R for Statistical Computing) is provided as additional Supplementary Material. We then applied a digital filtering algorithm (*ccgcrv* by Thoning et al., 1989; https://www.esrl.noaa.gov/gmd/ccgg/mbl/crvfit/crvfit.html) to the mean time series to extract the long-term trend and seasonal cycles, fitted as a 2-term polynomial (linear growth rate was used because the time series spanned only 3 years) and a 4-term harmonic function to account to seasonal asymmetry. Temporal data gaps were linearly interpolated by the algorithm. After subtracting the long-term trend and seasonal cycle, the *ccgcrv* algorithm filters the residuals in the frequency domain using a Fast-Fourier Transform (FFT) algorithm to retain short- and long-term interannual variation (additional details in Nakazawa et al., 1997; Pickers and Manning 2015). The cutoff for the short-term filter was set at the recommended value of 80 days (Thoning et al., 1989). The short-term cutoff of 80-days retains data variations that are evident, or maintained, for the time scale of 3-4 months (4.56 cycles/yr). The cutoff for the long-term filter was set to a large number (3000), which is longer than the number of days in our time series (365 days/yr * 3 yr= 1095 days) because, with such a short time series, we needed to force the estimation of a linear trend with no interannual variation; otherwise, the algorithm would be too sensitive and derive variation in the trend without practical justification. For all analyses here forth, we combined the seasonal cycle with the digitally filtered short-term variation and used the derived data points along the smoothed seasonal cycle curves for analysis.

### 2.6 Technical description of algorithm: Segmentation of seasonal cycles

The purpose of this section is to describe the technical algorithms used in the analysis. These algorithms are based on concepts put forth by Ehret and Zehe (2011), translated herein to the R computing language (R Development Core Team, 2008). Where Ehret and Zehe (2011) focused on the single hydrological events, we modify and restructure the algorithm to accommodate much longer non-stationary cyclic time series for general application to seasonal cycle analyses. An R package for the segmentation algorithm is freely available at the GitHub repository <https://github.com/lcalle/segmentTS>. A permanent version of the code is available in the Dryad Digital Repository <doi:10.5061/dryad.vk8ms62>. The computer code is annotated and provides data used in this study with demonstrations for applying the algorithm to remove local minima or maxima and the categorization of seasonal cycle segments.

#### 2.6.1 Categorize segments and isolate seasonal Rise and Fall cycles

We first determine the first derivatives numerically. The *ccgcrv* signal decomposition algorithm outputs a daily time series in the form of a multi-dimensional array, but we focus on a subset of the array, the 2-dimensional rectangular matrix representing points along the detrended seasonal cycle,

$$\boldsymbol{B} = \begin{bmatrix} b_{1,1} & b_{1,2} & b_{1,3} \\ \vdots & \vdots & \vdots \\ b_{n,1} & b_{n,2} & b_{n,3} \end{bmatrix} \tag{1}$$

, where the first column is the row index, the second column are dates, the third column is the detrended $XCO_2$ ppm with the short-term variation added back-in, the rows are the triplets of the index, time in the x-direction, and magnitude ($XCO_2$ ppm) in the y-direction.

We can numerically determine the first derivative in the y-direction at each point via differencing, as in,

$$\nabla b_{i,2} = b_{i,2} - b_{i-1,2} \tag{2}$$

We then classifying each row in first column ($b_{i,2}$ ... $b_{n,2}$) into one of the following categories below and expand **B** to a $n$ X 4 matrix to store the classified values. The main objective is to classify the endpoints (Trough, Peak) of the Rise and Fall segments:

$$\forall \mathrm{i} \in \{1 \dots n\},\ \mathbf{b}_{\boldsymbol{i},\mathbf{4}} = \begin{cases} Trough, & (\nabla\, b_{i,2} < 0) \wedge (\nabla\, b_{i+1,2} > 0) \\ Rise, & (\nabla\, b_{i,2} < 0) \wedge (\nabla\, b_{i+1,2} < 0) \\ Fall, & (\nabla\, b_{i,2} > 0) \wedge (\nabla\, b_{i+1,2} > 0) \\ Peak, & (\nabla\, b_{i,2} > 0) \wedge (\nabla\, b_{i+1,2} < 0) \\ Null, & otherwise \end{cases} \tag{3}$$

We then take the subset of endpoints ($S$) in the classified matrix **B**,

$$S \subset \mathbf{B} = \{\mathbf{B} \mid \mathbf{b}_{i,3}: Trough, Peak \tag{4}$$

, where $S$ retains the dimensions of the **B**. A unique segment ($s$) is defined as a set of two consecutive endpoints (rows) in $S$ that alternate in their classification of Trough or Peak, meeting the condition:

$$s \subset S = \{S \mid (S_{i,4}: Trough \wedge S_{i+1,4}: Peak) \vee (S_i: Peak \wedge S_{i+1,4}: Trough) \tag{5}$$

We identify local minima and maxima that are deviations in otherwise longer (seasonal) and more general Rise and Fall patterns based on two criteria below, and then reclassify the segments based on the class of the segment with the largest amplitude. The

amplitude of a segment ($a_s$) is defined as:

$$a_s = |s_{1,2} - s_{2,2}| \tag{6}$$

, where $s_{1,2}$ is the first endpoint in the second column ($XCO_2$ ppm), either a Trough or a Peak, and $s_{2,2}$ is the second endpoint for the specific segment, which, by definition the first endpoint must be classified ($s_{1,4}$) as one of Peak or Trough and must not have the same classification as the second endpoint ($s_{2,4}$).

The first criterion sets a minimum threshold for the amplitudes, redefining the set of endpoints defining the segments, as below:

$$s^* \subset s = \{s \mid a_s > \ minimum\ threshold \tag{7}$$

Segments that represent local minima or maxima that are not of interest to the user can be identified by a comparison of amplitudes of consecutive segments, dropping the segment with the lowest amplitude, as below:

$$s^{*\prime} \subset s^* = \{s^* \mid s^* \neq min(a_{s-1}, a_s, a_{s+1}) \tag{8}$$

This procedure results in a new subset of segment endpoints ($s^{*\prime}$) with consecutive elements that have similar classification (e.g., $s^{*\prime}_{1,4} \coloneqq Peak,$ and also, $s^{*\prime}_{2,4} \coloneqq Peak$), which needs to be rectified. We keep the endpoints with the lowest *Trough* value and the largest *Peak* value,

$$s[t]^* \subset \begin{Bmatrix} s[t]_{1,2} & s[t+1]_{1,2} \\ s[t]_{2,2} & s[t+1]_{2,2} \end{Bmatrix} =$$

$$\left\{ \begin{array}{l} s[t]^*_{1,2} = \begin{cases} min\big(s[t]_{1,2},\ s[t+1]_{1,2}\big), & s[t]_{1,4} \coloneqq Trough \wedge s[t+1]_{1,4} \coloneqq Trough \\ max\big(s[t]_{1,2},\ s[t+1]_{1,2}\big), & s[t]_{1,4} \coloneqq Peak \quad \wedge s[t+1]_{1,4} \coloneqq Peak \end{cases} \\ s[t]^*_{2,2} = \begin{cases} min\big(s[t]_{2,2},\ s[t+1]_{2,2}\big), & s[t]_{2,4} \coloneqq Trough \wedge s[t+1]_{2,4} \coloneqq Trough \\ max\big(s[t]_{2,2},\ s[t+1]_{2,2}\big), & s[t]_{2,4} \coloneqq Peak \quad \wedge s[t+1]_{2,4} \coloneqq Peak \end{cases} \end{array} \right\} \tag{9}$$

, where $s[t]$ is a unique segment in the set of *s* segments, $s[t+1]$ is the following consecutive segment, $s[.]_{1,2}$ and $s[.]_{2,2}$ are the segment first and last endpoints, respectively, and $s[t]^*$ is the updated segment with new endpoints $s[t]^*_{1,2}$ and $s[t]^*_{2,2}$, while segments $s[t], s[t+1]$ have been removed from the set of segments (*s*).

A (subjective) limit can also be set to exclude or include segments based on temporal proximity. For example, consecutive minima (*minima*/maxima/*minima*) should not be considered local minima if separated by 365 days; these are probably real local minima driven by processes unique to different seasons. By contrast, local minima separated by 60 days may represent signals within the overall seasonal Rise and Fall pattern (e.g., due to fire). For this study, we are more interested in assessing the general seasonal patterns. We therefore estimate the temporal distance, in 'days' ($D_s$), between the first endpoints of consecutive segments and evaluate the condition as below,

$$D_s = s[t+1]_{1,3} - s[t]_{1,3}\text{, given } s[t]_{1,4} \wedge s[t]_{1,4} \text{ are of the same class } (Trough, Peak) \tag{10}$$

$$s^* \subset s = \{s \mid D_s > \ minimum\ threshold \tag{11}$$

, where $s[.]_{1,3}$ is the endpoint date in the x-direction, and the minimum threshold for distance between endpoints is set at a conservative 250 days (~8 months), ensuring that only the main Rise and Fall patterns within a given year are captured. This conditional evaluation also results in a new subset of segments ($s^*$) with consecutive elements with similar classification, as above, but Eq. 9 can be re-applied to select the endpoints which represent general Rise and Fall patterns.

Additional criteria can be applied to automate the removal of local minima/maxima that are not relevant to the user, but we caution that visual inspection of the signal is important to avoid unwanted reclassification of segments in the time series.

### 2.6.2 Human-assisted pattern recognition via visual inspection

The procedure outline in Sect. 2.6.1, above, is applied to both the reference (*R*) and modeled (*M*) seasonal cycle time series. In the best of cases, the procedure would result in matrices for *R* and *M*, each with an equal number segments and the same sequence of endpoint classes (*Trough, Peak, Trough, Peak, ...*). In practice, however, the number and sequence of segments in *M* will not always equal the number or sequence of segments in *R*. When variability in the modeled seasonal cycle results in many local minima/maxima, and therefore many short Rise/Fall segments, there can be a mismatch between the indices of segments, wherein smaller/shorter segments in *M* are matched to much larger/longer segments in *R*; this is simply an artefact from automation of the procedure outlined previously. Although we have implemented automated procedures in the algorithm that reconcile these types of mismatches, we found that it was considerably quicker to (*i*) conduct a 'blind' run of the algorithm on the data, (*ii*) visually inspect the automated graphical plots of the seasonal cycles for mis-matching segments (Supplementary Material Fig. S1), (*iii*) identify the index of the mis-matching endpoints in *M*, and then finally (*iv*) re-run the algorithm specifying the index of the endpoint in *M* for removal.

### 2.6.3 Segment signal characteristics and error statistics

The amplitude (Eq. 6) and period ($p$ in 'days') for all segments are first characterized, with the period defined as,

$$p_s = s_n - s_0 \tag{12}$$

, where $s_n$ and $s_0$ are the end and start dates of a segment, respectively. Then, for each segment in *M* and *R*, a complementary vector $Mx$ and $Rx$ is created in the x-direction with a fixed number of, and equally-spaced, dates,

$$x = (x_1 \ldots x_k) \tag{13}$$

Each element in $Mx$ corresponds, by index, to an element in $Rx$, such that a matching pair exists. Similarly, a complementary vector $My$ and $Ry$ is created in the y-directions, with the length of the vector matching the length of the vector in the x-directions (*k*). For each element in $My$ and $Ry$, we perform a linear interpolation of the values of $XCO_2$ ppm in **B** ($\mathbf{b}_{.,2}$) for the indices given by the dates in $Mx$ and $Rx$; fortunately, the linear interpolation is automated by the *approx* function in R, which makes this procedural step straightforward. The end result is, for every segment in *M* and *R,* four vectors of equal length in $Mx, My$ and $Rx, Ry$, with the timing of the data and values of $XCO_2$ ppm that follow the corresponding seasonal cycles in **B**.

We can then decompose the corresponding errors in phase and magnitude along the time series,

$$Timing\ error = Mx - Rx \tag{14}$$

$$Magnitude\ error = My - Ry \tag{15}$$

Although in this paper we focus only on errors in amplitude, period, and phasing of the segments, the time series of errors in timing and magnitude are an additional level of detail in the error structure that is evaluated by the segmentation algorithm.

**2.7 Statistical summaries**

For each of the Rise and Fall segments within a region, we summarized the characteristics by averaging the amplitude (ppm), period (days), and the phase, which we estimated in two ways based on the day of year for the first and last endpoint of the corresponding segment (DOYstart, DOYend, respectively). For model biases, we used the total sum of the component tracers (land + fossil fuel + ocean) and we summarized model biases as the region-average of segment-to-segment differences between model and observation. Although we aggregate the biases among segment types, and therefore lose information, we do this to demonstrate that there are distinct general patterns in the Rise and Fall segments, regardless of region. Of course, one might be more interested in one bioregion over another, and while this is indeed possible and suggested, such analysis is not the intent of this paper.

The latitudinal variation of amplitude and period length for Rise and Fall segments was evaluated by comparing the regionally-averaged metrics against the average latitude of each TransCom region. We sought to evaluate a model's ability to reproduce the north to south gradient in seasonal cycle characteristics. We also use data from in-situ [CO2] flask samples for 2005-2015 (NOAA/ESRL/GMD CCGG cooperative air sampling network; https://www.esrl.noaa.gov/gmd/ccgg/flask.php) as a check to evaluate latitudinal variations of surface site seasonal amplitudes. Surface sites were selected if they had a minimum of five years of data between 2005-2015, with at least one flask sample per month. The peak-trough amplitude was then taken from monthly averaged data. Linear correlations were deemed statistically significant at levels of p=0.05.

The amplitude and period length asymmetries between Rise and Fall segments were calculated as in the following example. Given a sequence of data with segments of type {*Fall_1*, *Rise_1*, *Fall_2*, *Rise_2*}, representing seasonal cycles over two years, three asymmetries in amplitude and period length would be calculated for the sequence of segments, as (*i*) Fall_1 - Rise_1, (*ii*) Fall_2 - Rise_1, and (*iii*) Fall_2 - Rise_2. The asymmetries are referenced to Fall segments such that, for example, negative asymmetries mean that the amplitude (or period length) is greater in the Rise segment. The reason we calculated asymmetries between segments immediately before and after the Fall segments is because we assumed that there is some degree of autocorrelation in the relational values that is both real and could provide useful information, but the underlying causal mechanisms are speculative at this point.

## 2.8 Application of approach

We applied the approach to evaluate the effect of LUC on $XCO_2$ by using the segment characteristics setting the 'S2' scenario as the reference time series and then following procedures outlined in Sect. 2.6 to match corresponding Rise and Fall segments in the S3 and S2 simulations. We then calculated the difference in the amplitude, period, and phase between matching segments, hereafter defined as the 'LUCeffect'. To evaluate the relative influence of the LUCeffect on changes in amplitude, period and phase, we transformed the LUCeffect to percentages by (a) dividing the LUCeffect in amplitude by region-specific average amplitudes, and (b) dividing the LUCeffect in the period length and phase (DOYstart, DOYend) by the region-specific average period lengths. We then pooled the absolute values of the standardized LUCeffects for all regions, by model; the absolute values of LUCeffect was used because we were more interested in any significant change, rather than a directional change in the metric values. We conducted an Analysis of Variance to test for significant differences among models and type of LUCeffect (amplitude, period, and phase), in terms of the percent LUCeffect, also setting significant differences at $p=0.05$. In this manner, we were able to determine the relative importance of LUCeffect by metric and compare amongst models.

# 3. Results

## 3.1 Satellite coverage and $XCO_2$ seasonal cycles

The satellite data coverage had sufficient temporal density to extract smooth seasonal cycles (Fig. 3), except during Boreal Winter at high latitudes (> 50˚ N) and during the wet-season in Tropical Asia where there was clear evidence of linear interpolation over large data gaps (Supplementary Material Fig. S2-S4). We had to exclude North America Boreal and South America Tropical regions from all analyses because the data were too sparse and seasonal cycles could not be derived. The mean number of satellite retrievals per day in 5° bins was greater than 1 when averaged over a season, but the spatial distribution of the retrievals by month (Supplementary Material Fig. S2-S4) showed that only portions of the TransCom regions were being represented with satellite observations. The lack of a complete representative sample of satellite observations in a region suggests that the derived seasonal cycle will be biased towards the $XCO_2$ observations in those sub-regions with greater coverage. We take this finding as a caveat, but also demonstrate below that the derived seasonal cycles are a good representation of the general seasonal dynamics in the data.

There were noticeable deviations (local minimums) from otherwise consistent Rise and Fall patterns during a season (for example in North Africa in Fig. 3). We compared the seasonal cycles derived from DGVM $XCO_2$ co-located with GOSAT retrievals against DGVM seasonal cycles using all simulated $XCO_2$ and complete coverage (no-colocation). For the single DGVM studied in this side analysis, the local deviations were still evident in the seasonal cycles that used data with complete coverage (Supplementary Material Fig. S5). We believe that these deviations are not artefacts of the spatial distribution of satellite retrievals, but instead are true patterns in the $XCO_2$ seasonal cycle. However, the co-location sampling did appear to have a greater effect on the amplitudes and periods in Southern Hemisphere regions, whereas the effect of co-location sampling was less influential in Northern Hemisphere regions.

The magnitude of the GOSAT seasonal cycle residual error, averaged over all regions, was 0.15 ± 1.02 ppm, which was not a small fraction relative to the average amplitudes when taking into account the standard deviation. However, the residuals, were normally and randomly distributed around zero (Supplementary Material Fig. S6), which we took to suggest that there was no systematic bias and that the daily spatial variation in data coverage averaged out, and what we derived was a realistic estimate of seasonal variation in $XCO_2$.

### 3.2 Latitudinal variation in $XCO_2$ seasonal cycle amplitudes

Seasonal amplitude varied predictably with latitude (Fig. 4). Latitude explained between 82-84% of the variation in seasonal amplitudes in GOSAT, with the range taken from linear models of Rise and Fall segments (Fig. 4). There was an increase in amplitude of 0.74 ± 0.13 ppm ($\mu \pm$ S.E.) for Rise Segments and 0.77 ± 0.13 ppm for Fall Segments for every 10 degrees of latitude for GOSAT. Whereas the $XCO_2$ amplitudes exhibited a linear relationship with latitude, in-situ flask samples of $CO_2$ exhibited a log-linear relationship with latitude (Fig. 5; $R^2 = 0.90$, d.f.=45, $p < 0.001$), which indicates larger amplitude gradients at higher than at lower latitudes. The difference results in a latitudinal range (Equator to 70˚N) in seasonal amplitude of ~7 ppm for $XCO_2$ (taken as 70˚ * [0.077 + 1.95*0.013], as the largest possible amplitude gradient in $XCO_2$; $\mu$ + 1.95*S.E.) and ~17 ppm for surface $CO_2$. The dampened gradient in $XCO_2$ amplitude suggests substantial north-south atmospheric mixing, which is consistent with a previous study on the meridional versus zonal contribution to $XCO_2$ via atmospheric transport (Keppel-Aleks et al., 2012). In addition, the in-situ sampling stations are located in such a way that they sample the 'background' atmosphere, which reduces the influence of local to regional terrestrial fluxes, and instead they provide seasonal cycles representative of hemispheric- and continental-scales. The contrast between the latitudinal gradient in amplitude between $XCO_2$ in this study and in-situ surface samples may therefore be even greater than reported here (Olsen and Randerson, 2004; Sweeney et al., 2015).

Only LPX was able to simulate the GOSAT-derived latitudinal gradient (slope) in amplitude, but even in this model, the magnitudes of the amplitudes were consistently lower than GOSAT by ~1.5 ppm (Fig. 4). ORCHIDEE simulated the latitudinal gradient in amplitude reasonably well and CLM simulated a marginally stronger north-south gradient, whereas the gradient was much weaker in two models (OCN, VISIT) and there was no statistically detectable amplitude gradient in LPJ. The evidently enhanced meridional mixing of total column $CO_2$ complicates an interpretation of the finding that most models simulated a weaker gradient in $XCO_2$ seasonal amplitude (Fig. 4). It makes it difficult to determine why models do not reproduce the latitudinal gradient in amplitude very well – for example, are the magnitudes of the fluxes in certain regions too low or too high, such that they offset the seasonal amplitudes in the region of interest after atmospheric transport? We offer suggestions in the Discussion that might help answer these questions.

### 3.3 Latitudinal variation in $XCO_2$ seasonal cycle period

The period lengths of GOSAT $XCO_2$ seasonal cycles also varied predictably with latitude (Fig. 5) and there was no significant difference in the magnitude of the latitudinal gradients between Rise and Fall segments, although the direction of the gradient was positive for Rise segments and negative for Fall segments (Fig. 4). Latitude explained between 67-73% of the latitudinal variation in period lengths in GOSAT seasonal cycles. From South to North, the period lengths of Rise segments increased by 10 days per 10˚ of latitude for GOSAT. From South to North, the period lengths of Fall segments had negative gradient and decreased by -9 days/10˚ latitude for GOSAT. The opposite gradient in period lengths of Rise and Fall segments implies that around 2˚ N, the period of Rise and Fall segments of equal duration. North of this point of inversion in asymmetry, the period lengths of Rise segments are greater than in Fall segments, with an increasing asymmetry as latitude increases. We hypothesize that the latitude at the point of inversion of period asymmetry is a characteristic indicator global atmospheric dynamics and biosphere productivity. Our rationale is that if (i) the primary driver of the period of drawdown (Fall) or release (Rise) in $XCO_2$ seasonal cycles is the terrestrial biosphere, and (ii) DGVMs themselves simulate the terrestrial biosphere, then variation in the simulated point of inversion of asymmetry by different DGVMs suggests a strong influence of biosphere activity on this emergent pattern. The most obvious driver affecting the period being plant phenology. Furthermore, we already know that seasonal cycle in $XCO_2$ is dominated by flux seasonality in land biosphere, with the ocean and fossil fuel emission seasonality plays only a secondary role. Nevertheless, a north or south shift in the latitude of inversion (i.e., 2˚ N) would indicate that long-range transport of atmospheric signals, such as the poleward transport of southerly signals (Parazoo et al. 2016), has changed substantially. In which case, the relative contribution of long-range signals from southerly locations to seasonal cycle anomalies (in phase or amplitude) in northerly locations might be greater or less than expected. As of yet, however, it is unclear if this point of inversion is relatively stable over time or if, instead, the point shifts in latitude among years or decades depending on the relative influence of source-sink dynamics in biospheres in the Northern and Southern Hemispheres.

Most models correctly simulated the satellite-derived latitudinal gradient in period, but LPJ and VISIT did not simulate statistically significant gradients in either Rise or Fall segments, and LPX could only reproduce the gradient for Rise segments, but not for Fall segments (Fig. 4). For CLM, OCN and ORCHIDEE, the simulated gradients were statistically similar to GOSAT, although the absolute period lengths differed by up to 25 days. The latitudinal gradient in period of $XCO_2$ seasonal cycles is emergent from the underlying timing and duration of biosphere productivity, and as such, it serves as a high-level constraint on simulated dynamics. It may therefore be possible to add this emergent pattern as a benchmark to evaluate models that attempt to reproduce more direct indicators of biosphere activity, such as seasonal patterns in leaf area (Richardson et al., 2012), or primary production (Forkel et al., 2014).

### 3.4 GOSAT asymmetries in period and amplitude

The period asymmetry between Rise and Fall segments (Table 3.2) is clearer when comparing the periods of consecutive Rise and Fall segments (Fig. 6), taking the Fall segment as reference, as described in Sect. 2.7. The period asymmetries were in the same direction except for the Africa Northern, Africa Southern, and South America Temperate regions (Fig. 6A). The asymmetries exhibit stable patterns of consistent direction within many regions, and they also display quite a bit of interannual variation in the magnitude (or direction in some cases) of the asymmetries themselves (Fig. 6A and 6B). For example, the standard deviation in period asymmetry averaged 11% of the region-averaged periods for GOSAT seasonal cycles, and it was greatest for the Africa Southern region (42%). For context, a 10% change amounts to a change in period asymmetry by 5-29 days, and as much as 73 days in the Africa Southern regions, which is certainly a remarkable change in the atmospheric signal. The period asymmetries can provide insight into the underlying terrestrial dynamics, for example, from interannual variation in the duration of the carbon uptake period (Xia et al., 2015; Fu et al., 2017), but it is yet unclear how changes in carbon uptake period manifest to affect these patterns of asymmetry. Furthermore, one DGVM (ORCHIDEE) was able to simulate period asymmetries, consistent in direction, with that of the GOSAT record when using co-location sampling. Albeit, the magnitude of the period asymmetry for ORCHIDEE was about half that of GOSAT, but it does suggest that the surface fluxes from this DGVM were more realistic in timing and magnitude. All other models had greater interannual variation in the direction of the asymmetry, with no other model reproducing the direction of asymmetry in all regions.

The amplitude asymmetries between consecutive Rise and Fall segments were more variable in the direction of the asymmetry for GOSAT (Fig. 6B). There was no consistent pattern in the direction or magnitude of the amplitude asymmetries within or among regions, but we did not investigate if there were annual patterns that were consistent among all regions. No model successfully reproduced the direction of asymmetry in amplitude across all regions in all years. As of yet, the relevance of interannual variation in the asymmetries is speculative, but we do know that such variation is not simply due to data coverage (Supplementary Material Fig. S5), so there may be more insightful information in the signal.

### 3.5 Correlated biases between Rise and Fall segments

The correlations of model biases differed more among Northern and Southern Hemispheres (NH and SH, respectively) than among regions, so we present the following analyses not by region, but by NH and SH. The NH regions were comprised of Africa Northern, Europe, Eurasia Temperate, North America Temperate; the SH regions were comprised of Africa Southern, Australia, and South America Temperate. These analyses required data on both Rise and Fall segments, which eliminated the Asia Tropical and Eurasia Boreal regions from these analyses.

Among Rise and Fall segments, and among all models and regions, the model biases in amplitude were nearly perfectly correlated (NH $R^2 = 0.99$, d.f. = 28, t= 64.63, $p < 0.001$; SH $R^2 = 0.99$, d.f. = 16, t = 65.02, $p < 0.001$; Fig. 7a and 7e). Except for ORCHIDEE and CLM, which exhibited the smallest amplitude biases, the other models all had amplitudes that were too low. In the SH, there was a similar pattern of negative amplitude biases (Fig. 7e), with exception that CLM simulated amplitudes that were too large in two of three SH regions. The strong correlations suggest that knowing the amplitude biases in one part of the seasonal cycle is sufficient to gain information about amplitudes in the missing part of the seasonal cycle. This might be particularly useful for constraining estimates of $XCO_2$ seasonal cycle patterns during timeframes that have poor satellite coverage (Boreal Winter, Tropical Wet Season). Furthermore, it is revealing that models which simulate amplitudes that are too low do so almost equally for both Rise and Fall segments, which is suggestive of a systematic bias in the sensitivity of the models to seasonal changes in climate. Such systematic biases can be due to simulated fluxes that are overall lower in magnitude, or due to a pattern of spatio-temporal fluxes that end up offsetting or cancelling each other in the atmospheric domain, but we cannot yet definitively attribute the bias of individual models to one of these possible causes.

The average period biases of Rise and Fall segments were also strongly correlated, with a greater strength of correlation in the NH ($R^2 = 0.77$, d.f. = 22, t= -8.53, $p < 0.001$) than in the SH ($R^2 = 0.82$, d.f. = 21, t = -9.87, $p < 0.001$). In the NH, almost all models simulated periods that were too short in Rise segments and too long in Fall segments, in approximately equal and opposing amounts (Fig. 7b). In the SH, the period biases spanned both positive and negative values for both of the Fall and Rise segments, but also in approximately equal and opposing amounts of bias (Fig. 7f). There were only a few data points where the periods within a region were either biased (a) too short for Rise segments and also too short for Fall segments, or (b) where the Rise segment was biased too long and the Fall segment also biased too long. These patterns are suggestive of underlying constraints that compensate for biases in periods, such that situation (a) and (b), from above, rarely occur. Such constraints are likely associated with the underlying drivers of the period of Rise and Fall segments. For instance, models that simulate growing seasons that are too long will likely simulate Fall-segment periods that are also too long, and as a consequence, the dormant season will be shortened, as will the periods of associated Rise segments. Within a given model, the magnitude of compensating biases varied by region, so it is possible that biases in biosphere activity varied similarly by region. To incorporate such insights will require direct manipulation of the phenology represented by models, but improving the emergent patterns in period to better match the satellite-derived $XCO_2$ seasonal cycles will bolster confidence in the model's ability to represent both fine-scale dynamics and the emergent large-scale atmospheric patterns.

### 3.6 Application of Approach: LUCeffects on amplitude, period and phase metrics were non-trivial

We describe the LUCeffect as the percent change in the Rise and Fall segment amplitude, period, and phase (DOYstart, DOYend) when LUC processes are included in model simulations, relative to seasonal cycle metrics when LUC was not included in simulations. Among all models and Rise and Fall segments, the average LUCeffect was largest on amplitude (mean 13.4%, or 0.37 ppm), but there were also non-trivial changes in the period (7.2%, or 13.2 days), and phase metrics of the DOYend (6.5%, or 11.4 days) and DOYstart (6.2%, or 11.4 days). An Analysis of Variance suggested that the LUCeffects did not significantly differ between Rise and Fall segments ($F = 0.006$, d.f.=1, $p = 0.941$), and that the specific model explained 16% of the variation ($F = 15.183$, d.f.=5, $p < 0.001$) and the metric explained only 5% of the variation ($F = 7.815$, d.f.=3, $p < 0.001$). LPJ was an outlier in that it simulated larger LUCeffects in every metric (mean

LUCeffect=18%), approximately 8% greater than other models. The remaining variation in LUCeffect was explained by the larger LUCeffect on amplitude in LPX and VISIT (Fig. 8), whereas OCN simulated only marginally greater LUCeffects than CLM and ORCHIDEE. The LUCeffects were of similar magnitudes as the baseline interannual variation for these metrics, in terms of percent change, or greater in the case of the LUCeffect on amplitude (Table 3.3).

The importance of the LUCeffect on the amplitude of Rise and Fall segments was somewhat expected because LUC directly affects the type of land cover simulated in the models, for example, by converting forest to pasture or pasture to forest and thereby influencing the magnitude of surface fluxes directly (Arneth et al., 2017). However, the effect of LUC on the temporal metrics of the seasonal cycle (period, phase) is typically understated in the literature. The LUCeffects on period and phase are of the same relative magnitude as is observed in two-decades of advancement in the start and end dates of the carbon uptake period based on atmospheric inversion studies (Fu et al., 2017). It should not be a surprise then that LUC can affect the timing of surface fluxes, but this facet is often overlooked when the focus is solely on variability at annual or decadal timescales. At the very least, this work shows that land-surface modelers should consider the impact of LUC on the timing and duration of surface fluxes, in addition to its effect on the magnitude of the fluxes.

## 4. Discussion

### 4.1 Utility of a segment analysis for analyzing cyclic time series

We demonstrated that a segmentation analysis of satellite-derived $XCO_2$ seasonal cycles can generate direct estimates of amplitude, period, and phase at global and hemispheric scales, and that it can reveal stable patterns in the metrics which can be used as benchmarks to evaluate simulation models. There is obvious value in using standard statistics (RMSE, S.D., $R^2$, etc.) to characterize a time series and evaluate it against simulated reproductions (e.g., 'Taylor diagrams'; Taylor, 2001; Supplementary Fig. S7). We do this too, but we argue that applying statistical measures of goodness-of-fit over the entire time series misses an opportunity to extract valuable information from observational data and provide more direct measures of bias. Studies that have evaluated amplitude and period biases directly have been based on the mean harmonic of the seasonal cycle (Peng et al. 2015), which lacks interannual variation, and therefore does not fully represent the modeled biases. Furthermore, the metrics for the asymmetric Rise and Fall patterns in seasonal cycles are not typically estimated, nor evaluated for bias. In the Europe region, for example, the internanual variation in amplitude (1.25 ppm) and period (25 days) is certainly not trivial (Supplementary Fig. S8), and if excluded in evaluations it would cause a biased assessment of what the models can and cannot do well, limiting the potential of such assessments to inform potential improvements.

Our study focused on the Rise and Fall segments in $XCO_2$ seasonal cycles, corresponding to periods when terrestrial ecosystems generally release and uptake carbon dioxide, respectively. Other studies might be more interested in shorter-term, pulse-type signals, such as the ability of models to simulate the effect of large scale fires or volcano eruptions in an atmospheric time series. In either case, the segmentation algorithm could help standardize and decompose model bias into its component parts of amplitude, period and phase biases.

## 4.2 Asymmetries provide new insights into the interannual variation of atmospheric signals

By definition, the asymmetries (Fig. 6) are not anomalies, but similarly, the amplitude asymmetries are directly related to underlying processes generating the imbalance in the amplitude and period between Rise and Fall segments. Most likely, the asymmetries reflect the difference in the magnitude or in the timing of fluxes during the growing season for Fall segments and phenological dormancy for Rise segments (Randerson et al., 1997). Whereas the signature of the terrestrial biosphere may be a more dominant driver of the period asymmetries, the amplitude asymmetries may also be influenced by processes that the models simply do not simulate well, or in any sufficient manner in some cases, such as sub-seasonal representation of Fire and LUC (Earles et al., 2012) or volcano eruptions (Jones and Cox, 2001). The interannual variation in $XCO_2$ period and amplitude asymmetries are directly related the activity of terrestrial ecosystems, but questions remain – are the annual asymmetries in amplitudes or periods evident of a global response to large-scale climate phenomena, such as the El Niño-Southern Oscillation? Do some regions dominate and influence the signal more than others? To what degree do the asymmetries in one region provide information about asymmetries in other regions, and can we infer dynamics in Boreal regions, for example, by analyzing atmospheric signals in regions where satellite coverage is more complete? The asymmetries offer a new level of information on atmospheric dynamics that is ripe for exploring.

### 4.4 The effect of LUC on seasonal cycles is in addition to the effect on the long-term trend

Much focus has been put on accurately characterizing component fluxes from land use and land cover change simulated by DGVMs (Pongratz et al., 2014; Calle et al., 2016), but we also show that LUC influences the atmospheric seasonal cycle period and phase at a level that is comparable to the reference rates of interannual variation in those metrics (Table 3.3). This underscores a complex problem of trying to simultaneously resolve the contribution of LUC fluxes to the long-term trend in atmospheric $CO_2$ (Le Quéré et al., 2018), and also to represent realistic LUC effects on seasonal-scale biosphere activity (Betts et al., 2013; Bagley et al., 2014). For instance, when land is converted from forest to pasture, the dominant land cover will affect the duration and timing of the surface fluxes (Fleishcher et al., 2016) and this seems obvious on its own standing. However, DGVMs were not developed during the era of satellite $XCO_2$ observations, and so the main issue of trying to resolve the effect of large-scale changes in land use on both the long-term trend and seasonal cycle dynamics is not easily solved. But now that these data are available, perhaps a new approach is necessary to take advantage of these large-scale benchmarks.

The inclusion of LUC in the simulations, after including the contribution from fossil fuels and ocean, resulted in a combined long-term trend estimate which was too large, by 0.07 to 1.72 ppm yr $^{-1}$, compared to the long-term trend of GOSAT $XCO_2$ (2.16 ± 0.01 ppm yr $^{-1}$) (Supplementary Fig. S9). The GOSAT estimate is comparable to an independent estimate of the long-term trend of $XCO_2$ from SCIAMACHY for the 2000s (1.95 ± 0.05 ppm yr $^{-1}$; Schneising et al., 2014). If we assume that this study's simulated long-term trends of fossil fuel fluxes (4.44 ± 0.008 ppm yr $^{-1}$) and those of the ocean (-0.66 ± 0.0006 ppm yr $^{-1}$) are better constrained than the trends from the land fluxes, then according to the GOSAT benchmark, the simulated land sink is too weak. Despite the posibility that these simulated LUC fluxes are too high, the DGVM versions applied in this study do not simulate a suite of land management processes (shifting cultivation, wood harvesting, pasture harvest, agriculture mgmt.) that have been shown to increase the annual LUC flux by 20-60% (Arneth et al., 2017), further pointing to a simulated land sink that is too weak. DGVM-based estimates of the terrestrial land sink have been compared against a residual term in the global carbon budget that is taken as the average flux over a decade (Le Quéré et al., 2018), but perhaps we are overlooking something here. The cumulative fluxes simulated by the models in this study (from 2002-2012) resulted in a long-term trend that is at odds with the satellite record, and it is unclear why. We must therefore attempt to reconcile biases in both the long-term trend and seasonal cycle dynamics if we are to use $XCO_2$, or other integrated atmospheric measurements to constrain model dynamics, and not simply assess these patterns independently.

### 4.5 Caveats, limitations and ways forward

The $XCO_2$ gradient in amplitude is approximately half the gradient in amplitude of in-situ surface $CO_2$. The dampened $XCO_2$ gradient suggests the presence of strong meridional mixing, which complicates accurate attribution of model biases to any specific bioregion. In effect, the $XCO_2$ seasonal cycle is comprised of the fluxes from all regions to varying degrees (Olsen and Randerson, 2004; Sweeney et al., 2015; Lan et al., 2017). Given this, simulating the atmospheric transport of the surface fluxes from all regions at once would allow us to both, (a) obtain useable estimates of model bias and (b) to provide attribution to those biases. Indeed, the model biases were fully described, but only in terms of $XCO_2$, not in terms of terrestrial surface fluxes themselves. An approach for attribution of model bias in $XCO_2$ might be laid out similar to Liptak et al. (2017), wherein the surface fluxes from each region (by year) undergo independent atmospheric transport. In a framework similar to this study, such simulations might prove instrumental in determining the fractional contribution of each region's fluxes the $XCO_2$ seasonal cycle characteristics while also providing better guidance for model development.

Model evaluations also showed that few models have low bias in all seasonal cycle metrics of amplitude, period, and phasing of simulated $XCO_2$. An inherent requirement for reproducing the $XCO_2$ signal is that the land-to-atmosphere fluxes are reasonable in magnitude, duration and timing *in all land regions*, or at the very least, in land regions with large vegetative areas that might disproportionately dominate the signal. Even though such requirement may be necessary to simulate the amplitude asymmetries, this is an extreme level of proficiency that, simply, the models do not currently exhibit.

Lastly, the relative contribution of land, ocean and fossil fuel fluxes to the seasonal cycle differs by region, latitude, and time period (Randerson et al., 1997). This poses some concern because fossil fuel and cement fluxes are considered to have low uncertainty, but they may be biased too high in some regions (Saeki and Patra 2017), affecting our interpretation of the contribution of simulated land fluxes to the seasonal cycle amplitudes, especially if the fossil fuel seasonal cycle signal is additive to (or offsets) the signal from the land fluxes. Other land uncertainties were not addressed in this study as it was not our intent to determine which DGVM had zero bias. Instead, we sought to extract unique patterns in the observed signals so that they may inform model development and subsequent evaluations in the future. Model improvements in their representation of important land processes such as forest demography, wetland and permafrost dynamics, agriculture and land management, and a greater diversity of functional plant diversity are all on the horizon (Pugh et al., 2016; Fisher et al., 2018) and may further improve simulated atmospheric signals. The patterns in $XCO_2$ seasonal cycles are emergent from surface fluxes over the globe, and we foresee that a segment-based analysis of atmospheric seasonal cycles as a way to extract emergent patterns in the reference data to help guide future development and an improved understanding of the terrestrial biosphere.

**Acknowledgements**

We thank Ehret and Zehe (2011) for their initial foray into alternative approaches to automate pattern matching in time series, which inspired this study. We thank the TRENDY Version 2 DGVM modelling community for their extensive efforts in continuing to advance model representation and making simulation data freely available. We acknowledge the developers at NOAA ESRL that have maintained the C program of the ccgcrv algorithm and made it freely available. LC was supported by a National

Aeronautics and Space Administration Earth and Space Science Fellowship (NASA ESSF 2016-2019). PKP acknowledges support from the Tougou (Theme B) project of the Ministry of Education, Culture, Sports, Science and Technology.

**Author Contribution**

LC, BP, and PKP conceived of the study. PKP conducted the atmospheric simulations. LC prepared and analyzed simulated and satellite data. LC developed the code for the segmentation algorithm. LC prepared the manuscript with contributions from all co-authors.

**Data Availability**

Data used in the analysis and code for the segmentation algorithm is freely-available from the GitHub repository <https://github.com/lcalle/segmentTS>. The permanent version of the algorithm is archived and freely available at the Dryad Digital Repository < doi:10.5061/dryad.vk8ms62>.

**References**

Anav, A., Friedlingstein, P., Beer, C., Ciais, P., Harper, A., Jones, C., Murray-Tortarolo, G., Papale, D., Parazoo, N. C., Peylin, P., Piao, S., Sitch, S., Viovy, N., Wiltshire, A., & Zhao, M.: Spatiotemporal patterns of terrestrial gross primary production – a review. Reviews of Geophysics, 53, 785-818. doi:10.1002/2015RG000483, 2015.

Arneth, A., Sitch, S., J. Pongratz, Stocker, B. D., Ciais, P., Poulter, B., Bayer, A. D., Bondeau, A., Calle, L., Chini, L. P., Gasser, T., Fader, M., Friedlingstein, P., Kato, E., Li, W., Lindeskog, M., Nabel, J. E. M. S., Pugh, T. A. M., Robertson, E., Viovy, N., Yue, C., & Zaehle, S.: Historical carbon dioxide emissions caused by land-use changes are possibly larger than assumed. Nature Geoscience, 10. doi:10.1038/NGEO2882, 2017.

Bagley, J. E., Desai, A. R., Harding, K. J., Snyder, P. K. & Foley, J. A.: Drought and deforestation – Has land cover change influence recent precipitation extremes in the Amazon? Journal of Climate 27:345-361, doi:10.1175/JCLI-D-12-00369.1, 2014.

Belikov, D. A., Maksyutov, S., Ganshin, A., Zhuravlev, R., Deutscher, N. M., Wunch, D., Feist, D. G., Morino, I., Parker, R. J., Strong, K., Yoshida, Y., Bril, A., Oshchepkov, S., Boesch, H., Dubey, M. K., Griffith, D., Hewson, W., Kivi, R., Mendonca, J., Notholt, J., Schneider, M., Sussmann, R., Velazco, V. A. & Aoki, S.: Study of the footprints of short-term variation in $XCO_2$ observed by TCCON sites using NIES and FLEXPART atmospheric transport models. Atmospheric Chemistry and Physics 17:143-157, doi:10.5194/acp-17-143-2017.

Betts, A. K., Desjardins, R., Worth, D. & Cerkowniak, D.: Impact of land use change on the diurnal cycle climate of the Canadian Prairies. Journal of Geophysical Research – Atmospheres 188(11):996-12011, doi:10.1002/2013JD020717, 2013.

Bonan, G. B.: Forests and climate change – forcings, feedbacks, and the climate benefits of forests. Science, 320, 1444. doi:10.1126/science.1155121, 2008.

Calle, L., Canadell, J. G., Patra, P. K., Ciais, P., Ichii, K., Tian, H., Kondo, M., Piao, S., Arneth, A., Harper, A. B., Ito, A., Kato, E., Koven, C., Sitch, S., Stocker, B. D., Vivoy, N., Wiltshire, A., Zaehle, S., and Poulter, B.: Regional carbon fluxes from land use and land cover change in Asia, 1980-2009. Environmental Research Letters 11:074011, 2016.

Ciais, P., Dolman, A. J., Bombelli, A., Duren, R., Peregon, A., Rayner, P. J., Miller, C., Gobron, N., Kinderman, G., Marland, G., Gruber, N., Chevallier, F., Andres, R. J., Balsamo, G., Bopp, L., Bréon, F.-M., Broquet, G., Dargaville, R., Battin, T. J., Borges, A., Bovensmann, H., Buchwitz, M., Butler, J., Canadell, J. G., Cook, R. B., DeFries, R., Engelen, R., Gurney, K. R., Heinze, C., Heimann, M., Held, A., Henry, M., Law, B., Luyssaert, S., Miller, J., Moriyama, T., Moulin, C., Myneni, R. B., Nussli, C., Obersteiner, M., Ojima, D., Pan, Y., Paris, J.-D., Piao, S. L., Poulter, B., Plummer, S., Quegan, S., Raymond, P., Reichstein, M., Rivier, L., Sabine, C., Schimel, D., Tarasova, O., Valentini, R., Wang, R., van der Werf, G., Wickland, D., Williams, M. & Zehner, C.: Current systematic carbon-cycle observations and the need for implementing a policy-relevant carbon observing system. Biogeosciences, 11, 3547-3602, doi:10.5194/bg-11-3547-2014, 2015.

Crisp, D., Fisher, B. M., O'Dell, C. O., Frankenberg, C., Basilio, R., Bösch, H., Brown, L. R., Castano, R., Conner, B., Deutscher, N. M., Eldering, A., Griffith, D., Gunson, M., Kuze, A., Mandrake, L., McDuffie, J., Messerschmidt, J., Miller, C. E., Morino, I., Natraj, V., Notholt, J., O'Brien, D. M., Oyafuso, F., Polonsky, I., Robinson, J., Salawitch, R., Sherlock, V., Smyth, M., Suto, H., Taylor, T. E., Thompson, D. R., Wennberg, P. O., Wunch, D., & Yung, Y. L.: The ACOS $CO_2$ retrieval algorithm – Part II – Global $XCO_2$ data characterization. Atmospheric Measurement Techniques, 5, 687-707. doi:10.5194/amt-5-687-2012, 2012.

Earles, J. M., Yeh, S. & Skog, K. E.: Timing of carbon emissions from global forest clearance. Nature Climate Change 2:682-685, doi:10.1038/NCLIMATE1535, 2012.

Ehret, U., & Zehe, E.: Series distance – an intuitive metric to quantify hydrograph similarity in terms of occurrence, amplitude and timing of hydrological events. Hydrology and Earth Systems Science, 15, 877-896. doi:10.5194/hess-15-877-2011, 2011.

Fisher, R. A., Koven, C. D., Anderegg, W. R. L., Christoffersen, B. O., Dietze, M. C., Farrior, C. E., Holm, J. A., Hurtt, G. C., Knox, R. G., Lawrence, P. J., Lichstein, J. W., Longo, M., Matheny, A. M., Medvigy, D., Muller-Landau, H. C., Powell, T. L., Serbin, S. P., Sato, H., Shuman, J. K., Smith, B., Trugman, A. T., Viskari, T., Verbeeck, H., Wang, E., Xu, C., Xu, X., Zhang, T., Moorcroft, P. R.: Vegetation demographics in Earth System Models – A review of progress and priorities. Global Change Biology 24:35-54, doi:10.1111/gcb.13910, 2018.

Fleishcher, E., Khashimov, I., Hölzel, N. & Klemm, O.: Carbon exchange fluxes over peatlands in Western Siberia – possible feedback between land-use change and climate change. Science of the Total Environment, doi:10.1016/j.scitotenv.2015.12.073, 2016.

Forkel, M., Carvalhais, N., Schaphoff, S., Bloh, W. v., Migliavacca, M., Thurner, M., & Thonicke, K.: Identifying environmental controls on vegetation greenness phenology through model-data integration. Biogeosciences, 11, 7025-7050. doi:10.5194/bg-11-7025-2014, 2014.

Fu, Z., Dong, J., Zhou, Y., Stoy, P. C. & Niu, S.: Long term trend and interannual variability of land carbon uptake – the attribution and processes. Environmental Research Letters 12: 014018, doi:10.1088/1748-9326/aa5685, 2017.

Glecker, P. J., Taylor, K. E., & Doutriaux, C.: Performance metrics for climate models. Journal of Geophysical Research - Atmospheres, 113, D06104. doi:10.1029/2007/JD008972, 2008.

Goldewijk, K. K., Beusen, A., van Drecht, G., & de Vos, M.: The HYDE 3.1 spatially explicit database of human-induced global land-use change over the past 12,000 years. Global Ecology and Biogeography., 20, 73-86. doi:10.1111/j.1466-8238.2010.00587.x, 2011.

Guerlet, S., Butz, A., Schepers, D., Basu, S., Hasekamp, O. P., Kuze, A., Yokota, T., Blavier, J. F., Deutscher, N. M., Grif- fith, D. W. T., Hase, F., Kyro, E., Morino, I., Sherlock, V., Suss- mann, R., Galli, A., and Aben, I.: Impact of aerosol and thin cirrus on retrieving and validating $XCO_2$ from GOSAT shortwave infrared measurements. Journal Geophysical Research - Atmospheres, 118, 4887– 4905, doi:10.1002/jgrd.50332, 2013.

Hammerling, D. M., Kawa, S. R., Schaefer, K., Doney, S. & Michalak, A. M.: Detectability of $CO_2$ flux signals by a space-based lidar mission. Journal of Geophysical Research – Atmospheres 120, 1794–1807, doi:10.1002/ 2014JD022483, 2015.

Jones, C. D. & Cox, P. M.: Modeling the volcanic signal in the atmospheric $CO_2$ record. Global Biogeochemical Cycles 15(2):452-465, 2001.

Kato, E., Kinoshita, T., Ito, A., Kawamiya, M., & Yamagata, Y.: Evaluation of spatially explicit emission scenario of land-use change and biomass burning using a process-based biogeochemical model. Journal of Land Use Science, 8:1, 104-122. doi:10.1080/1747423X.2011.628705, 2013.

Keeling, C. D., Whorf, T. P., Wahlen, M., & van der Plicht, J.: Interannual extremes in the rate of rise of atmospheric carbon dioxide since 1980. Nature, 375, 666-670, 1995.

Krinner, G., Viovy, N., de Noblet-Ducoudré, N., Ogeé, J., Polcher, J., Friedlingstein, P., Ciais, P., Sitch, S., & Prentice, I. C.: A dynamic global vegetation model for studies of the coupled atmosphere–biosphere system. Global Biogeochemical Cycles, 19, GB1015. doi:10.1029/2003GB002199, 2005.

Lawrence, D. M., Oleson, K. W., Flanner, M. G., Thornton, P. E., Swenson, S. C., Lawrence, P. J., Zeng, X., Yang, Z. L., Levis, S., Sakaguchi, K., Bonan, G. B., & Slater, A. G.: Parameterization improvements and functional and structural advances in version 4 of the Community Land Model. Journal of Advances in Modeling Earth Systems, 3, M03001. doi:10.1029/2011MS000045, 2011.

Le Quéré, C., Andrew, R. M., Friedlingstein, P., Sitch, S., Pongratz, J., Manning, A. C., Korsbakken, J. I., Peters, G. P., Canadell, J. G., Jackson, R. B., Boden, T. A., Tans, P. P., Andrews, O. D., Arora, V. K., Bakker, D. C. E., Barbero, L., Becker, M., Betts, R. A., Bopp, L., Chevallier, F., Chini, L. P., Ciais, P., Cosca, C. E., Cross, J., Currie, K., Gasser, T., Harris, I., Hauck, J., Haverd, V., Houghton, R. A., Hunt, C. W., Hurtt, G. C., Ilyina, T., Jain, A. K., Kato, E., Kautz, M., Keeling, R. F., Goldewijk, K. K., Körtzinger, Landschützer, P., Lefèvre, N., Lenton, A., Lienert, S., Lima, I., Lombardozzi, D., Metzl, N., Millero, F., Monteiro, P. M. S., Munro, D. R., Nabel, J. E. M. S., Nakaoka, S., Nojiri, Y., Padin, X. A., Peregon, A., Pfeil, B., Pierrot, D., Poulter, B., Rehder, G., Reimer, J., Rödenbeck, C., Schwinger, J., Séférian, R., Skjelvan, I., Stocker, B. D., Tian, H., Tilbrook, B., Tubiello, F. N., van der Laan-Luijkx, I. T., van der Werf, G. R., van Heuven, S., Viovy, N., Vuichard, N., Walker, A. P., Watson, A. J., Wiltshire, A. J., Zaehle, S. & Zhu, D.: Global Carbon Budget, Earth System Science Data, 10, 405-448, doi:10.5194/essd-10-405-2018, 2018.

Lindqvist, H., O'Dell, C. W., Basu, S., Boesch, H., Chevallier, F., Deutscher, N., Feng, L., Fisher, B., Hase, F., Inoue, M., Kivi, R., Morino, I., Palmer, P. I., Parker, R., Schneider, M., Sussmann, R., and Yoshida, Y.: Does GOSAT capture the true seasonal cycle of carbon dioxide?, Atmospheric Chemistry and Physics, 15, 13023–13040, https://doi.org/10.5194/acp-15-13023-2015, 2015.

Liptak, J., Keppel-Aleks, G. & Lindsay, K.: Drivers of multi-century trends in the atmospheric $CO_2$ mean annual cycle in a prognostic ESM. Biogeosciences 14:1383-1401, doi:10.5194/bg-14-1383-2017, 2017.

Nakazawa, T., Ishizawa, M., Higuchi, K., & Trivett, N. B. A.: Two curve fitting methods applied to CO2 flask data. Environmetrics, 8, 197-218, 1997.

O'Dell, C. W., Conner, B., Bösch, H., O'Brien, D. O., Frankenberg, C., Castano, R., Christi, M., Crisp, D., Eldering, A., Fisher, B., Gunson, M., McDuffie, J., Miller, C. E., Natraj, V., Oyafuso, F., Polonsky, I., Smyth, M., Taylor, T., Toon, G. C., Wennberg, P. O., & Wunch, D.: The ACOS $CO_2$ retrieval algorithm – Part 1 – Description and validation against synthetic observations. Atmospheric Measurement Techniques, 5, 99-121. doi:10.5194/amt-5-99-2012, 2012.

Olsen, S. C. & Randerson, J. T. Differences between surface and column atmospheric $CO_2$ and implications for carbon cycle research. Journal of Geophysical Research 109:D02301, doi:10.1029/2003JD003968, 2004.

Parazoo, N. C., Commane, R., Wofsy, S. C., Koven, C. D., Sweeney, C., Lawrence, D. M., Lindaas, J., Chang, R. Y.-W., & Miller C. E.: Detecting regional patterns of changing $CO_2$ flux in Alaska. Proceedings of the National Academies of Science of the United States of America, 113, 7733-7738, doi:10.1073/pnas.1601085113, 2016.

Patra, P. K., Takigawa, M., Dutton, G. S., Uhse, K., Ishijima, K., Lintner, B. R., Miyazaki, K., & Elkins, J. W.: Transport mechanisms for synoptic, seasonal and interannual SF6 variations and 'age' of air in troposphere. Atmospheric Chemistry and Physics, 9, 1209-1225, 2009.

Peng, S., Ciais, P., Chevallier, F., Peylin, P., Cadule, P., Sitch, S., Piao, S., Ahlström, A., Huntingford, C., Levy, P., Li, X., Liu, Y., Lomas, M., Pouler, B., Viovy, N., Wang, T., Wang, X., Zaehle, S., Zeng, N., Zhao, F., & Zhao, H.: Benchmarking the seasonal cycle of CO2 fluxes simulated by terrestrial ecosystem models. Global Biogeochemical Cycles, 29, 46-64. doi:10.1002/2014GB004931, 2015.

Pickers, P. A., & Manning, A. C.: Investigating bias in the application of curve fitting programs to atmospheric time series. Atmospheric Measurement Techniques, 8, 1469-1489. doi:10.5194/amt-8-1469-2015, 2015.

Pongratz, J., Reick, C. H., Houghton, R. A. & House, J. I.: Terminology as a key uncertainty in net land use and land cover change flux estimates. Earth System Dynamics 5:177-195, doi:10.5194/esd-5-177-2014, 2014.

Poulter, B., Ciais, P., Hodsen, E., Lischke, H., Maignan, F., Plummer, S., & Zimmermann, N. E.: Plant functional type mapping for earth system models. Geoscientific Model Development, 4, 993-1010. doi:10.5194/gmd-4-993-2011, 2011.

Prentice, I. C., Kelley, D. I., Foster, P. N., Friedlingstein, P., Harrison, S. P., & Bartlein, P. J.: Modeling fire and the terrestrial carbon balance. Global Biogeochemical Cycles 25:GB3005, 2011.

Pugh, T. A. M., Müller, C., Arneth, A., Haverd, V. & Smith, B.: Key knowledge and data gaps in modelling the influence of $CO_2$ concentration on the terrestrial carbon sink. Journal of Plant Physiology 203:3-15, 2016.

R Development Core Team. R: A language and environment for statistical computing. R Foundation for Statistical Computing, Vienna, Austria. ISBN 3-900051-07-0, URL http://www.R-project.org., 2008.

Randerson, J. T., Thompson, M. V., Conway, T. J., Fung, I. Y. & Field, C. B.: The contribution of terrestrial sources and sinks to trends in the seasonal cycle of atmospheric carbon dioxide. Global Biogeochemical Cycles 11(4):535-560, 1997.

Richardson, A. D., Anderson, R. S., Arain, M. A., Barr, A. G., Bohrer, G., Chen, G., Chen, J. M., Ciais, P., Davis, K. J., Desai, A. R., Dietze, M. C., Dragnoi, D., Garrity, S. R., Gough, C. M., Grant, R., Hollinger, D. Y., Margolis, H. A., McCaughey, H., Migliavacca, M., Monson, R. K., Munger, J. W., Poulter, B., Raczka, B. M., Ricciuto, D. M., Sahoo, A. K., Schaefer, K., Tian, H., Vargas, R., Verbeeck, H., Xiao, J., & Xue, Y.: Terrestrial biosphere models need better representation of vegetation phenology – results from the North American Carbon Program site synthesis. Global Change Biology, 18, 566-584. doi:10.1111/j.1365-2486.2011.02562.x, 2012.

Saeki, T. & Patra, P. K.: Implications of overestimated anthropogenic $CO_2$ emissions on East Asian and global land $CO_2$ flux inversion. Geoscience Letters 4:9, doi:10.1186/s40562-017-0074-7, 2017.

Saito, R., Patra, P. K., Deutscher, N., Wunch, D., Ishijima, K., Sherlock, V., Blumenstock, T., Dohe, S., Griffith, D., Hase, F., Heikkinen, P., Kyro, E., Macatangay, R., Mendonca, J., Messerschmidt, J., Morino, I., Notholt, J., Rettinger, M., Strong, K., Sussmann, R. & Warneke, T.: Technical Note – Latitude-time variations of atmospheric column-average dry air mole fractions of CO2, CH4, N2O. Atmospheric Chemistry and Physics 12:7767-7777, doi:10.5194/acp-12-7767-2012, 2012.

Schneising, O., Reuter, M., Buchwitz, M., Heymann, J., Bovensmann, H. & Burrows, J. P.: Terrestrial carbon sink observed from space – variation of growth rates and seasonal cycle amplitudes in response to interannual surface temperature variability. Atmospheric Chemistry and Physics 14:133-141, doi:10.5194/acp-14-133-2014, 2014.

Sitch, S., Smith, B., Prentice, I. C., Arneth, A., Bondeau, A., Cramer, W., Kaplan, J. O., Levis, S., Lucht, W., Sykes, M. T., Thonicke, K., & Venevsky, S.: Evaluation of ecosystem dynamics, plant geography and terrestrial carbon cycling in the LPJ dynamic global vegetation model. Global Change Biology 9:161–185, 2003.

Sitch, S., Friedlingstein, P., Grubber, N., Jones, S. D., Murray-Tortarolo, G., Ahlström, A., Doney, S. C., Graven, H., Heinze, C., Huntingford, C., Levis, S., Levy, P. E., Lomas, M., Poulter, B., Viovy, N., Zaehle, S., Zeng, N., Arneth, A., Bonan, G., Bopp, L., Canandell, J. G., Chevallier, F., Ciais, P., Ellis, R., Gloor, M., Peylin, P., Piao, S. L., Le Quére, C., Smith, B., Zhu, Z., and Myneni, R.: Recent trends and drivers of regional sources and sinks of carbon dioxide. Biogeosciences, 12, 653-679. doi:10.5194/bg-12-653-2015, 2015.

Smith, B., Prentice, I. C., & Sykes, M. T.: Representation of vegetation dynamics in the modelling of terrestrial ecosystems: comparing two contrasting approaches within European climate space. Global Ecology and Biogeography 10:621–638, 2001.

Sweeney, C., Karion, A., Wolter, S., Newberger, T., Guenther, D., Higgs, J. A., Andrews, A. E., Lang, P. M., Neff, D., Dlugokencky, E., Miller, J. B., Montzka, S. A., Miller, B. R., Masarie, K. A., Biraud, S. C., Novelli, P. C., Crotwell, M., Crotwell, A. M., Thoning, K. & Tans, P. P. (2015). Seasonal climatology of $CO_2$ across North America from aircraft measurements in the NOAA/ESRL Global Greenhouse Gas Reference Network. Journal of Geophysical Research - Atmospheres 120:5155–5190, doi:10.1002/ 2014JD022591, 2015.

Taylor, K. E.: Summarizing multiple aspects of model performance in a single diagram. Journal of Geophysical Research - Atmospheres, 106, 7183-7192, 2001.

Thoning, K. W., Tans, P. P., & Komhyr, W. D.: Atmospheric carbon dioxide at Mauna Loa Observatory, 2. Analysis of the NOAA CMCC data, 1974-1985. Journal of Geophysical Research, 94, 8549-8565, 1989.

Wunch, D., Wennberg, P. O., Toon, G. C., Connor, B. J., Fisher, B., Osterman, G. B., Frankenberg, C., Mandrake, L., O'Dell, C., Ahonen, P., Biraud, S. C., Castano, R., Cressie, N., Crisp, D., Deutscher, N. M., Eldering, A., Fisher, M. L., Griffith, D. W. T., Gunson, M., Heikkinen, P., Keppel-Aleks, G., Kyro, E., Lindenmaier, R., Macatangay, R., Mendonca, J., Messerschmidt, J., Miller, C. E., Morino, I., Notholt, J., Oyafuso, F. A., Rettinger, M. A., Robinson, J., Roehl, C. M., Salawitch, R. J., Sherlock, V., Strong, K., Sussmann, R., Tanaka, T., Thompson, D. R., Uchino, O., Warneke, T., & Wofsy, S. C. A method for evaluating bias in global measurements of CO2 total columns from space. Atmospheric Chemistry and Physics, 11, 12317-12337, 2011.

Xia, J., Niu, S., Ciais, P., Janssens, I. A., Chen, J., Ammann, C., Arain, A., Blanken, P. D., Cescatti, A., Bonal, D., Buchmann, N., Curtis, P. S., Chen, S., Dong, J., Flanagan, L. B., Frankenberg, C., Georgiadis, T., Gough, C. M., Hui, D., Kiely, G., Li, J., Lund, M., Magliulo, V., Marcolla, B., Merbold, L., Montagnani, L, Moors, E. J., Olesen, J. E., Piao, S., Raschi, A., Roupsard, O., Suyker, A. E., Urbaniak, M., Vaccari, F. P., Varlagin, A., Vesala, T., Wilkinson, M., Weng, E., Wohlfahrt, G., Yan, L. & Luo, Y.: Joint control of terrestrial gross primary production by plant phenology and physiology. Proceedings of the National Academies of Science of the United States of America 112(9):2788-2793, doi:10.1073/pnas.1413090112, 2015.

Yoshida, Y., Ota, Y., Eguchi, N., Kikuchi, N., Nobuta, K., Tran, H., Morino, I., and Yokota, T.: Retrieval algorithm for $CO_2$ and $CH_4$ column abundances from short-wavelength infrared spectral observations by the greenhouse gases observing satellite. Atmospheric Measurement and Techniques, 4, 717–734, doi:10.5194/amt-4-717-2011, 2011.

Zaehle, S., & Friend, A. D.: Carbon and nitrogen cycle dynamics in the O-CN land surface model: 1. Model description, site-scale evaluation, and sensitivity to parameter estimates. Global Biogeochemical Cycles, 24, GB1005. doi:10.1029/2009GB003521, 2010.

**Table 3.1. Terrestrial ecosystem models from the TRENDY v.2 model inter-comparison used to simulate terrestrial Net Ecosystem Exchange.**

| Model | Abbrev. | Spatial Resolution | Land Surface Model | Fire Simulation | C-N coupled cycle | Source |
|---|---|---|---|---|---|---|
| Community Land Model v.4.5 | CLM | 2.5 X 2.5 | Yes | Yes | Yes | Lawrence et al. (2011) |
| Lund-Potsdam-Jena | LPJ | 0.5 X 0.5 | No | Yes | No | Sitch et al. (2003) |
| Land-surface Processes and exchanges | LPX | 1.0 X 1.0 | No | Yes | Yes | Prentice et al. (2011) |
| ORganizing Carbon and Hydrology in Dynamic EcosystEms | ORCHIDEE | 3.74 X 2.5 | Yes | Yes | No | Krinner et al. (2005) |
| ORCHIDEE with coupled C-N cycling | OCN | 1.0 X 1.0 | Yes | Yes | Yes | Zaehle and Friend (2010) |
| Vegetation Integrative SImulator for Trace gases | VISIT | 0.5 X 0.5 | No | Yes | Yes | Kato et al. (2013) |

**Table 3.2. Signal characteristics for Rise and Fall segments of the GOSAT-derived $XCO_2$ seasonal cycles (2009-2012) by TransCom region. The timeframe of one Rise plus one Fall segment approximately equates to one year. North America Boreal and South America Tropical regions were excluded for lack of observations to derive signals for Rise or Fall segments.**

| | | Period (days) | | Amplitude (ppm) | |
|---|---|---|---|---|---|
| **Region** | **Segment** | **Fall** | **Rise** | **Fall** | **Rise** |
| Africa Northern | 1,2 | 118 | 241 | 5.4 | 6.1 |
| | 3,4 | 130 | 229 | 5.5 | 5.2 |
| | 5,6 | 135 | 232 | 6.0 | 5.8 |
| | 7 | 135 | NA | 5.7 | NA |
| Africa Southern | 1,2 | 174 | 216 | 2.5 | 3.0 |
| | 3,4 | 131 | 131 | 4.0 | 3.6 |
| | 5,6 | 218 | 147 | 3.2 | 3.0 |
| Asia Tropical | 1,2 | NA | 194 | NA | 6.4 |
| | 3,4 | NA | 200 | NA | 7.5 |
| | 5,6 | NA | 190 | NA | 7.0 |
| Australia | 1,2 | 140 | 225 | 2.0 | 1.2 |
| | 3,4 | 136 | 209 | 2.0 | 2.5 |
| | 5,6 | 155 | 228 | 2.4 | 2.4 |
| Europe* | 2,1 | 115 | 236 | 6.8 | 8.0 |
| | 3,4 | 131 | 239 | 7.9 | 6.4 |
| | 5,6 | 132 | 244 | 6.1 | 7.4 |
| Eurasia Temperate* | 2,1 | 109 | 248 | 6.2 | 7.1 |
| | 3,4 | 108 | 255 | 7.2 | 6.4 |
| | 5,6 | 118 | 253 | 5.7 | 6.5 |
| Eurasia Boreal | 1,2 | 102 | NA | 10.9 | NA |
| | 3,4 | 100 | NA | 11.7 | NA |
| | 5,6 | 104 | NA | 11.2 | NA |
| North America Temperate | 1,2 | 129 | 235 | 6.4 | 6.8 |
| | 3,4 | 126 | 243 | 5.6 | 5.4 |
| | 5,6 | 127 | 233 | 6.0 | 5.3 |
| | 7 | 129 | NA | 5.6 | NA |
| South America Temperate | 1,2 | 232 | 91 | 2.1 | 2.0 |
| | 3,4 | 238 | 137 | 2.2 | 2.4 |
| | 5,6 | 234 | 154 | 2.9 | 2.6 |

* the first differentiable segment is a Rise segment, starting approximately ~100+ days after the first segment in other regions because the initial drawdown (Fall segment) in the region is a partial or incomplete segment.

**Table 3.3. The interannual variation (IAV) in $XCO_2$ seasonal cycle metrics, presented as the relative standard deviation (i.e., RSD or coefficient of variation) and the LUCeffect, defined as the change in the $XCO_2$ seasonal cycle metrics when land-use change is included in simulations, relative to simulations with only natural vegetation. The values for IAV and LUCeffect presented below are first calculated for each region and segment type (Rise, Fall), and then averaged over all regions, and models (for LUCeffect). The values for the phasing metrics (day of year, 'DOY') are calculated using the period as the divisor.**

| metric | GOSAT IAV (%) | LUCeffect (%) |
|---|---|---|
| amplitude | 12.3 | 14.2 |
| period | 14.5 | 7.5 |
| DOYstart | 9.3 | 6.5 |
| DOYend | 7.5 | 6.8 |

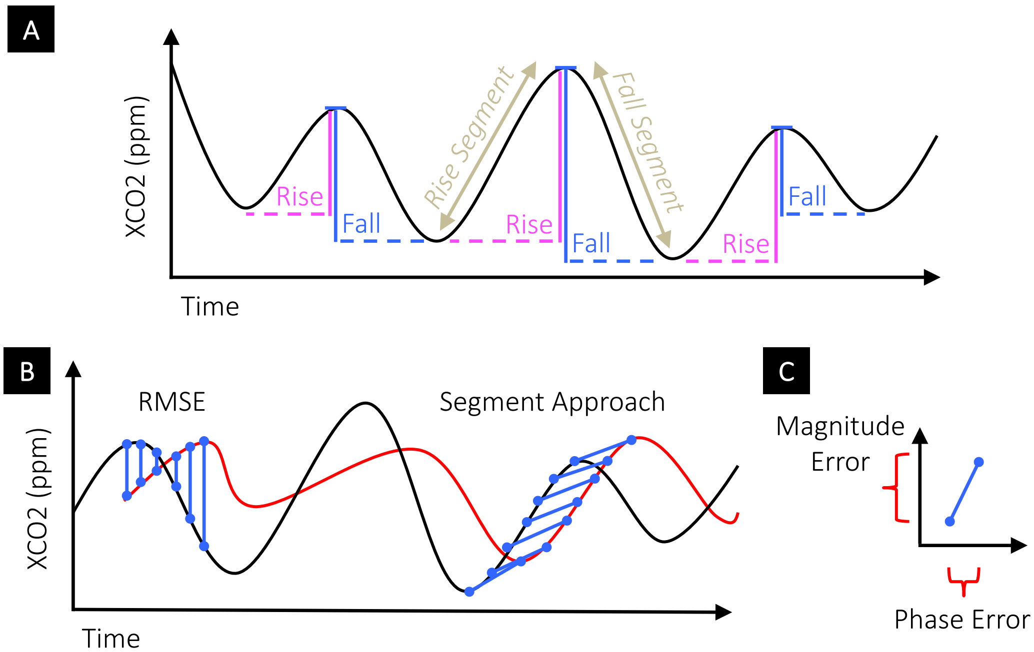


**Figure 3.1. Conceptual diagram for the segmentation analysis. (A) interannual variation in seasonal cycle amplitudes (vertical, solid colored lines) and periods (horizontal, dashed colored lines); such interannual variation may also differ among Rise and Fall segments. (B) a reference (black) and a modeled seasonal cycle (red) are compared using the Root Mean Squared Error (RMSE), which is taken as the difference in magnitude at the same exact time in reference and modeled seasonal cycles; in out-of-phase signals, the RMSE misrepresents bias; the segmentation approach matches segments in the reference and modeled seasonal cycles, Rise-to-Rise and Fall-to-Fall, so that the errors in magnitude and phase can be decomposed and directly represented (C).**


**Figure 3.2. TransCom region map.**

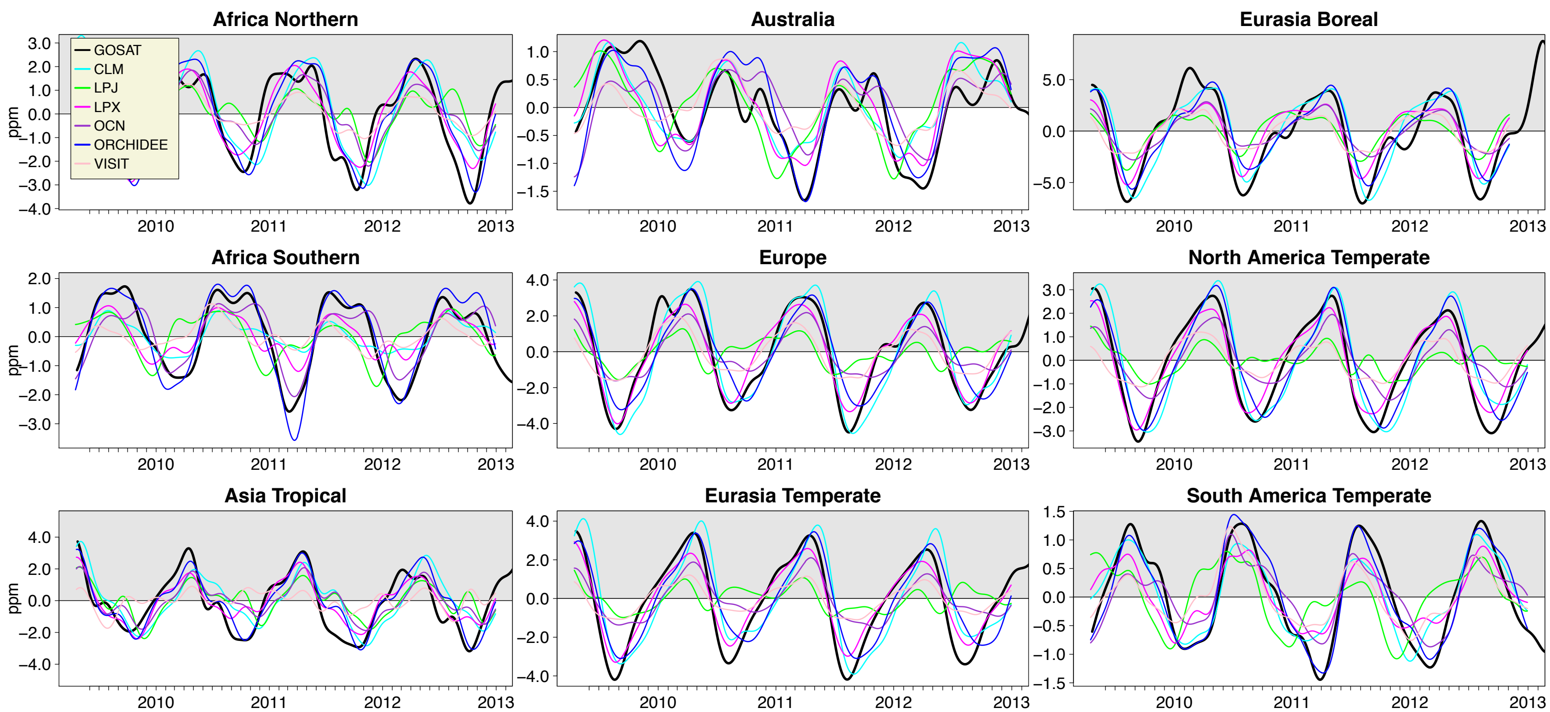


**Figure 3.3. Detrended $XCO_2$ seasonal cycles by TransCom region. Simulated seasonal cycles are the sum of transported fluxes from DGVM, Fossil Fuel and Ocean, but only the DGVM model name is listed.**

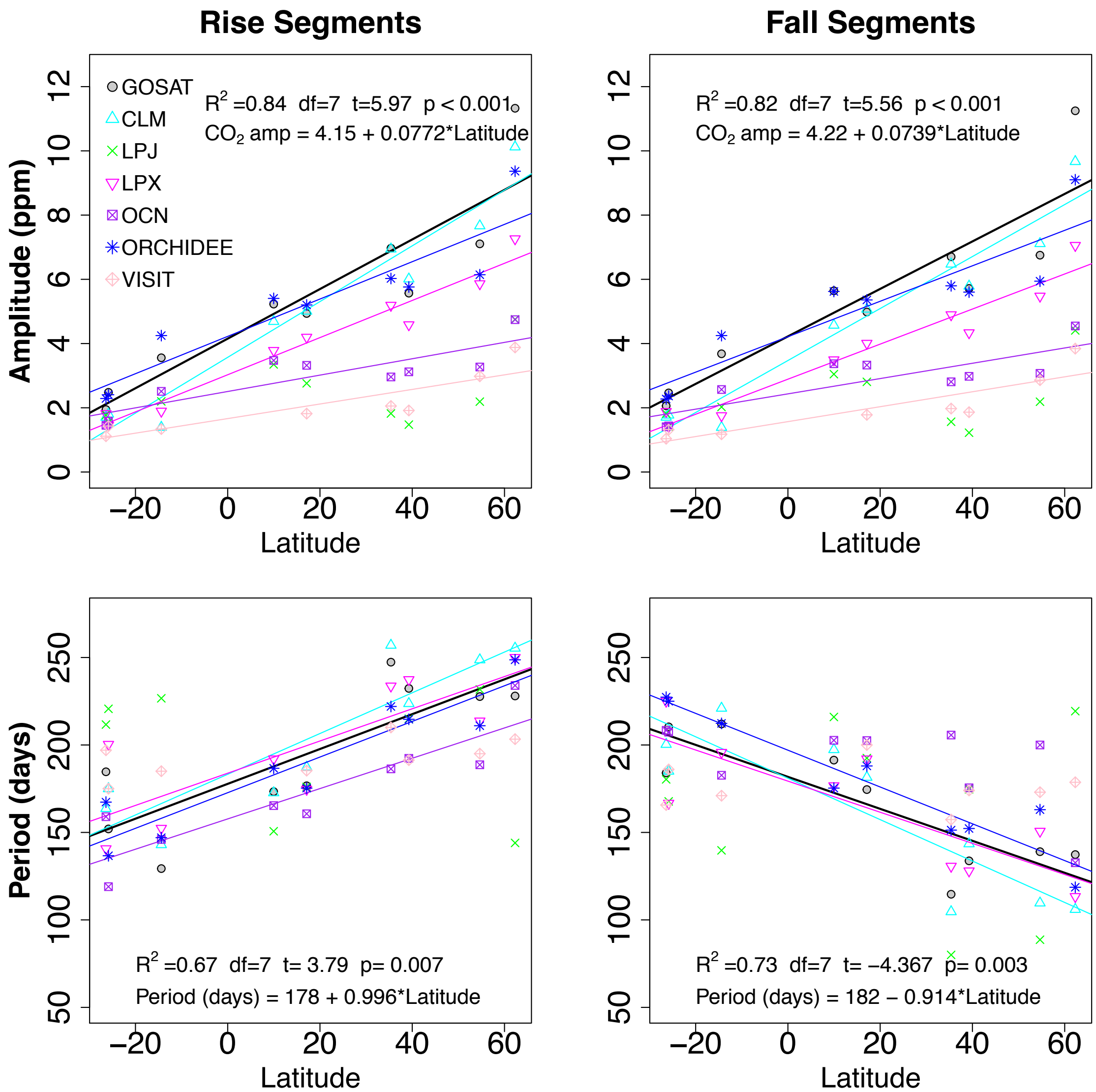


**Figure 3.4. Latitudinal variation in amplitude and period in Rise and Fall segments among TransCom regions, using the average latitude for each region. Linear regressions shown when significant ($p < 0.05$). Regression statistics and equation only given for GOSAT.**

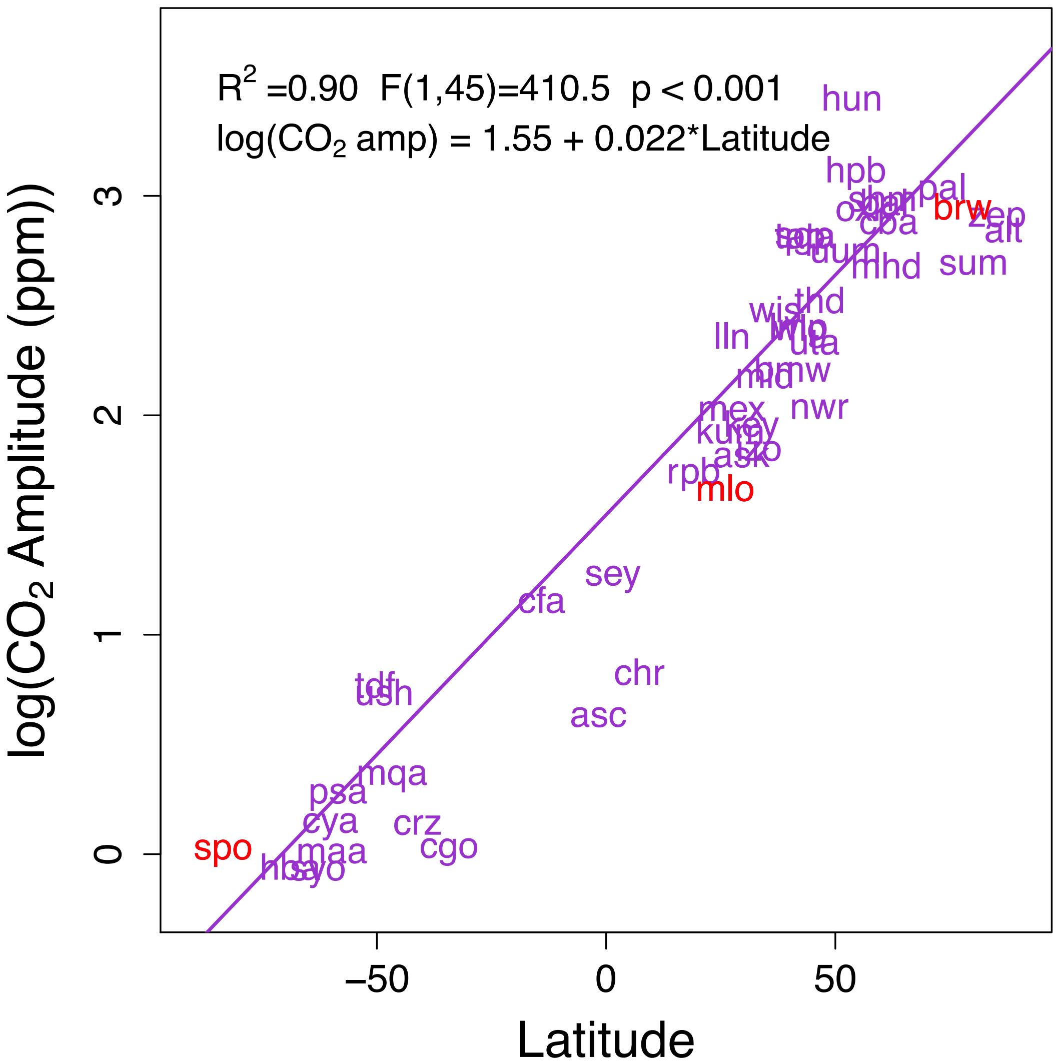


**Figure 3.5. Latitudinal variation in the amplitude for detrended in-situ surface $CO_2$ samples. Data are the average of peak-trough amplitudes for 2005-2015, only including sites with a minimum of 5 years of data. Points are labeled according to the three-letter code of the sampling station. South Pole (spo), Mauna Loa (mlo), and Barrow Island (brw) are highlighted in red for reference as these sites are commonly referenced in literature. The latitudinal range in surface site $CO_2$ seasonal amplitudes (~ 19 ppm), is more than 2 times the latitudinal range in seasonal amplitudes of $XCO_2$.**

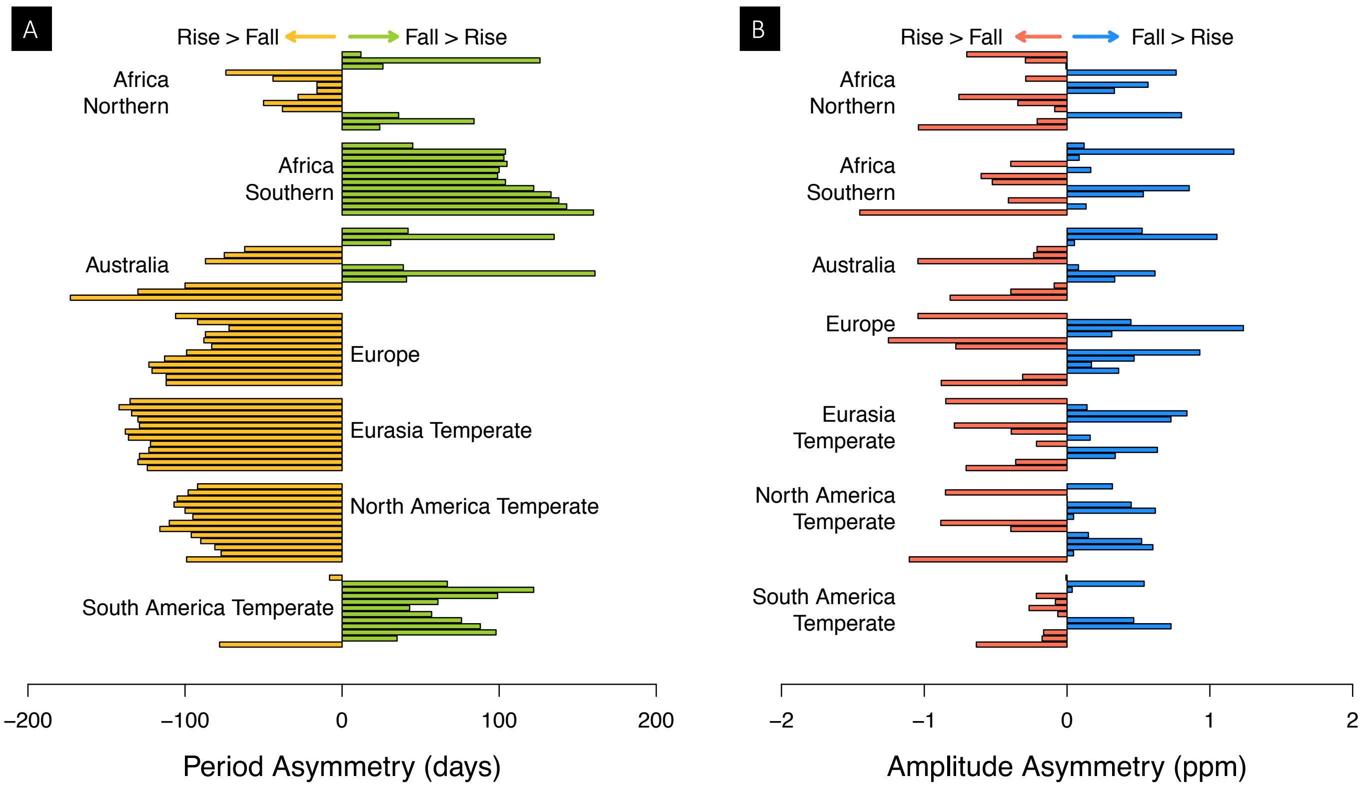


**Figure 3.6. Period asymmetries (A) and Amplitude asymmetries (B) in GOSAT $XCO_2$ seasonal cycles. The bars represent differences in amplitude or period for consecutive Fall (F) and Rise (R) segments, taking the Fall segment as reference. For example, if the time series follows the sequence F1, R1, F2, R2, F3, R3, (i.e., 3 seasonal cycles), then the difference between the first segment (F1) and the second segment (R2) is calculated as 'F1-R2'; a zero value would indicate that the metric (amplitude or period) were equal, whereas an asymmetry would be indicated by a positive (F1 > R2) or negative (F1 < R2) value. By definition, consecutive segments cannot be categorized as F-F or R-R. Asymmetry statistics are not traditional summaries, but nevertheless, they are characteristic and in some regions persistent patterns of the seasonal cycle that are undoubtedly influenced by biosphere activity.**

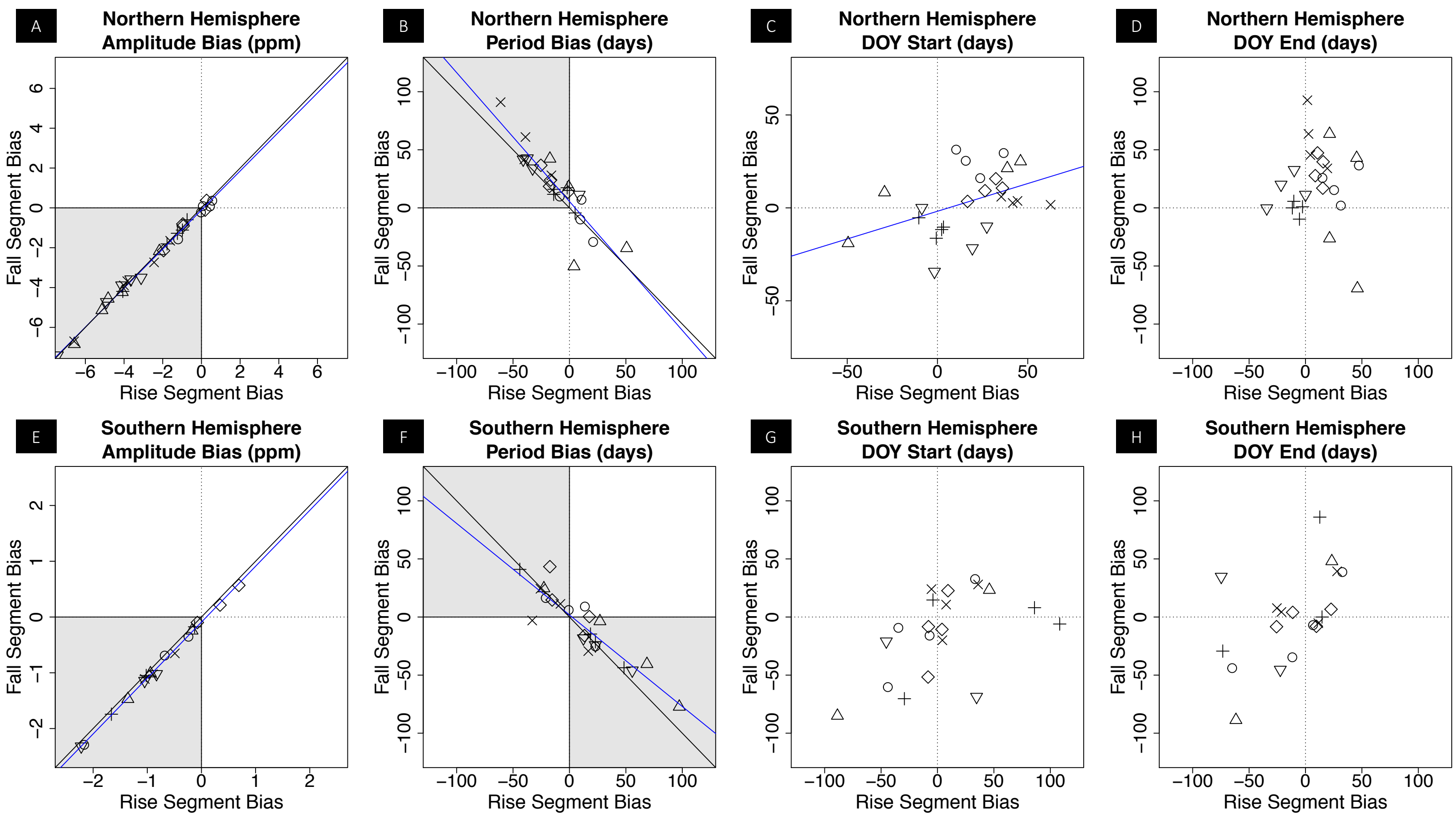


**Figure 3.7. Emergent correlations among biases for Rise (x-axes) and Fall (y-axes) segments model biases, using GOSAT $XCO_2$ as reference, for TransCom regions in the Northern Hemisphere (top row) and Southern Hemisphere (bottom row). Data points are the average bias by model (unique symbols, not shown) for a particular region. Data for the Eurasia Boreal and Asia Tropical regions were excluded for lack of data in both Rise and Fall segments. Diagonal black lines are the 1:1 correspondence lines, blue lines are significant linear correlations.**

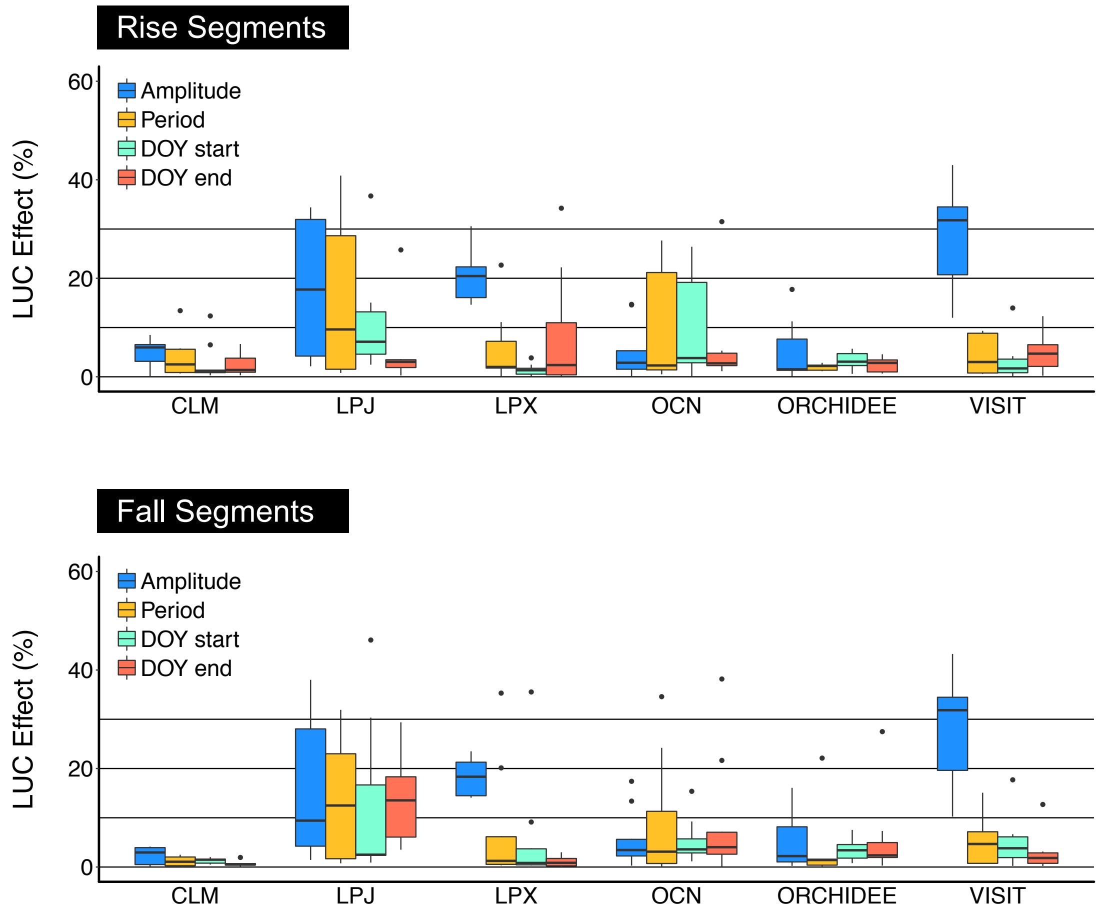


**Figure 3.8. Land Use Change effect on amplitude, period, and day of year (DOY). The percentages were calculated from the difference in the metrics between simulations (S3-S2), scaled relative to amplitude and period of Rise and Fall segments for each region and model; DOY was scaled against the period.**

# CHAPTER FOUR

# ECOSYSTEM AGE-CLASS DYNAMICS AND DISTRIBUTION IN A GLOBAL ECOSYSTEM MODEL

## Contribution of Authors and Co-Authors

Manuscript in Chapter Four

Author: Leonardo Calle

Contributions: wrote manuscript, performed simulations and processed data, developed methods and performed analyses, interpreted results, generated tables and figures

Manuscript Information

Leonardo Calle

Biogeosciences

Status of Manuscript:
_X__ Prepared for submission to a peer-reviewed journal
____ Officially submitted to a peer-reviewed journal
____ Accepted by a peer-reviewed journal
____ Published in a peer-reviewed journal

Published by the European Geoscience Union

# CHAPTER FOUR

# ECOSYSTEM AGE-CLASS DYNAMICS AND DISTRIBUTION IN A GLOBAL ECOSYSTEM MODEL

The following work is currently in progress to be submitted for publication

Leonardo Calle

Montana State University, Department of Ecology, Bozeman, Montana 59717, USA

## 1. ABSTRACT

Forested ecosystems follow classic responses with age, peaking production around canopy closure and declining thereafter. Although age dynamics might be more dominant in certain regions over others, demographic effects on Net Primary Production (NPP) and Heterotrophic Respiration (Rh) are bound to exist. Yet, explicit representation of ecosystem demography is notably absent in global ecosystem models. This is concerning because the global community relies on these models to regularly update our collective understanding of the global carbon cycle. This paper presents the technical developments of a computationally-efficient approach for representing age-class dynamics within a global ecosystem model, the LPJ Dynamic Global Vegetation Model. Age-classes are created by fire feedbacks, wood harvesting, and abandonment of managed land. Analyses are presented of model behavior, in terms of age-structure and age-functional patterns, and show that the age-module can capture classic demographic patterns in stem density, tree height, NPP, and Rh. Simulations show that, between 1860 and 2016, zonal age distribution on Earth was driven predominately by fire, causing a ~45 year difference in ages between Boreal (50N-90N) and Tropical (23S-23N) latitudes. Land use change and land management was responsible for an additional decrease in zonal age by -6 yrs in Boreal and by -21 yrs in Temperate (23N-50N) and Tropical latitudes, with the anthropogenic effect on zonal age distribution increasing over time. A statistical model helped reduced LPJ complexity by predicting per-grid-cell annual NPP and Rh fluxes by three terms: precipitation, temperature and age-class; at global scales, $R^2$ was between

0.95 and 0.98. As determined by the statistical model, the demographic effect on ecosystem function was often less than 0.10 kg C $m^{-2}$ $yr^{-1}$ but as high as 0.60 kg C $m^{-2}$ $yr^{-1}$ where the effect was greatest. In eastern forests of North America, the demographic effect was of similar magnitude, or greater than, the effects of climate; demographic effects were similarly important in large regions of every vegetated continent. Spatial datasets are provided for global ecosystem ages and the estimated coefficients for effects of precipitation, temperature and demography on ecosystem function. The discussion focuses on the increasing role of demography in the global carbon cycle, the consequences of omitting demography in global models, which alters relaxation times (resilience) following a disturbance event, and the 40 Pg C increase in turnover from age dynamics at global scales. A frank discussion is provided on model limitations and suggestions are offered for model improvement. Whereas time is the only mechanism that increases ecosystem age, any additional disturbance not explicitly modeled will decrease age. Arguably, the LPJ Age-module simulates the upper limit of age-class distributions on Earth and represents another step forward towards understanding the role of demography in global ecosystems.

## 1. INTRODUCTION

Ecosystem production follows predictable patterns with the time since disturbance – the classic forest age-production curves from Odum (1969), where Net Ecosystem Production (NEP) peaks around canopy closure, declining thereafter due to hydraulic limitations on gross primary production (Ryan et al. 2004, Drake et al. 2010, 2011) and increases in Heterotrophic Respiration from biomass turnover, as well as from stand-level declines in population density (Ptrezsch and Biber 2005, Stephenson et al. 2014). That younger forests are more productive than older forests has been long-standing knowledge in forestry, as evidenced by yield and growth tables dating back to the 18$^{th}$ Century that incorporated stand age into their calculations of lumber production (Pretzsch et al. 2008).

On global scales, forest age is a considerable factor in global carbon cycling. Regrowth following disturbance comprises ~60% of the total land carbon sink based on country-level forest inventories (Pan et al. 2011a; tropical regrowth sink of 1.6 ± 0.5 Pg C yr$^{-1}$) and model-based studies (Pugh et al. 2019; global regrowth sink of 1.02-1.23 Pg C yr$^{-1}$). In the last decade, explicit model representation of forests as a function of time since disturbance (hereafter simply, 'ecosystem age') has been a grand challenge in an effort to quantify the demographic response of forests to changes in climate, atmospheric $CO_2$, and disturbances (Friend et al. 2014, Kondo et al 2018, Pugh et al. 2019), and from fire and Land Use Change and Land Management (LUCLM) (Gitz and Ciais 2003, *Model*: OSCAR; Shevliakova et al. 2009, *Model*: LM3V; Haverd et al. 2014, *Model*: CABLE-

POP; Yue et al. 2018, *Model*: ORCHIDEE MICT). Much of the focus of these global modeling studies has been on the effect of natural and anthropogenic disturbances on the carbon dynamics in old-growth versus second-growth (history of land use) forests (Gitz and Ciais 2003, Shevliakova et al. 2009, Kondo et al 2018, Yue et al. 2018, Pugh et al. 2019), lacking finer distinction of demographic effects, for example, when age-classes near canopy closure have the greatest NEP.

Large-scale (> 0.1 ha) ecosystem disturbances that reset ecosystem age, including here both natural and anthropogenic causes, can be generally ranked in the following order according to global area disturbed: fire > windstorms > timber harvest > shifting cultivation (Frolking et al. 2009). Much of the evidence for the relative importance and global distribution of large disturbances has come from either satellite retrievals of spectral indices indicating burn scars on the land (Potter et al. 2003, Frolking et al. 2009), national forest inventory records of land use change and timber harvest (Houghton 1999, FAO-FRA 2015, Williams et al. 2016), or from model-based studies (Goldewijck 2001, Arneth et al. 2017) that integrate information on historical land use (Goldewijck 2001, Hurtt et al. 2006). Other natural disturbances such as pest and pathogen outbreaks, flooding, ice storms, and volcano eruptions are less widespread globally (Frolking et al. 2009) but are still influential drivers of landscape patch dynamics (Dale et al. 2001, Turner 2010). In the conterminous United States, timber harvest is the predominate forest disturbance (1.4% of forested area logged annually), followed Fire (0.01-0.5% of forested area burned annually 1997-2008) (Williams et al. 2016). Although pest and pathogens, namely bark beetle infestations, affected a much larger area (up to 6% of total forested area in U.S.) than both logging and fire, the effects do not always cause stand replacement. It is arguable whether fire and timber harvest are the two most important global drivers of ecosystem age (Pan et al. 2011b), but nevertheless these are the drivers applied in a model framework in this study, in a manner that moves modeling one step forward to assess global age-class dynamics.

The overall aim of this study was to fill a gap in existing knowledge by simulating the time-evolution of global age-class distributions in a global ecosystem model and to determine if explicit representation of demography influenced ecosystem stocks and fluxes at global scales or at the level of a grid-cell. Technical details are presented for a module representing age-class dynamics, driven by fire feedbacks, land abandonment and wood harvesting in the Lund Potsdam Jena (LPJ; Sitch et al. 2003) Dynamic Global Vegetation Model (DGVM). Analyses are presented of model behavior, in terms of age-structure and age-functional patterns, the temporal evolution of age distributions and their causative drivers, and a statistical model of ecosystem production and respiration as a function of demography and climate. We offer an extended discussion on the consequences of omitting demography in global ecosystem models and offer suggestions to improve representation of disturbance types and plant physiology that might alter the age-production patterns in this study.

## 2. METHODS

### 2.1 LPJ General Model Description

LPJ simulates soil hydrology and vegetation dynamics in 0.5˚ grid-cells, wherein climate, atmospheric $CO_2$, and soil texture is assumed to be the same (Figure 4.1). Vegetation is categorized into Plant Functional Types (PFT; Box 1996). Plant populations compete for light, space, and soil water, depending on demand; nutrient cycles are not considered in this model version. LPJ is a 'big-leaf' ecosystem model, whereby leaf-level photosynthesis and respiration (Haxeltine and Prentice 1996, Farquhar et al. 1980) occur at daily time-steps, accounting for the photosynthetically active period (daytime), and is scaled to the stand-level using a mean-individual approximation, which assumes that important state variables (carbon stocks and fluxes) can be determined by using the average properties of a population. Plant populations are categorized using 10 PFTs in this study (phenology parameters and bioclimatic limits listed in SM Table 4.1); the same PFTs in Sitch et al. (2003). Left unchanged are the PFT-specific bioclimatic limits, turnover rates, C:N tissue ratios, allometric ratios, and other parameters not explicitly commented on here, but as described in Sitch et al. (2003). Mortality occurs via reductions in population density if a PFT's annual carbon balance is less than zero or if fire occurs; further details on fire module described in *Section 2.2.2*.

## 2.2 Age-class Module

### *2.2.1 An age-based model of ecosystems – sub-gridcell patch dynamics*

Age-classes are represented as patches within a grid-cell (Figure 4.1), such that every patch has the same climate, atmospheric $CO_2$, and soil texture, but the properties of the patch, such as available soil water and light availability, are determined by feedbacks from plant demand; hereafter, 'age-class' and 'patch' are used interchangeably depending on context but describe the same entity. Plant processes (competition, photosynthesis, respiration) are simulated at the level of the patch. The age-class module has a fixed number of age-classes that can be represented, but all age-classes are not always represented within a grid-cell. In this version of the module, age-classes are classified into 12 age-classes (patches) in fixed age-width bins, defined as the *unequalbin* or the *10yr-equalbin* age-width setup (Table 4.1). The age-widths of the age-classes in the *10yr-equalbin* setup correspond to common age-widths of classes used in forest inventories. The *10yr-equal*bin age setup is used for all global simulations, whereas the *unequalbin* setup is applied to explore model dynamics at the level of a single grid-cell; simulation details in next section.

Age-classes are only created by fire, timber harvest, or land abandonment and are initialized to the youngest age-class. The fraction of the patch that burns gets its age 'reset' to the youngest age-class, 1-10 yr. The same process occurs for the fractional area that experienced timber harvest or when managed land is abandoned and allow to regrow

– the fractional area undergoing an age-transition is reclassified as a 1-10 yr age-class. This process allows the model to accurately track the carbon stocks, fluxes and feedbacks associated with these state variables. For example, if a fire burns 50% of a patch, then 50% might have bare ground and 50% will have vegetation at pre-burn levels. If the probability of another fire is dependent on live vegetation, then feedbacks will result in a lower chance of fire on the bare-ground fraction versus the fully-vegetated fraction that was not previously burned. The improvements are in the accounting of stocks and fluxes.

The most novel advancement in this study is a new method of age-class transition modeling, called 'vector-tracking of fractional transitions' (VTFT), which improves the computational efficiency of modeling age-classes in global models. The method is a solution to the problem of dilution, which manifests as an advective process when state variables, such as carbon stocks or tree density, are made to merge by area-weighted averaging. The concept of merging two unique model entities ('patch' or age-class) on the basis of similarity is a computational solution to constrain the number simulated patches in accordance with computer resources, but it also troublesome and quite impractical. Along what axis is a patch considered to be most similar to another patch – in terms of PFT composition, biomass in plant organs, plant height, or stem density? Existing age-class models (Medvigy et al. 2009, *Model*: ED2; Lawrence et al. 2019, *Model*: CLMv5.0; Yu et al. 2018, *Model*: ORCHIDEE-MICT) employ merging rules with varying thresholds to ensure that patches are only merged if the difference among one state variable (biomass, tree height) is less than a fixed threshold. Merging rules are arbitrary distinctions of similarity and VTFT circumvents these issues by not using merging rules at all. By design, VTFT allows age-classes to advance in a natural progression from young to old and ensures that age-class transitions always occur between the most similar age-classes along multiple state variables.

VTFT describes a vector associated with every age-class of length ( $w$ ), equal to the age-width of the age-class, with elements ( $f$ ) that are the fractional areas contributing to the total fractional area of the patch ( $f_{total}$ ). When a young age-class ($a_1$) is first created, VTFT vectors are initialized to zero and the first element ( $f_1$ ) is set to the *incoming* fractional area. *Within-class Fractional Transitions*: For every simulation year, the position of each element ( $f_x$ ) in the VTFT vector is incremented by the representative time of each element ( $x$ ), which is simply 1. No changes occur to the state variables of the age-class in within-class transitions. *Between-class Fractional Transitions*: Upon incrementing the position of each element, if the value at ( $f_w$ ) is non-zero, then the corresponding fractional area $f_w$, defined as the *outgoing* fraction, is used in an area-weighted average between the state variables of $a_1 f_w$ and the next oldest age-class $a_2$ $f_{total}$. Lastly, upon incrementing element position, if all elements $< f_1 \dots f_w >$ in the VTFT vector of the preceding age-class, in this example ($a_1$), are zeros, then the age-class is simply deleted from computational memory.

Two examples are provided in Figure 4.2 that demonstrate the procedure when there is a young age-class is created, and another scenario when there are fractional age-class transitions between age-classes. With VTFT, any number of age-classes and age-widths can be modeled, but it is demonstrated that the age-widths employed in this study are sufficient to minimize the dilution of state variables when area-weighted averaging is used to merge fractional patches while also simulating stand-age patterns in state variables of carbon stocks, stem density and fluxes.

### *2.2.2 Integration with fire and Land Use Change and Land Management (LUCLM) modules*

*Fire* – The fractional area burned initiates the creation of a youngest age-class, or it gets merged with a youngest age-class if one exists already. Fire simulation is based on the semi-empirical Glob-FIRM model by Thonicke et al. (2001), with implementation details described in Sitch et al (2003). In short, fire is dependent on the length of the fire season, calculated as the number of dry days in a year above a threshold and a minimum fuel load, defined only as the mass of carbon in litter. When a fire occurs, PFT-specific fire resistances determine the fraction of the PFT population that gets burned. The biomass of burned PFTs, along with the aboveground litter in the patch, gets calculated as an immediate flux to the atmosphere. The fraction of the PFT population that does not burn maintains state variables (e.g., tree height, carbon in leaf and wood) at previous values; said another way, it is possible to have so called 'survivor' trees on the youngest age-class that then skews the age-height distribution of the patch.

*LUCLM* – Age-classes get created when managed land is abandoned and allowed to regrow into secondary forests, or when timber harvest occurs on forested lands. In both cases, the fractional area abandoned/logged initiates the creation of a youngest age-class, or it gets merged with a youngest age-class if one exists already. To improve accounting of primary forests, defined here as natural land without history of LUCLM, and second-growth forests, defined as natural land with a history of LUCLM; transitions between these classes are unidirectional from primary -> secondary. In the LUCLM module, gross transitions between land uses (Pongratz et al. 2014, Stocker et al. 2014) are simulated, such that if the fraction of abandoned land equals the fraction of land deforested in the same year (net zero land use change), the fluxes from the gross transitions are tracked independently and gives an overall more accurate accounting (and higher magnitude) of emissions from LUC (Arneth et al. 2017).

General rules distinguishing primary and secondary stands within the age-class context: (1a) the primary grid-cell fraction only decreases in size and never gets mixed with existing secondary forests or with abandoned managed land. Only fire creates young age-classes on primary lands. (2a) secondary grid-cell fractions can be mixed with other secondary forest fractions, recently abandoned land, fractions with timber harvest, and recently burned area. General priority rules for deforestation and timber harvest: (1b) For simplicity, deforestation always occurs in the ranking of oldest to youngest age-class, proceeding to deforest each age-class until the prescribed fractional area of deforestation is met. This rule is a conservative estimate of fluxes from deforestation, typically resulting in greater land-to-atmosphere fluxes than if rules were employed that allowed younger age-classes to be preferentially deforested. (2b) timber harvest also occurs in the ranking of oldest to youngest age-class until two conditions are met. Timber harvest occurs on each age-class until a prescribed harvest mass or harvest area is met.

Treatment of immediate emissions and residues: Deforestation results in 100% of heartwood biomass and 50% of sapwood biomass being stored for delay emission in product pools; root biomass is entirely part of belowground litter pools, while 100% leaf and 50% of sapwood biomass becomes part of aboveground litter pools. Grid-cell fractions that underwent land-use change were not mixed with existing managed lands or secondary fractions until all land-use transitions had occurred; this avoids a computational sequence that results in a lower flux if deforestation and abandonment occur in the same year. For timber harvest, 100% of leaf biomass and 40% of the sapwood and heartwood enters the aboveground litter pools, and 100% of root biomass the belowground litter pools; 60% of sapwood and heartwood are assumed to go into a product pool for delayed emission.

Timber from deforestation and harvest in product pools for delayed emission (Earles et al. 2012): For deforestation, 60% of exported wood (i.e., not in litter) goes into a 2-yr product pool and 40% goes into a 25-yr product pool, following the 40:60 efficiency assumption from McGuire et al. (2001). For timber harvest, the model uses space-time explicit data on harvest fractions going into roundwood, fuelwood and biofuel product pools; dataset described further in Sect. *2.3.2*. We use three product pools and assume that 100% of the fuelwood and biofuel fraction goes into the 1-year product pool (emitted in the same year of wood harvest), 50% of the roundwood fraction goes into the 10-year product pool (emitted at rate 10% per year) and the remaining 50% of the roundwood fraction goes into the 100-year product pool (emitted at rate 1% per year).

## 2.3 Experimental Design and Analysis

### *2.3.1 Model inputs*

Inputs to the model are gridded soil texture (sand, silt, clay fractions) from the USDA Harmonized World Soils (Nachtergaele et al. 2008), annually-varying global-mean [$CO_2$] (time series available in supplement), and monthly-varying air temperature, precipitation, precipitation frequency, and radiation from the Climate Research Unit (CRU, version TS3.26) data for 1901-2016. Land use, land use change, and timber harvest was prescribed annually based on the Land Use Harmonization dataset version 2 (LUHv2; Hurtt et al. 2017), which is used as forcing land-use for the 6th Coupled Model Intercomparison Project (CMIP6; Eyring et al. 2016 CMIP citation in GMD). The dataset includes fractional area of bi-directional (gross) land use transitions between forested and managed lands, as well as the total biomass of timber harvest on a specified fractional area logged. In this version of LPJ, managed lands (crops, pastures) are treated as grasslands with no irrigation, no fire, and tree PFTs were not allowed to establish. Model representation of land management is an oversimplification to focus on effects of timber harvest.

*2.3.2 Regional simulation – age dynamics of stand structure and ecosystem function*

The objectives were to evaluate demographic patterns of stand structure and function when simulating age-classes using different age-width binning. Two ideal simulations were conducted at a regional scale to sample simulated annual stem density, average tree height, and NEP. The first simulation used the *unequalbin* age-width setup, $\mathbf{S_{unequalbin}}$, and another used the *10-yr-equalbin* age-width setup, $\mathbf{S_{10yrbin}}$ (Table 4.2). For both simulations, Fire and LUCLM were not simulated. Instead, 5% of the fractional area of age-classes > 25 yrs were cleared of biomass annually; the fractional area cleared was re-classified and merged with the youngest age-class. The intent of the setup was to ensure that each grid-cell maintained patches in every age-class for each year of the simulation and avoided situations in which age-classes were only present in 'bad years', or when growing conditions were poor. Both simulations were conducted with a 1000-yr 'spinup' using fixed $CO_2$ (287 ppm, 'pre-industrial' values) and climate randomly sampled from 1901-1920 to ensure that age distributions were developed and state variables were in dynamic equilibrium (i.e., no trend). A transient simulation then used time-varying $CO_2$ and climate, as prescribed by model inputs. Stand structure data were analyzed for 1980-2016.

The idealized simulations were performed for the mixed deciduous and evergreen forests of Michigan, Minnesota and Wisconsin, U.S.A (bounding box defined by left: 97.00º W;

right: 82.50º W, top: 49.50º N, bottom: 42.00º W). These forests are of moderate temperate climates, with total annual rainfall 815.0 mm/yr (average over 1980-2016, based on CRU TS3.26) with monthly minimum 21.0 mm/mo and maximums of 148.5 mm/mo. Mean annual temperature (1980-2016, CRU TS3.26) was 5.98º C with monthly minimum of –11.45º C and maximum 20.98º C.

Data were pooled for the region over the time period and by age-class. Date were plotted in box plots to show median value, interquartile range and outliers. No attempt was made to de-trend data because there was enough between age-class variation to evaluate general demographic patterns visually.

*2.3.3 Idealized simulation of a single event of deforestation, abandonment, regrowth*

The objective was to evaluate the effect of age-classes on relaxation times following a single deforestation, abandonment and regrowth event within a single grid-cell (Table 4.2). The relaxation time is defined as the time required for a variable to recover to previous state and is a direct measure of ecosystem resilience (*sensu* Pimm 1984). Two simulations were conducted, the first simulation used the *10-yr-equalbin* age-width setup, $\mathbf{S_{age\_event}}$, and another did not simulate age-classes, $\mathbf{S_{noage\_event}}$ (Table 4.2). Both simulations were conducted with a 1000-yr 'spinup' using fixed $CO_2$ (287 ppm, pre-industrial value) and climate randomly sampled from 1901-1920 to ensure that state variables were in dynamic equilibrium. A transient simulation then used time-varying

$CO_2$ and climate, as prescribed by model inputs. Fire and LUCLM were not simulated. Instead, 25% of the fractional area was deforested in year 1910 of the simulation and classified as managed land. Deforestation rules were equally applied for both simulations as described in *Section 2.2.2*. In the following year (1911), the managed land fraction was abandoned and allowed to regrow. The following state variables were plotted over time and visually evaluated: NBP, NEP, NPP, Rh, Carbon in Biomass.

The idealized simulations were performed for a single grid-cell in a mixed broadleaf and evergreen needleleaf forest in British Columbia, CAN (121.25º W 57.25º N). The grid-cell is a Boreal climate with total annual rainfall 473.7 mm/yr (average over 1980-2016, based on CRU TS3.26) with monthly minimum 9.11 mm/mo and maximums of 105.8 mm/mo. Mean annual temperature (1980-2016, CRU TS3.26) was 0.59º C with monthly minimum of –16.9º C and maximum 14.7º C.

*2.3.4 Global simulation objectives and setup*

There were three main objectives for global simulations. The first objective was to simply evaluate if there were differences in global stocks and fluxes when including age-classes in simulations, $\mathbf{S_{age}}$, compared to a simulation that did not include age-classes, $\mathbf{S_{noage}}$ (Table 4.2). The second objective was to determine the relative influence of fire and LUCLM on the spatial and temporal distribution of ecosystem ages. For this objective, a Fire-only simulation ($\mathbf{S_{Fire}}$) only had age-classes created by fire, whereas a LUCLM-only simulation ($\mathbf{S_{LU}}$) had age-classes only created by abandonment of managed land or by timber harvest (Table 4.2). A simulation with both Fire and LUCLM ($\mathbf{S_{FireLU}}$) was used as the baseline for comparison against $\mathbf{S_{Fire}}$ and $\mathbf{S_{LU}}$. The third objective used data from $\mathbf{S_{age}}$ to identify the relative influence of demography versus climate on simulated fluxes (NEP, NPP, and Rh).

For all three simulations, a spinup simulation was run for 1000 yrs using randomly sampled climate conditions from 1901-1920 and atmospheric $CO_2$ fixed at pre-industrial levels (287 ppm); spinup ensured that age distributions were initialized under natural conditions and state variables were in dynamic equilibrium (i.e., no trend). A second 'land-use-spinup' procedure was run for 398 years to initialize land use at values for year 1860, resampling climate and fixing $CO_2$ as in the first spinup. After spinup procedures, climate and $CO_2$ were allowed to vary until simulation year 2016; in $\mathbf{S_{LU}}$ and $\mathbf{S_{FireLU}}$, land use change and timber harvest varied annually as prescribed by the LUHv2 dataset.

In the first objective (as above), global values for stocks and fluxes include both natural and managed lands. These global estimates conform to typical presentation of global values (Le Quéré et al. 2018), in Petagrams ($10^{15}$) of Carbon. Comparisons are made among simulation types and to values from the literature.

For the second objective, a time series of zonal mean ecosystem ages were analyzed to determine the relative importance of $\mathbf{S_{Fire}}$ and $\mathbf{S_{LU}}$ on the observed distributions in $\mathbf{S_{FireLU}}$.

The first assessment was made by visual inspection of zonally-averaged time-series (i.e., Hovmöller plots) for the entire period of transient simulation, years 1860-2016. In addition, for each of $\mathbf{S_{Fire}}$ and $\mathbf{S_{FireLU}}$, a simple linear regression model (Age ~ Year, setting 1860 as the reference year and defined as 1) was applied to identify trends in ecosystem age by the following zonal bands: Boreal (50˚ N to 90˚ N), Temperate (23˚ N to 50˚ N), and Tropics (23˚ S to 23˚ N). Trends in LUCLM are, by definition, prescribed *a priori* by the forcing data, but age distributions are not prescribed by inputs per se; instead, the age module is a necessary model structure that allows full realization of the effect of forcing data on age distributions. By contrast, fire is a fully simulated process that integrates feedbacks from climate conditions and fuel loads.

For the third objective, to reduce dimensionality of the data and to assess the relative influence of demography and climate on simulated fluxes, annual flux data from $\mathbf{S_{age}}$ (Table 4.2) were analyzed from 2000-2016 using generalized linear regression model (*Flux* = Total Annual Precipitation + Mean Annual Temperature + Age-class), where *Flux* was one of [NEP, NPP, Rh] in kg C $m^{-2}$ $yr^{-1}$, Precipitation (mm) and Temperature (Celsius) data from CRU TS3.26, and Age-class was categorical, defined by the age-class code (Table 4.1). An initial test of the data model attempted to estimate globally-consistent predictor effects, but the model was found to be a terrible fit (*not shown*) and it was assumed that there was too much variation among grid-cells to detect globally-consistent effects. Instead of adding additional gridded fields of predictor variables to account for grid-cell-level variation, the same statistical model was applied and analyzed per-grid-cell. This allowed coefficients of Precipitation, Temperature and Age-class to vary by grid-cell, in essence, reducing the effect of variation in PFT composition, soil texture and hydrology that might otherwise reduce predictive power.

In the subsequent per-grid-cell analysis, the intercept term was intentionally omitted from the data model by adding a '-1' term to the data model. The Age-class term, as a categorical variable, effectively takes the place of the intercept term anyhow, so the outcome is that estimates are for the absolute effect of each age-class on the predicted flux as opposed to estimates that were relative to the first age-class; this had no impact on estimated coefficients but it did simplify analyses. In grid-cells where only a single age-class was present, the statistical model was defined as (*Flux* = Total Annual Precipitation + Mean Annual Temperature), leaving the intercept term to be estimated from the data and then re-classifying the intercept term by the age-class code for the grid-cell.

The degrees of freedom (d.f.) of a model for a grid-cell with a single age-class was d.f.=14, based on 17 annual data points to estimate coefficients of three predictors. The degrees of freedom for a grid-cell that had a maximum of 12 age-classes was d.f.=190, based on 204 annual data points to estimate coefficients for 14 predictors. Because the analysis produced statistical results for every grid-cell, the degrees of freedom are not presented elsewhere. Coefficients were only analyzed or mapped when significant at p=0.05.

## 3. RESULTS

### 3.1 Model Age Dynamics

#### 3.1.1 *Dynamics of stand structure and function – regional simulations*

Forest structural characteristics of stem density, height, and NEP followed the expected patterns with age with a few exceptions. In $\mathbf{S_{unequalbin}}$ (Table 4.2), stem density increased from near zero to maximum in the 21-25 yr age-class, before declining non-linearly (Figure 4.3). By contrast, the gradual increase in stem density in the first age-class in $\mathbf{S_{10\text{-}yrbin}}$ (Table 4.1) was not readily apparent because this process, which is evident in $\mathbf{S_{unequalbin}}$, occurs entirely within the youngest 1-10 yr age-class in $\mathbf{S_{10\text{-}yrbin}}$. Both simulation setups approach the same stem densities after age ~25; prior differences are due to binning of age-widths.

For average tree height in $\mathbf{S_{unequalbin}}$, there were large tree heights in the youngest age-class, which results from so-called 'survivor' trees (Figure 4.3). Not all trees are killed-off when a stand-clearing disturbance occurs in LPJ. Although the stand is 'reset' to the youngest age-class, the survivor trees skew the height distribution until the density of establishing saplings subsequently increases and brings down the average tree height to smaller values. This pattern is more akin to what occurs during natural fires or selective harvesting, which can reduce the overall age of a stand but might not result in a complete removal of all trees. By contrast, the skewed age-height pattern is not apparent in $\mathbf{S_{10\text{-}yrbin}}$ (Figure 4.3) only because the same process is effectively hidden. Both simulation types approach the same average tree heights after age ~25 (Figure 4.3).

NEP peaked at age-class 5-6 in $\mathbf{S_{unequalbin}}$, before declining non-linearly to the lowest average value in the oldest age-class (Figure 4.3). Although the unimodal peak was not apparent in $\mathbf{S_{10\text{-}yrbin}}$, the maximum NEP occurred in the youngest age-class and also declined non-linearly thereafter (Figure 4.3). The decline in NEP after a maximum at 5-6 years was driven mainly by an increase in Rh due to increases in turnover rather than a larger decline in NPP (Figure 4.4). The peak in NEP did not coincide with maximum stand density at ~20 years. Instead, model dynamics suggest that the total foliar projective cover of tree canopies reaches near maximum (80-95% cover, *not shown*) at 5-6 years, thereafter plant competition reduces NPP while biomass turnover increases, which together cause the apparent decline in NEP. The time period of canopy closure, at 5-6 years, in LPJ is probably too early, in part due to advanced regeneration (saplings establish at 1.5 m height) and constant establishment rates. Although there is room for improvement, the age module demonstrates NEP-Age relationships consistent with field-based evidence (Ryan et al. 2004, Turner 2010).

Lastly, an emergent pattern was found in the declining portion of the NEP-Age curve and approximately follows the functional form $NEPmax{*}0.70^{age-agemax}$, where *NEPmax* is the maximum NEP flux at the initial point of decline, *age* is the age of the stand, and *agemax* is the age of the stand where NEP is maximal. In plain terms, the non-linear decline in NEP is approximately 30% with increasing age. The functional equation holds between year 5-6 to year 25, after which NEP decreases only by 20% with increasing age and the functional form becomes $NEP_{25yr}*0.80^{age-25}$, where $NEP_{25yr}$ is the NEP at year 25. The functional form of the decline in NEP is consistent among climate regions when simulated data is analyzed separately for all U.S. States (*not shown*). It is unclear whether this emergent pattern is strictly the result of model dynamics around canopy closure or if the pattern would be apparent in field data. Nevertheless, it is an interesting simplification to complex age dynamics simulated by the model.

**3.1.2** *Time-series evolution of a deforestation, abandonment and regrow event*

A single event of deforestation, abandonment and subsequent forest regrowth caused long-lasting effects and unrealistic model behavior when omitting age-class dynamics. In the simulation without age-classes, $\mathbf{S_{noage\_event}}$ (Table 4.2), NEP takes ~30 years to recover to values prior the event, whereas the age-class simulation, $\mathbf{S_{age\_event}}$, takes only 5-6 years to recover (Figure 4.5) – a 5-fold change in relaxation times. The quick recovery of NEP in $\mathbf{S_{age\_event}}$ is due partly to the fact that the fraction of the grid-cell (75%) that was *not* deforested maintained its state variables (carbon stocks in vegetation, soil, litter) un-changed from its prior state, which buffered NEP and dampened the effect of the smaller fraction (25% of grid-cell) that was deforested. Age-class dynamics also contributed an elevated NEP (Figure 4.4) that quickens the recovery at the grid-cell level.

In $\mathbf{S_{age\_event}}$, there is an elevated NEP in the secondary stand that is sustained for more than 30 years following the event.

In $\mathbf{S_{noage\_event}}$, vegetation dynamics cause turnover to increase, resulting in an elevated Rh that is consistently higher than NPP for 30 years after the event; which is more striking because NPP does recover quicker than in the $\mathbf{S_{noage\_event}}$ and maintains an elevated value for ~30 yrs. The underlying mechanics of this issue is that LPJ treats plants populations using the mean-individual approximation. Following a disturbance event, stem density and foliar projective cover is reduced but the state variables of the plant populations (carbon in plant organ pools of leaf, stem, root) maintain prior values; this is the reason NPP recovers quickly in the standard-no-age simulation. As stand density increases again, canopy closure initiates competitive dynamics that result in mortality of individuals of the population that are generally larger than if the stand had progressed from small to large individuals (as in $\mathbf{S_{age\_event}}$). This model behavior is an artefact of the model structure and is clearly an unrealistic representation. This same artefact of model behavior will occur in other models that simulate competitive vegetation dynamics and also force sub-grid-cell tiles to merge so as to reduce computational load. The VTFT age-class module also uses the mean-individual approximation, but these unrealistic model dynamics are effectively dampened because stand dynamics are always allowed to occur in natural progression and the relatively small age-widths (10-yrs) ensure that stand age dynamics (NEP-Age trajectories in Figures 4.3 and 4.4) most evident in the first 50 years are discretely modeled.

### 3.2 Global Stocks, Fluxes, and Age Distribution

**3.2.1** *Stocks and fluxes – $S_{noage}$ versus $S_{FireLU}$ and convergence in global NEP.*

Carbon stocks in biomass are lower in $\mathbf{S_{age}}$ than in $\mathbf{S_{noage}}$ by ~40 Pg C globally (Figure 4.6). Greater global biomass in $\mathbf{S_{age}}$ is a byproduct of the simulated stand structure and can be explained by feedbacks from LUC and Fire that create younger age-classes that have lower overall biomass than in older stands. In addition, age dynamics cause turnover to increase (as in Figures 4.3 and 4.4), causing soil carbon to be greater by ~35 Pg C and litter carbon to be greater by 5 Pg C. Taken together, age-class dynamics cause 40 Pg C to be re-allocated from the living biomass pool to the soil-detrital pool, which compounds to alter the magnitude of fluxes from heterotrophic respiration. Demographic changes in turnover, such as these, are already known to be a large source of uncertainty among projections by global ecosystem models (Friend et al. 2014). What these numbers emphasize, however, is that uncertainty among models could be reduced by explicitly modeling age dynamics.

Net Ecosystem Exchange (NEE; positive fluxes to atmosphere) is only marginally different between $\mathbf{S_{noage}}$ and $\mathbf{S_{age}}$ simulations (mean difference of 0.25 Pg C $yr^{-1}$ over 2000-2010). Compensatory fluxes in Fire and Rh explain the small difference in NEE at global scales. Fire fluxes in $\mathbf{S_{age}}$ are lower by 0.92 Pg C $yr^{-1}$ in the 2000s than in the $\mathbf{S_{noage}}$, but fluxes from Rh are greater in $\mathbf{S_{age}}$ by 1.61 Pg C $yr^{-1}$ and NPP also greater by

0.55 Pg C $yr^{-1}$. The fluxes in Fire, Rh and NPP largely offset to minimize differences in NEE from age dynamics.

The question still remains – should there be an expectation for greater differences in NEE?, perhaps not. Consider that deforestation (areal changes prescribed the same in $\mathbf{S_{noage}}$ and $\mathbf{S_{age}}$) occurs from the oldest to youngest age-class in $\mathbf{S_{age}}$, following greater to lower overall biomass, respectively. The deforestation flux is greater in the $\mathbf{S_{age}}$ by only 0.04 Pg C $yr^{-1}$ in 2000s compared to deforestation fluxes in $\mathbf{S_{nosge}}$, which makes sense given that low-biomass age-classes are not preferentially deforested or harvested. By contrast, Fire is not prescribed in LPJ but it is simulated based on soil moisture and a minimum fuel load. It is not clear outright how age-dynamics affect soil moisture, but fluxes from fire would need to be proportional to the biomass in a patch. By definition in $\mathbf{S_{age}}$, there is explicit representation of lower-biomass patches (younger age-classes) than in $\mathbf{S_{noage}}$, and a series of fires or disturbances within the grid-cell would drive the age distribution towards younger states, exacerbating differences in downstream fluxes as well. That global NEE only changed marginally when simulating global age dynamics was a surprise, but explained by shifts in the carbon pools and compensatory fluxes the patterns appear to make sense. In light of these compensation effects, however, there is a great need to benchmark fluxes from critical feedbacks, particularly from fire in this case. It is beyond the scope of this paper to do so, and best available datasets, such as the Global Fire Emission Database (GFEDv4s; van der Werf et al. 2017) do not lend themselves to direct comparison with fire fluxes from LPJ. GFED includes fires from deforestation and land management that are tracked differently in LPJ – as a land use change flux, which cannot simply be added to the fire flux for direct comparison to GFED without double counting. In any manner, this issue is stated as a suggestion for future development and refinement.

**3.2.2** *Global age-class distribution – contribution of fire and LUCLM to age distributions*

Average ecosystem age among continents differed greatly (Figure 4.7), with large areas of old-growth forests in Asia, Europe, North and South America skewing the distribution towards older ages. The largest area of young ecosystems was located in Africa and Australia (Figure 4.1), wherein age-classes comprised an ~1:1 age to fractional area ratio of vegetated land (age-classes < 20 yrs comprise ~20% of the vegetated land area in Africa and Australia and age-classes < 40 yrs ~ 40% of vegetated land area; Figure 4.7).

The primary driver of zonal age distributions was Fire (Figure 4.8), which was responsible for a ~23 yr difference in zonal ages (Table 4.3). There was a significant decrease in zonal ecosystem age over time due to fire (Table 4.3), most likely from feedbacks due to enhanced fuel (biomass) production from $CO_2$ fertilization. The causes were not explored further because feedbacks between fire-climate-$CO_2$ are largely constrained by the fire module itself. A proper attribution to trends in fire is better suited to fire model inter-comparisons ('FireMIP' *in* Hanston et al. 2016). The emphasis here is simply that fire was a major driver of age distributions and fire-age relationships show an apparent trend over time. Between simulation years 1860 and 2016, fire caused a total change in ecosystem age, integrated over the time period, by -1.5 yrs in Boreal zones (negative values for a decrease in age), whereas the change was greater in Temperate (-6.7 yrs) and Tropical (-8.24 yrs) zonal bands (Table 4.3). The larger trend in Temperate and Tropical latitudes might be due to increasing warming temperatures in contemporary times, causing dryer conditions more suitable for fire, or from increases in fuel loads from $CO_2$ fertilization. A more convincing argument would require support from additional factorial experiments to identify to the casual driver of the trend differences.

After accounting for the effects of fire, LUCLM caused a much greater change over time in the zonal ecosystem age (Figure 4.9). Integrating from 1860 to 2016, LUCLM caused a zonal change in ecosystem age by -6.1 yrs in Boreal zones, whereas the change in ecosystem age from LUCLM in Temperate and Tropical zones was -21.6 yrs, with no significant difference in the trend due to LUCLM among these zonal bands (Table 4.3). These patterns are consistent with the concentration of deforestation in the Tropics and land use change in Temperate latitudes, as described by the forcing data (Hurtt et al. 2011, Hurtt et al. 2017).

## 3.3 Global Demographic Effects on NPP and Rh

### **3.3.1** *Simplification of LPJ via a statistical model*

The statistical model (Flux = Precipitation + Temperature + Age-class) had great predictive power for NPP and Rh, with $R^2$ between 0.95-0.98 (Figure 4.10). The predicted fluxes are at annual time scales, with annual variation being mainly driven by total annual precipitation and mean annual temperature, whereas the mean state (intercept) being predicted by the age-class. The predictive power for a model of NEP was slightly worse ($R^2$ between 0.60-0.65; SM Figure 4.1). The effect of precipitation, temperature and age-class on NEP was not consistent enough for robust predictions, but more specifically, the predictors had different effects on NPP versus Rh leading to poorer model fit. As it is, NEP is better derived as predictions of NPP minus predictions of Rh rather than having a standalone model for NEP. The fact that NPP and Rh fluxes simulated by a complex ecosystem model can be predicted by three terms will prove, as described below, to be incredibly useful for evaluating demographic effects on carbon fluxes.

### **3.3.2** *The Effective Range of Predictors – assessing relative importance of demography on predicted fluxes*

The "Effective Range of the Predictors" were mapped to visualize spatial patterns of the range of effects, given observed values for the predictors (Figure 4.11). In essence, the effective range of the predictor is a measure of the dynamic range in the predicted flux due to changes in precipitation, temperature or demography. It is calculated as the grid-cell-specific beta coefficient multiplied by the observed range of the predictor for a given grid-cell, which helps constrain the effect of the predictor on the predicted flux to realistic values. For example, for the LPJ grid-cell at location [110.75 W 50.25 N], the ß estimate for the effect of precipitation on NPP was 0.0028, and the range of observed precipitation (based on CRU TS36) was 282 mm, then the effective range of the predictor on the flux was calculated as 0.0028*282 = 0.79 kg C $m^{-2}$ $yr^{-1}$.

The effect of precipitation on NPP was clearly greater in the central USA and Eastern Australia (range of effect ~ 0.70 kg C $m^{-2}$ $yr^{-1}$ due to precipitation) than in other locations, and overall, precipitation had a stronger (positive) effect on NPP than on Rh (Figure 4.11). It was also clear from the maps that the direction of the effect of temperature on NPP was more spatially varied in the direction of effect (both positive and negative) than other predictors (Figure 4.11). The effects of precipitation and temperature displayed similar spatial patterns in both Primary and Secondary stands, which was a good sanity check because the distinction between Primary and Secondary stands is mainly to track land use histories within LPJ and there was no reason, *a priori*, that climate effects should differ substantially between the two stand types.

The effective range of demography on fluxes was generally lower than the effective range of precipitation and temperature, but there were regions where the range of demographic effects were just as important as, or greater than, the climate predictors. The demographic effect on NPP ranged between 0.30-0.60 kg C $m^{-2}$ $yr^{-1}$ in Eastern North America, Western Europe, Central Africa, Eastern China, Tropical Asia, and distributed smaller areas of South America (Figure 4.11), whereas it was at maximum ~0.10 kg C $m^{-2}$ $yr^{-1}$ in other regions. The higher demographic effect was predominately on Secondary stands (Figure 4.12), but there was also a distinct absence of Primary stands in these same areas (Figure 4.11) so it could not be said definitively if the higher demographic effect was due to a wider age distribution, and therefore a greater demographic effect, or simply due to the productivity of these locations.

### **3.3.3** *Frequency distribution of demographic effects*

The global mean demographic effect on NPP on Primary stands was 0.078 ± 0.063 [0, 1.37] kg C $m^{-2}$ $yr^{-1}$ (μ ± stdev. [min, max]), whereas on Secondary stands it was 0.160 ± 0.141 [0, 1.33] kg C $m^{-2}$ $yr^{-1}$. There were differences in the spatial distribution of Primary and Secondary stands that led to the disparity in global mean values of the demographic effect. On Primary stands, the distribution of age-classes with maximum NPP flux was skewed towards the second (11-20 yrs) age-class having the maximum NPP flux, whereas on Secondary stands, the maximum NPP flux was in the first (1-10 yrs) and also in the second age-class (Figure 4.12). Recall that the first class was categorized as 1-10 yrs, but in the presence of constant renewal, an age-class can effectively be younger than an equivalent age-class without such recurrent disturbance. Furthermore, on Primary stands, fire is the only mechanism that creates young age-classes, whereas land management also creates young age-classes on Secondary stands. It is possible for timber harvest, a form of simulated land management, to result in advanced regeneration of younger stands if harvest demand is met without ‘clear-cutting’ the prescribed fractional area under harvest. Currently, the model structure does not lend itself to say definitively the cause of the difference in the age-class of maximum flux, but the only process that differs between Primary and Secondary stands is land management, so it is reasonable to assume that land management is the cause of the difference. In any manner, global values for Age-effects for NPP on Primary and Secondary stands were also skewed towards greater values on Secondary stands, but more due to the absence of Primary stands in productive areas where Secondary stands dominated (e.g., Eastern U.S.A.).

Following a similar pattern, the demographic effects on Rh were greater on Secondary stands than on Primary stands (Figures 4.11 and 4.12), which could be partly explained by the differential coverage of Secondary and Primary stands, but also by historical land use. LUCLM leads to overall greater inputs to soil and litter carbon pools than does fire, and the latter is simulated in the same manner on Secondary stands as on Primary stands. In LPJ, timber harvest is only 60% efficient, leaving dead biomass ‘residue’ as a legacy flux. An increase of carbon in the litter and soil pools would add additional mass that can be respired during heterotrophic respiration, and which manifests as a larger demographic effect on Rh, ranging from 0.25 to 0.70 kg C $m^{-2}$ $yr^{-1}$ on the high-end (Figure 4.12).

# 4. DISCUSSION

## 4.1 Distribution of Ecosystem Age on Earth

The LPJ Age-module simulates the upper limit of age-class distributions on Earth (Figure 4.13) and captures important demographics effects on NPP and Rh. Simulations demonstrate that fire and LUCLM have been driving the latitudinal age distribution towards younger states in contemporary times (Figure 4.8), suggesting an increasing role of age dynamics on global ecosystem functioning. Whereas time is the only mechanism that increases ecosystem age, any additional disturbance not explicitly modeled in this study will decrease age.

The simulations omit widespread disturbances of windstorms, flood, pest and disease outbreak, selective logging, and other processes that would modify stand structure and function. For instance, small-scale logging activity is a dominant disturbance in South Eastern U.S.A. (Williams et al. 2016) but it is underestimated by the LUCLM driver data in this study (‘LUHv2’, Hurtt et al. 2017); otherwise the simulated age of Secondary forests in this region (~100 yrs) would be lower and closer to inventory-based age estimates of these forests (< 50 yrs; *Figure 4 in* Pan et al. 2011b). Furthermore, the fire module has been well evaluated at global scale (Thonicke et al. 2001) but it is overly simplistic (Hantson et al. 2016), so it is more likely that effects of fire are much greater than simulated in this study. It is clear then that this study underestimates disturbances rather than overestimates them, and as such, these simulations overestimate ecosystem age. But again, additional disturbances would only lead to younger age-classes, enhancing the role of age dynamics in regional and global carbon cycles.

Even with these caveats in mind, the findings presented retain utility as insight into the way age-class dynamics integrate into our broader understanding of global carbon dynamics. Ecosystem demographics likely play a larger role than suggested here, and on regional scales, demographic effects on NPP and Rh are already identified by this study as more important in East Asia, Tropical Asia, Europe, Central Africa, Eastern North America, and Tropical South America than they are in other regions, where average ecosystem ages are much older.

### 4.2 Age Dynamics Increase Turnover

In an analysis by Friend et al. (2014), it was determined that demographic processes (age-dependent mortality and turnover) influence carbon residence time (1/Turnover), which was found to be a major source of uncertainty in future projections by global ecosystem models. In this study, it was demonstrated that simulation of age-classes led to a ~40 Pg C shift from live vegetation to the soil-litter pool, effectively an increase in biomass turnover. Further, relaxation times, or the time to return to a previous state, were up to 30 yrs in the no-age simulation ($\mathbf{S_{noage\_event}}$; Figure 4.5) but relaxation times were less 10 yrs when simulating age-classes, suggesting that uncertainty in carbon residence time can be reduced by improving representation of demographics in models. Omitting age-class representation in models can leave long-lasting patterns in simulated fluxes that could inflate land use change fluxes at global scales when considering legacy fluxes from past land use change (Pongratz et al. 2014). The current state of knowledge is that fluxes from gross land use change and land management cause greater-than-expected land use fluxes (Arneth et al. 2017), but existing models that estimate the global land use flux (Arneth et al. 2017, Le Quéré et al. 2018) do not include age dynamics. If resiliency is inversely proportional to relaxation times (a quicker return to previous states is represented by shorter relaxation times, therefore greater resiliency; Pimm 1984, Tilman and Downing 1994), then instead of land use change fluxes being 'greater than assumed' (Arneth et al. 2017), we might rethink the land as being 'more resilient than expected' when demographic effects are considered at large scales.

### 4.3 Forecasting Demographic Effects with a Simplified Statistical Model

The modeling community has made increasing effort to simplify complex models using a traceability framework (Friedlingstein et al. 2006, Xia et al. 2013). Statistical emulators, from matrix models (Huang et al. 2018) to accounting-type statistical models, which track individual carbon pools (Xia et al. 2013, Ahlström et al. 2015), have been developed to reduce the dimensionality of simulated state variables. However, statistical modeling by linear regression can be a more straightforward approach, as long as the statistical model shows promise.

It was extremely satisfying then that LPJ fluxes of NPP and Rh could be predicted at annual timescales by three terms (precipitation, temperature and age-class). Part of the success of the data model came from allowing coefficients to vary by grid-cell. This allowed the intercept (age-class) term to effectively capture grid-cell level variation in soil texture (which influences soil hydrology and plant available water), PFT composition and cloud cover. Another insight was that climate and age-class had differential effects on NPP versus Rh, which makes sense and ultimately led to poorer fit of the NEP model (NEP = NPP – Rh). It might have been possible to improve upon the NPP model further by separately modeling GPP and Autotrophic Respiration (NPP = GPP – Ra) because climate might also have differential effects on GPP than on Ra, but suffice to say that the NPP statistical model was robust.

Although unexplored in this study, the spatial datasets of predictor coefficients could be used within an emulator (Xia et al. 2013, Ahlström et al. 2015) to forecast NPP and Rh, while exploring extreme climate scenarios (Reichstein et al. 2013), such as drought. Such application would allow for a much quicker exploration of scenarios and could include a more explicit treatment of uncertainty that would otherwise be too costly for the simulation model in terms of computing time. The spatial dataset of precipitation coefficients has an equivalent meaning to spatial maps of climatic sensitivity. In fact, the maps of the effective range of precipitation on NPP (Figure 4.11) show areas where the precipitation effect is largest, notably in semi-arid biomes – a biome that is known to be highly sensitive to precipitation and has been shown to play an important role in the inter-annual variability of global-scale fluxes (Poulter et al. 2014, Ahlström et al. 2015). But what if, in a given year, semi-arid biomes received their maximum annual precipitation, while every other biome received its lowest annual precipitation – can anomalously high annual precipitation and high productivity events in some regions overcome anomalously low precipitation and low productivity events in other regions? This type of question is best suited for exploration within a simplified statistical model that maintains fidelity to the process-based model because effects of climate on fluxes can be explored quicker, easier, and with a better treatment of statistical uncertainty.

## 4.2 Vector Tracking of Fractional Transitions (VTFT) – modeling age-classes in global models

Total runtime for global age-class simulations ($\mathbf{S_{age}}$) was ~8 hrs on 32 Intel Xeon CPUs, whereas runtime for the no-age simulations ($\mathbf{S_{noage}}$) was ~3 hrs. On a limited sample of single grid-cell simulations, there was a 4- to 6-fold increase in runtimes, but not all grid-cells require simultaneous tracking of every age-class so the increase in runtime of global simulations was lower than expected from per-grid-cell estimates. These runtimes are also orders of magnitude lower than other global age-class models (LPJ-GUESS takes multiple days to run global simulations using a fixed number of 100 sub-grid-cell patches; Tom Pugh, *pers. comm.*).

The VTFT approach simulated classic demographic responses in NPP and Rh (Figure 4.4), a differential in younger age-classes that led to a larger carbon sink in the youngest stands. These demographic responses are inherent within the original formulation in LPJ; that is, establishment rates and the process of self-thinning of stand density over time as plants grow and compete (for space, light, water resources) have been unchanged. In the original formulation of LPJ (prior to this study), and under a hypothetical scenario where a disturbance clears the biomass from the entire grid-cell (0.5° ~ 2,500 km$^2$), the resultant evolution of stand structure and fluxes would produce the same pattern as in the age-module, such as the Age-NPP pattern from Figure 4.4. It is often the case, however, that smaller disturbances (<< 2,500 km$^2$) occur regularly as opposed to a much larger disturbance the size of the entire grid-cell. As such, in the original formulation of LPJ, the potential benefits of demographic responses are often masked (as demonstrated in *Section 3.1.2*; Figure 4.5). One can then say that the VTFT age-module reveals intrinsic demographic responses and model behavior that would rarely emerge otherwise.

**4.3 Opportunities for Improving Modelled Age-dynamics**

There a number of opportunities for refining the age-module. The low-hanging fruit is to incorporate additional disturbances within the model, which will help simulate age distributions more consistent with inventory data (Pan et al. 2011a) and contribute to more scientifically relevant questions. Modeled disturbances need not be complex to explore their effects on age distributions, they only need to reset a fractional area to the youngest age-class. For example, windstorms from Hurricanes are known to be a large disturbance of Eastern North American forests (Dale et al. 2001). Data on Hurricane return intervals and locations of landfall in Eastern North America have been available for some time (Keim et al. 2007), and could be used to prescribe a periodic resetting of age-classes to assess the demographic effect of Hurricanes on ecosystem function. In another example, forest gaps represent areas of high production because of high resource abundance relative to the surrounding areas. The distribution of forest gaps also has a predictable power-law relationship with size of the gap (Asner et al. 2013), and this fact lends itself well for representing gaps within the framework of the current age-module; gaps can effectively be thought of as a young age-class. If forest gaps represent a constant fraction of the landscape, what is effective age of these forests in steady state? and what is the cumulative contribution of forest gaps to regional fluxes (Miller et al. 2016)? Having the model structure to track age-classes is a boon that opens doors to more scientific and management related questions.

There are limitations to the current framework of the model, which are more difficult and will require more effort in model development to overcome. In this version of the model, plant composition and competitive dynamics in young age-classes are not representative of early successional dynamics because there is a lack of plant trait variation in the current set of PFTs that could otherwise represent a wider range of growth strategies, turnover, and production (Pütz et al. 2011, Fischer et al. 2016, Miller et al. 2016). There is also no height variation within an age-class, for lack of a radiative transfer model; each age-class in this version of LPJ is an even-height stand. Demographic patterns in this study (Age-NPP, Age-Rh, relaxation times by age-class) will inevitably differ when, and if, additional trait and height variation is incorporated into the model. Such requests, or suggestions, for future development are no small task, but will lead to a model that can represent a greater range of demographic effects than in this study.

## 5. ACKNOWLEDGEMENTS

Computational efforts were performed on the Hyalite High Performance Computing System, operated and supported by University Information Technology Research Cyberinfrastructure at Montana State University. LC was supported by a National Aeronautics and Space Administration Earth and Space Science Fellowship (NASA ESSF 2016-2019). Global datasets of ecosystem ages, predictor coefficients (precipitation, temperature and age-class effects on ecosystem function), and analysis code are available at https://github.com/lcalle/VTFT_demography and stored for posterity at the Dryad Digital Repository.

## 6. LITERATURE CITED

Ahlström, A., Xia, J., Arneth, A., Luo, Y., and Smith, B.: Importance of vegetation dynamics for future terrestrial carbon cycling. *Environmental Research Letters*, doi:10.1088/1748-9326/10/5/054019, 2015.

Ahlström, A., Raupach, M. R., Schurgers, G., Smith, B., Arneth, A., Jung, M., Reichstein, M., Canadell, J. G., Friedlingstein, P., Jain, A. K., Kato, E., Poulter, B., Sitch, S., Stocker, B. D., Viovy, N., Wang, Y. P., Wiltshire, A., Zaehle, S., and Zeng, N.: The dominant role of semi-arid ecosystems in the trend and variability of the land $CO_2$ sink. *Science*, 348, 895-898, doi:10.1126/science.aaa1668, 2015.

Arneth, A., Sitch, S., J. Pongratz, Stocker, B. D., Ciais, P., Poulter, B., Bayer, A. D., Bondeau, A., Calle, L., Chini, L. P., Gasser, T., Fader, M., Friedlingstein, P., Kato, E., Li, W., Lindeskog, M., Nabel, J. E. M. S., Pugh, T. A. M., Robertson, E., Viovy, N., Yue, C., and Zaehle, S.: Historical carbon dioxide emissions caused by land-use changes are possibly larger than assumed. *Nature Geoscience*, 10, doi:10.1038/NGEO2882, 2017.

Asner, G. P., Kellner, J. R., Kennedy-Bowdoin, T., Knapp, D. E., Anderson, C., and Martin, R. E.: Forest canopy gap distributions in the Southern Peruvian Amazon. *PLoS ONE*, 8, e60875, doi:10.1371/journal.pone.0060875, 2013.

Box, E. O.: Plant functional types and climate at the global scale. *Journal of Vegetation Science*, 7, 309-320, 1996.

Earles, J. M., Yeh, S. and Skog, K. E.: Timing of carbon emissions from global forest clearance. *Nature Climate Change*, 2, 682-685, doi:10.1038/NCLIMATE1535, 2012.

Dale, V. H., Joyce, L. A., McNulty, S., Neilson, R. P., Ayres, M. P., Flannigan, M. D., Hanson, P. J., Irland, L. C., Lugo, A. E., Peterson, C. J., Simberloff, D., Swanson, F. J., Stocks, B. J., and Wotton, B. M.: Climate change and forest disturbance. *BioScience*, 51, 723-734, 2001.

Drake, J. E., Raetz, L. M., Davis, S. C., and DeLucia, E. H.: Hydraulic limitation not declining nitrogen availability causes the age-related photosynthetic decline in loblolly pine (*Pinus taeda* L.). *Plant, Cell and Environment*, 33, 1756-1766, doi:10.1111/j.1365-3040.2010.02180.x, 2010.

Drake, J. E., Davis, S. C., Raetz, L. M., and DeLucia, E. H.: Mechanisms of age-related changes in forest production: the influence of physiological and successional changes. *Global Change Biology*, 17, 1522-1535, doi:10.1111/j.1365-2486.2010.02342.x, 2011.

Eyring, V., Bony, S., Meehl, G. A., Senior, C. A., Stevens, B., Stouffer, R. J., and Taylor, K. E.: Overview of the Coupled Model Intercomparison Project Phase 6 (CMIP6) experimental design and organization. *Geoscientific Model Development*, 9, 1937-1958, doi:10.5194/gmd-9-1937-2016, 2016.

FAO-FRA. U.N. Food and Agriculture Organization 2015 Forest Resource Assessment.

Farquhar, G. D., von Caemmerer, S., and Berry, J. A.: A biochemical model of photosynthetic $CO_2$ assimilation in leaves of $C_3$ plants. *Planta*, 149, 78-90, 1980.

Fischer, R., Bohn, F., de Paula, M. D., Dislich, C., Groeneveld, J., Gutiérrez, A. G., Kazmierczak, M., Knapp, N., Lehmann, S., Paulick, S., Pütz, S., Rödig, E., Taubert, F., Köhler, P., and Huth, A.: Lessons learned from applying a forest gap model to understand ecosystem and carbon dynamics of complex tropical forests. *Ecological Modelling*, 326, 124-133, doi:10.1016/j.ecolmodel.2015.11.018, 2016.

Friend, A. D., Lucht, W., Rademacher, T. T., Keribin, R., Betts, R., Cadule, P., Ciais, P., Clark, D. B., Dankers, R., Falloon, P. D., Ito, A., Kahana, R., Kleidon, A., Lomas, M. R., Nishina, K., Ostberg, S., Pavlick, R., Peylin, P., Schaphoff, S., Vuichard, N., Warszawski, Wiltshire, A., and Woodward, F. I.: Carbon residence time dominates uncertainty in terrestrial vegetation responses to future climate and atmospheric $CO_2$. *Proceedings of the National Academies of Science of the United States of America*, 111, 3280-3285, doi:10.1073/pnas.1222477110, 2014.

Friedlingstein, P., Cox, P., Betts, R., Bopp, L., von Bloh, W., Brovkin, V., Cadule, Pl, Doney, S., Eby, M., Fung, I., Bala, G., John, J., Jones, C., Joos, F., Kato, T., Kawamiya, M., Knorr, W., Lindsay, K., Matthews, H. D., Raddatz, T., Rayner, P., Reick, C., Roeckner, E., Schnitzler, K.-G., Schnur, R., Strassmann, K., Weaver, A. J., Yoshikawa, C., and Zeng, N.: Climate-carbon cycle feedback analysis: Results from the $C^4$MIP Model Intercomparison. *Journal of Climate*, 19, 3337-3353, 2006.

Frolking, S., Palace, M. W., Clark, D. B., Chambers, J. Q., Shugart, H. H., and Hurtt, G. C.: Forest disturbance and recovery: A general review in the context of spaceborne remote sensing of impacts on aboveground biomass and canopy structure. *Journal of Geophysical Research,* 114, G00E02, doi:10.1029/2008JG000911, 2009.

Gitz, V., and Ciais, P.: Amplifying effects of land-use change on future atmospheric $CO_2$ levels. *Global Biogeochemical Cycles,* 17, 1024, doi:10.1029/2002GB001963, 2003.

Goldewijk, K. K.: Estimating global land use change over the past 300 years: The HYDE Database. *Global Biogeochemical Cycles*, 15, 417-433, 2001.

Hantson, S., Arneth, A., Harrison, S. P., Kelley, D. I., Prentice, I. C., Rabin, S. S., Archibald, S., Mouillot, F., Arnold, S. R., Artaxo, P., Bachelet, D., Ciais, P., Forrest, M., Friedlingstein, P., Hickler, T., Kaplan, J. O., Kloster, S., Knorr, W., Lasslop, G., Li, F., Mangeon, S., Melton, J. R., Meyn, A., Sitch, S., Spessa, A., van der Werf, G. R., Voulgarakis, A., and Yue, C.: The status and challenge of global fire modelling. *Biogeosciences*, 13, 335903375, doi:10.5194/bg-13-3359-2016, 2016.

Haxeltine, A., and Prentice, I. C.: A general model for the light-use efficiency of primary production. *Functional Ecology*, 10, 551-561, 1996.

Haverd, V., Smith, B., Nieradzik, L. P., and Briggs, P. R.: A stand-alone tree demography and landscape structure module for Earth system models: integration with inventory data from temperate and boreal forests. *Biogeosciences*, 11, 4039-4055, doi:10.5194/bg-11-4039-2014, 2014.

Houghton, R. A.: The annual net flux of carbon to the atmosphere from changes in land use 1850-1990. *Tellus B*, 51B, 298-313, 1999.

Huang, Y., Lu, X., Shi, Z., Lawrence, D., Koven, C. D., Xia, J., Du, Z., Kluzek, E., and Luo, Y.: Matrix approach to land carbon cycle modeling: A case study with the Community Land Model. *Global Change Biology*, 24, 1394-1404, doi:10.1111/gcb.13948, 2018.

Hurtt, G. C., Frolking, S., Fearon, M. G., Moore, B., Shevliakova, E., Malyshev, S., Pacala, S. W., and Houghton, R. A.: The underpinnings of land-use history: three centuries of global gridded land-use transitions, wood-harvest activity, and resulting secondary lands. *Global Change Biology*, 12, 1208-1229, doi:10.1111/j.1365-2486.2006.01150.x, 2006.

Hurtt, G. C., Chini, L. P., Frolking, S., Betts, R. A., Feddema, J., Fischer, G., Fisk, J. P., Hibbard, K., Houghton, R. A., Janetos, A., Jones, C. D., Kindermann, G., Kinoshita, T., Goldewijk, K. K., Riahi, K., Shevliakova, E., Smith, S., Stehfest, E., Thomson, A., Thornton, P., van Vuuren, D. P., and Wang, Y. P.: Harmonization of land-use scenarios for the period 1500-2100: 600 years of global gridded annual land-use transitions, wood harvest, and resulting secondary lands. *Climatic Change*, 109, 117-161, doi:10.1007/s10584-011-0153-2, 2011.

Hurtt G, Chini L, Sahajpal R, and Frolking S.: (2017) Harmonization of global land-use change and management for the period 850-2100, version 2. Available at luh.umd.edu/data.shtml.

Keim, B. D., Muller, R. A., and Stone, G. W.: Spatiotemporal patterns and return periods of tropical storm and hurricane strikes from Texas to Maine. *Journal of Climate*, 20, 3498-3509, doi:10.1175/JCLI4187.1, 2007.

Kondo, M., Ichii, K., Patra, P. K., Poulter, B., Calle, L., Koven, C., Pugh, T. A. M., Kato, E., Harper, A., Zaehle, S., and Wiltshire, A.: Plant regrowth as a driver of recent enhancement of terrestrial CO2 uptake. *Geophysical Research Letters*, 45, 4820-4830, doi:10.1029/2018GL077633, 2018.

Lawrence, D.M., Fisher, R.A., Koven, C.D., Oleson, K.W., Swenson, S.C., Vertenstein, M., Andre, B., Bonan, G., Ghimire, B., van Kampenhout, L., Kennedy, D., Kluzek, E., Knox, R., Lawrence, P. J., Li, F., Li, H., Lombardozzi, D., Lu, Y., Perket, J., Riley, W.J. Sacks, W.J., Shi, M., Wieder, W.R., Xu, C., Ali, A., Badger, A., Bisht, G., Broxton, P., Brunke, M., Buzan, J., Clark, M., Craig, A., Dahlin, K., Drewniak, B., Fisher, J. B., Flanner, M., Gentine, P., Lenaerts, J., Levis, S., Leung, L. R., Lipscomb, W. H., Pelletier, J. D., T., Ricciuto, D. M., Sanderson, B. M., Shuman, J., Slater, A., Subin, Z., Tang, J., Tawfik, A., Thomas, R. Q., Tilmes, S., Vitt, F., and Zeng, X.: Technical description of version 5.0 of the Community Land Model (CLM). The National Center for Atmospheric Research, 2019.

Le Quéré, C., Andrew, R. M., Friedlingstein, P., Sitch, S., Pongratz, J., Manning, A. C., Korsbakken, J. I., Peters, G. P., Canadell, J. G., Jackson, R. B., Boden, T. A., Tans, P. P., Andrews, O. D., Arora, V. K., Bakker, D. C. E., Barbero, L., Becker, M., Betts, R. A., Bopp, L., Chevallier, F., Chini, L. P., Ciais, P., Cosca, C. E., Cross, J., Currie, K., Gasser, T., Harris, I., Hauck, J., Haverd, V., Houghton, R. A., Hunt, C. W., Hurtt, G. C., Ilyina, T., Jain, A. K., Kato, E., Kautz, M., Keeling, R. F., Goldewijk, K. K., Körtzinger, Landschützer, P., Lefèvre, N., Lenton, A., Lienert, S., Lima, I., Lombardozzi, D., Metzl, N., Millero, F., Monteiro, P. M. S., Munro, D. R., Nabel, J. E. M. S., Nakaoka, S., Nojiri, Y., Padin, X. A., Peregon, A., Pfeil, B., Pierrot, D., Poulter, B., Rehder, G., Reimer, J., Rödenbeck, C., Schwinger, J., Séférian, R., Skjelvan, I., Stocker, B. D., Tian, H., Tilbrook, B., Tubiello, F. N., van der Laan-Luijkx, I. T., van der Werf, G. R., van Heuven, S., Viovy, N., Vuichard, N., Walker, A. P., Watson, A. J., Wiltshire, A. J., Zaehle, S. & Zhu, D.: Global Carbon Budget. *Earth System Science Data*, 10, 405-448, doi:10.5194/essd-10-405-2018, 2018.

McGuire, A. D., Sitch, S., Clein, J. S., Dargaville, R., Esser, G., Foley, J., Heimann, M., Joos, F., Kaplan, J., Kicklighter, D. W., Meier, R. A., Melillo, J. M., Moore III, B., Prentice, I. C., Ramankutty, N., Reichenau, T., Schloss, A., Tian, H., Williams, L. J., and Wittenberg, U.: Carbon balance of the terrestrial biosphere in the twentieth century: Analyses of $CO_2$, climate and land use effects with four process-based ecosystem models. *Global Biogeochemical Cycles*, 15, 183-206, 2001.

Medvigy, D., Wofsy, S. C., Munger, J. W., Hollinger, D. Y., and Moorcroft, P. R.: Mechanistic scaling of ecosystem function and dynamics in space and time: Ecosystem Demography model version 2. *Journal of Geophysical Research*, 114, G01002, doi:10.1029/2008JG000812, 2009.

Miller, A. D., Dietze, M. C., DeLucia, E. H., and Anderson-Teixeira, K. J.: Alteration of forest succession and carbon cycling under elevated $CO_2$. *Global Change Biology*, 22, 351-363, doi:10.1111/gcb.13077, 2016.

Nachtergaele, F., Van Velthuizen, H., Verelst, L., Batjes, N., Dijkshoorn, K., Van Engelen, V., Fischer, G., Jones, A., Montanarella, L., and Petri, M.: Harmonized world soil database, FAO, Rome, Italy and IIASA, Laxenburg, Austria, 2008.

Odum, E. P.: The strategy of ecosystem development. *Science* 164:262-270, 1969.

Pan, Y., Chen, J. M., Birdsey, R., McCullough, K., He, L, and Deng, F.: Age structure and disturbance legacy of North American forests. *Biogeosciences*, 8, 715-732, doi:10.5194/bg-8-715-2011, 2011a.

Pan, Y., Birdsey, R. A., Fang, J., Houghton, R., Kauppi, P. E., Kurz, W. A., Phillips, O. L., Shvidenko, A., Lewis, S. L., Canadell, J. G., Ciais, P., Jackson, R. B., Pacala, S. W., McGuire, A. D., Piao, S., Rautiainen, A., Sitch, S., and Hayes, D.: A large and persistent carbon sink in the world's forests. *Science*, 333, 988-993, 2011b.

Pimm, S. L.: The complexity and stability of ecosystems. *Nature*, 307, 321-326, 1984.

Pongratz, J., Reick, C. H., Houghton, R. A., and House, J. I.: Terminology as a key uncertainty in net land use and land cover change carbon flux estimates. *Earth System Dynamics*, 5, 177-195, doi:10.5194/esd-5-177-2014, 2014.

Potter, C., Tan, P.-N., Steinbach, M., Klooster, S., Kumar, V., Myneni, R., and Genovese, V.: Major disturbance events in terrestrial ecosystems detected using global satellite data sets. *Global Change Biology*, 9, 1005-1021, 2003.

Poulter, B., Frank, D., Ciais, P., Myneni, R. B., Andela, N., Bi, J., Broquet, G., Canadell, J. G., Chevallier, F., Liu, Y. Y., Running, S. W., Sitch, S., and van der Werf, G. R.: Contribution of semi-arid ecosystems to interannual variability of the global carbon cycle. *Nature*, 509, 600-603, doi:10.1038/nature13376, 2014.

Pretzsch, H., and Biber, P.: A re-evaluation of Reineke's Rule and stand density index. *Forest Science*, 51, 304-320, 2005.

Pretzsch, H., Grote, R., Reineking, B., Rötzer, TH., and Seifert, ST.: Models for Forest Ecosystem Mangement: A European Perspective. *Annals of Botany*, 101, 1065-87, doi:10.1093/aob/mcm246, 2008.

Pugh, T. A. M., Lineskog, M., Smith, B., Poulter, B., Arneth, A., Haverd, V., and Calle, L.: Role of forest regrowth in global carbon sink dynamics. *Proceedings of the National Academies of Science of the United States of America*, doi:10.1073/pnas.1810512116, 2019.

Pütz, S., Groeneveld, J., Alves, L. F., Metzger, J. P., and Huth, A.: Fragmentation drives tropical forest fragments to early successional states: A modelling study for Brazilian Atlantic forests. *Ecological Modelling*, 222, 1986-1997, doi:10.1016/j.ecolmodel.2011.03.038, 2011.

Reichstein, M., Bahn, M., Ciais, P., Frank, D., Mahecha, M. D., Seneviratne, S. I., Zscheischler, J., Beer, C., Buchmann, N., Frank, D. C., Papale, D., Rammig, A., Smith, P., Thonicke, K., van der Velde, M., Vicca, S., Walz, A., and Wattenbach, M.: Climate extremes and the carbon cycle. *Nature*, 500, 287-295, doi:10.1038/nature12350, 2013.

Ryan, M. G., Binkley, D., Fownes, J. H., Giardina, C. P., and Senock, R. S.: An experimental test of the causes of forest growth decline with stand age. *Ecological Monographs*, 74, 393-414, 2004.

Shevliakova, E., Pacala, S. W., Malyshev, S., Hurtt, G. C., Milly, P. C. D., Caspersen, J. P., Sentman, L. T., Fisk, J. P., Wirth, C., and Crevoisier, C.: Carbon cycling under 300 years of land use change: Importance of the secondary vegetation sink. *Global Biogeochemical Cycles*, 23, GB2022, doi:10.1029/2007GB003176, 2009.

Sitch, S., Smith, B., Prentice, I. C., Arneth, A., Bondeau, A., Cramer, W., Kaplan, J. O., Levis, S., Lucht, W., Sykes, M. T., Thonicke, K., and Venevsky, S.: Evaluation of ecosystem dynamics, plant geography and terrestrial carbon cycling in the LPJ dynamic global vegetation model. *Global Change Biology*, 9, 161-185, 2003.

Stephenson, N. L., Das., A. J., Condit, R., Russo, S. E., Baker, P. J., Beckman, N. G., Coomes, D. A., Lines, E. R., Morris, W. K., Rüger, N., Alvarez, E., Blundo, C., Bunyavejchewin, S., Chuyong, G., Davies, S. J., Duque, A., Ewango, C. N., Flores, O., Franklin, J. F., Grau, H. R., Hao, Z., Harmon, M. E., Hubbell, S. P., Kenfack, D., Lin, Y., Makana, J.-R., Malizia, A., Malizia, L. R., Pabst, R. J., Pongpattananurak, N., Su, S.-H., Sun, I-F., Tan, S., Thomas, D., van Mantgem, P. J., Wang, X., Wiser, S. K., and Zavala, M. A.: Rate of tree carbon accumulation increases continuously with tree size. *Nature*, 507, 90-93, doi:10.1038/nature12914, 2014.

Stocker, B. D., Feissli, F., Strassmann, K. M., Spahni, R., and Joos, F.: Past and future carbon fluxes from land use change, shifting cultivation and wood harvest. *Tellus B*, 66, 23188, http://dx.doi.org/10.3402/tellusb.v66.23188,2014.

Thonicke, K., Venevsky, S., Sitch, S., and Cramer, W.: The role of fire disturbance for global vegetation dynamics: coupling fire into a Dynamic Global Vegetation Model. *Global Ecology & Biogeography*, 10, 661-677, 2001.

Tilman, D., and Downing, J. A.: Biodiversity and stability in grasslands. *Nature*, 367, 363-365, 1994.

Turner, M. G.: Disturbance and landscape dynamics in a changing world. *Ecology*, 91, 2833-2849, 2010.

van der Werf, G. R., Randerson, J. T., Giglio, L., van Leeuwen, T. T., Chen, Y., Rogers, B. R., Mu, M., van Marle, M. J. E., Morton, D. C., Collatz, G. J., Yokelson, R. J., and Kasibhatla, P. S.: Global fire emissions estimates during 1997-2016. *Earth System Science Data*, 9, 697-720, doi:10.5194/essd-9-697-2017, 2017.

Williams, C A., Gu, H., MacLean, R., Masek, J. G., and Collatz, G. J.: Disturbance and the carbon balance of US forests: A quantitative review of impacts from harvests, fires, insects, and droughts. *Global and Planetary Change*, 143, 66-80, doi:10.1016/j.gloplacha.2016.06.002, 2016.

Yue, C., Ciais, P., Luyssaert, S., Li, W., McGrath, M. J., Chang, J., and Peng, S.: Representing anthropogenic gross land use change, wood harvest and forest age dynamics in a global vegetation model ORCHIDEE-MICT v8.4.2. *Geoscientific Model Development*, 11, 409–428, https://doi.org/10.5194/gmd-11-409-2018, 2018.

Xia, J., Luo, Y., Wang, Y.-P., and Hararuk, O.: Traceable components of terrestrial carbon storage capacity in biogeochemical models. *Global Change Biology*, 19, 2104–16, 2013.

**Table 4.1. Age-class widths corresponding to two different simulation age-class setups in LPJ. The age-class codes are referenced in Figures.**

| | *Age-Widths (years)* | |
|---|---|---|
| **Code** | **Unequal Bins** | **10-yr Equal Bins** |
| 1 | 1-2 | 1-10 |
| 2 | 3-4 | 11-20 |
| 3 | 5-6 | 21-30 |
| 4 | 7-8 | 31-40 |
| 5 | 9-10 | 41-50 |
| 6 | 11-15 | 51-60 |
| 7 | 16-20 | 61-70 |
| 8 | 21-25 | 71-80 |
| 9 | 26-50 | 81-90 |
| 10 | 51-75 | 91-100 |
| 11 | 76-100 | 101-150 |
| 12 | +101 | +151 |

**Table 4.2. Description of LPJ simulations in this study, corresponding objectives and related science questions. Land Use Change and Land Management (LUCLM, LU).**

| Simulation | Description | Objective and Questions | *Structure/Processes Included* Age-classes | Fire | LUCLM |
|---|---|---|---|---|---|
| *Single-cell* | | | | | |
| $\mathbf{S_{age\_event}}$ | Idealized simulations of a deforest, abandon, and regrow event in British Columbia, CAN [121.25W 57.25N] | Evaluate recovery dynamics of a single regrow event. Do age dynamics influence relaxation times? | ✓ | ✓ | ✓ |
| $\mathbf{S_{noage\_event}}$ | | | *x* | ✓ | ✓ |
| *Regional* | | | | | |
| $\mathbf{S_{unequalbin}}$* | Idealized simulation with 5% of grid-cell cleared annually to create a wide age-class distribution in mixed broadleaf and evergreen temperate forests of Michigan (MI), Minnesota, and Wisconsin (WI) of U.S.A. | Does the model capture 'classic' demographic patterns in stand structure (tree density and height) and function (NEP, NPP, Rh)? | ✓* | *x* | *x* |
| $\mathbf{S_{10yrbin}}$‡ | | | ✓‡ | *x* | *x* |
| *Global* | | | | | |
| $\mathbf{S_{noage}}$ | Standard-forcing factorial simulations at global scale. | Do age dynamics influence global stocks and fluxes? | *x* | ✓ | ✓ |
| $\mathbf{S_{Fire}}$ | | What is the relative contribution of Fire and LU to ecosystem age? | ✓ | ✓ | *x* |
| $\mathbf{S_{LU}}$ | | Are demographic effects evident in fluxes, and where is the effect greatest? | ✓ | *x* | ✓ |
| $\mathbf{S_{FireLU}}$ ($\mathbf{S_{age}}$) | | What is the relative contribution of climate versus demography on fluxes? | ✓ | ✓ | ✓ |

* unequal age-width simulation. Age-widths as described in Table 4.1

‡ 10-yr interval age-width simulation. Age-widths as described in Table 4.2

**Table 4.2. Linear trend statistics by zonal band from LPJ simulations, based on model (age = $\beta 0 + \beta 1$*year) where year at 1860 is indexed at 1. Coefficients listed as $\mu \pm$ S.E. All d.f. are 113 and $p < 0.001$.**

| Zonal Band | Simulation | $\beta 0$ | $\beta 1$ | $R^2$ |
|---|---|---|---|---|
| Boreal | Fire Only (**$S_{Fire}$**) | 141.7 ± 0.01 | -0.0098 ± 0.0002 | 0.95 |
| | Fire and LUCLM (**$S_{FireLU}$**) | 139.7 ± 0.13 | -0.0388 ± 0.0019 | 0.78 |
| Temperate | Fire Only (**$S_{Fire}$**) | 118.5 ± 0.05 | -0.0525 ± 0.0008 | 0.98 |
| | Fire and LUCLM (**$S_{FireLU}$**) | 112.6 ± 0.21 | -0.1383 ± 0.0032 | 0.94 |
| Tropics | Fire Only (**$S_{Fire}$**) | 95.9 ± 0.06 | -0.0429 ± 0.0009 | 0.95 |
| | Fire and LUCLM (**$S_{FireLU}$**) | 88.9 ± 0.16 | -0.1382 ± 0.0024 | 0.97 |

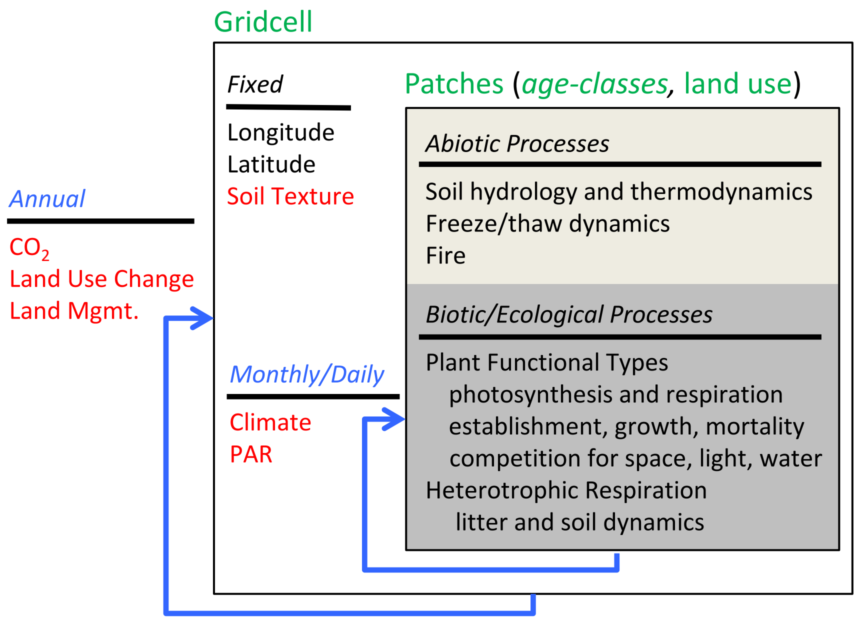


**Figure 4.1. LPJ model structure of inputs (red), time-steps (blue) and the level at which state variables are tracked within grid-cells and sub-grid-cell patches (green), such as age-classes or land uses. Simulation of abiotic, biotic and ecological processes occurs at the scale of a patch.**

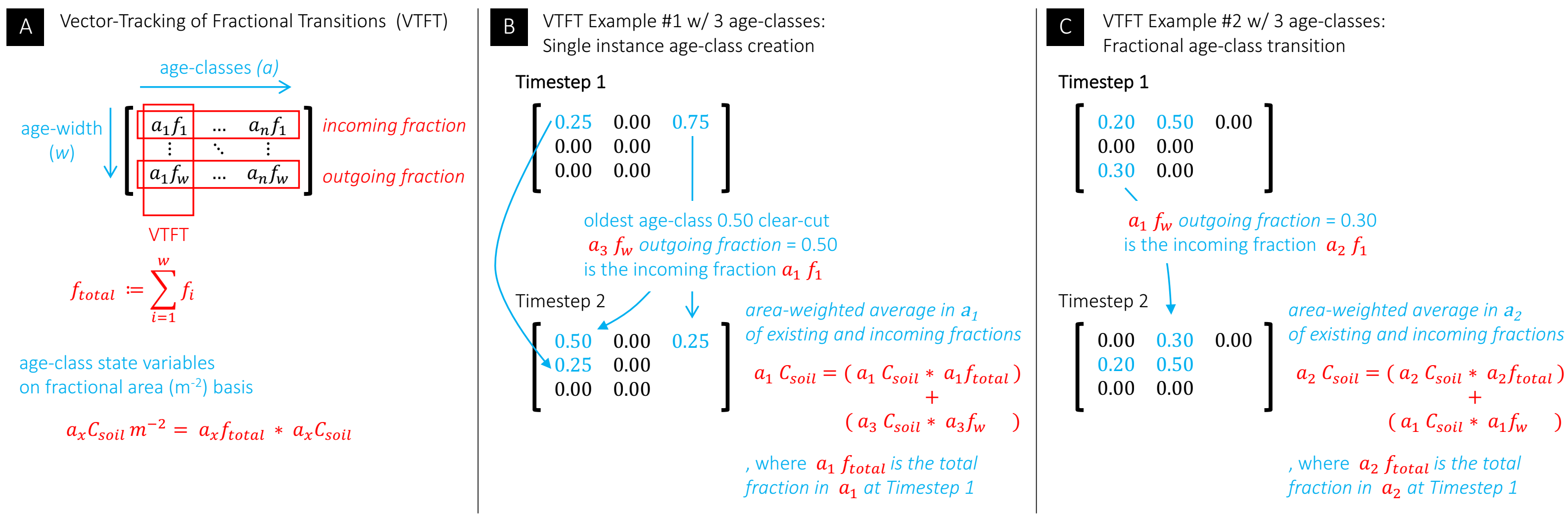


**Figure 4.2. Methodological examples of the matrix based method called Vector-Tracking of Fractional Transitions for computationally-efficient simulation of age-classes in large-scale models. (a) Hypothetical matrix of VTFT vectors of fractional areas (*f*). The total area of the age-class is the sum of the fractional areas in the corresponding VTFT vector. State variables are calculated on area basis by accounting for the fractional area of the age-class, in this example $C_{soil}$ is the carbon in soil. (b) An example of the VTFT method for a newly created age-class by clear-cut timber harvest. An area-weighted average updates age-class state variables in the youngest age-class using the preceding total fractional area of the age-class and the incoming fraction. (c) A VTFT example for a fractional age-class transition. An area-weighted average updates state variables in an age-class using the preceding total fractional area of the age-class and the incoming fraction from the younger age-class.**

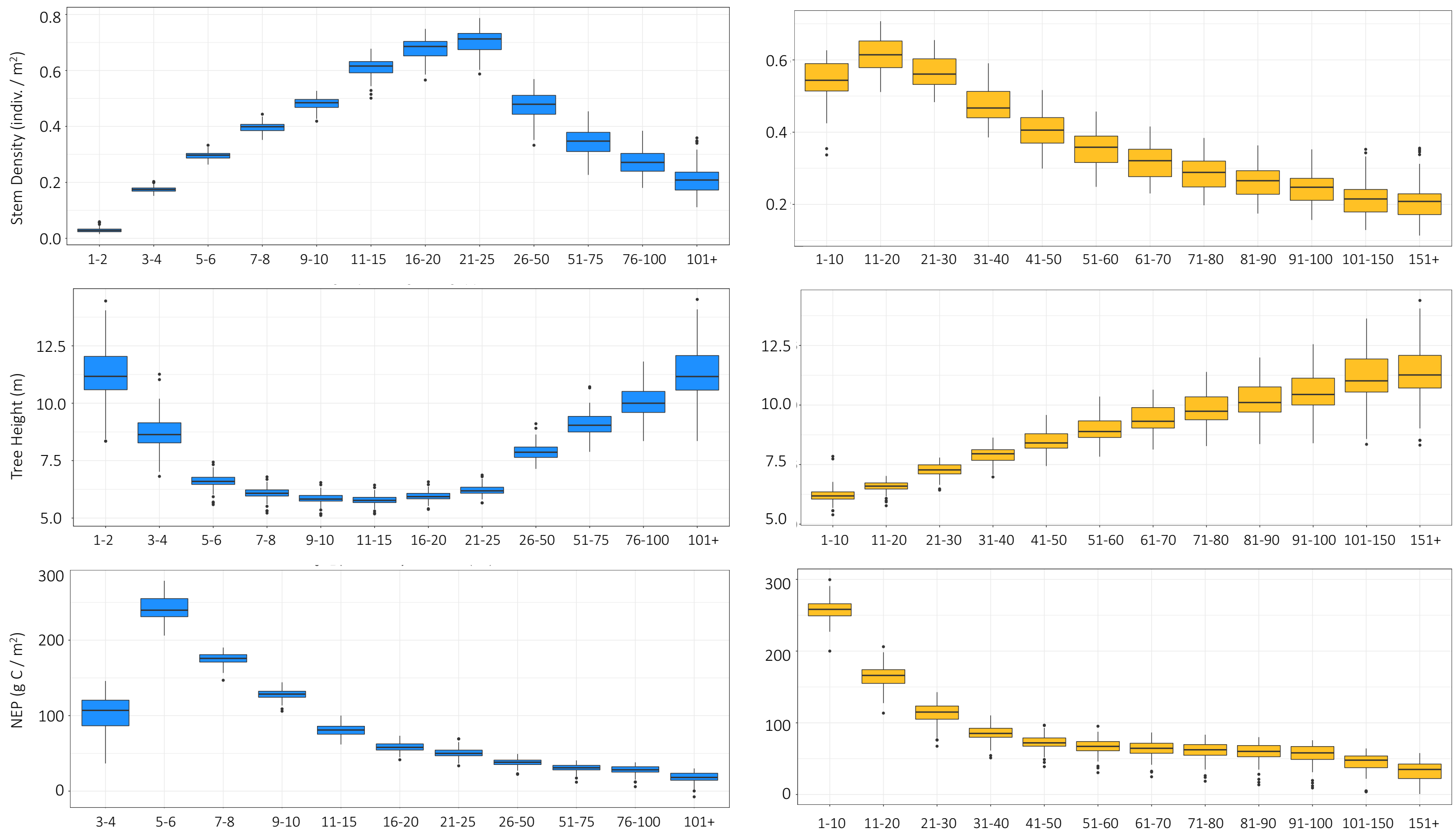


**Figure 4.3. Boxplots by age-classes (x-axis, *in years*) from LPJ simulations for MI, MN, WI. (blue, left) Age-classes defined with *unequalbin* age widths (Table 4.1); small age-widths in the youngest age-classes towards progressively larger width age classes. Density peaks in the 21-25 year age-class and NEP peaks in the 5-6 year age-class. For average tree height (middle row), large tree height in the youngest age-class represents the 'survivor' trees; average tree height decreases as the density of establishing saplings increases. (gold, right) Age-classes in *10-yr-equalbin* age-widths (Table 4.1), the standard age-class setup used in global age-class simulations. Peaks in Density and NEP roughly follow the age-class patterns when finer age-widths are employed (blue, left).**

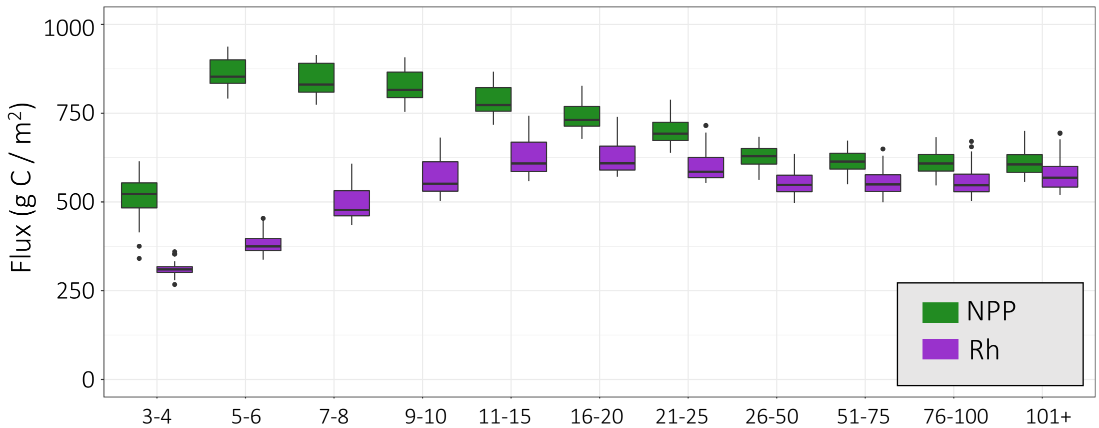


**Figure 4.4. Boxplots of NPP and Rh by age-classes (x-axis, *in years*) from LPJ simulations for U.S. States MI, MN, WI. Age-classes defined with *unequabinl* age widths (Table 4.1); small age-widths in the youngest age-classes towards progressively larger age-widths.**

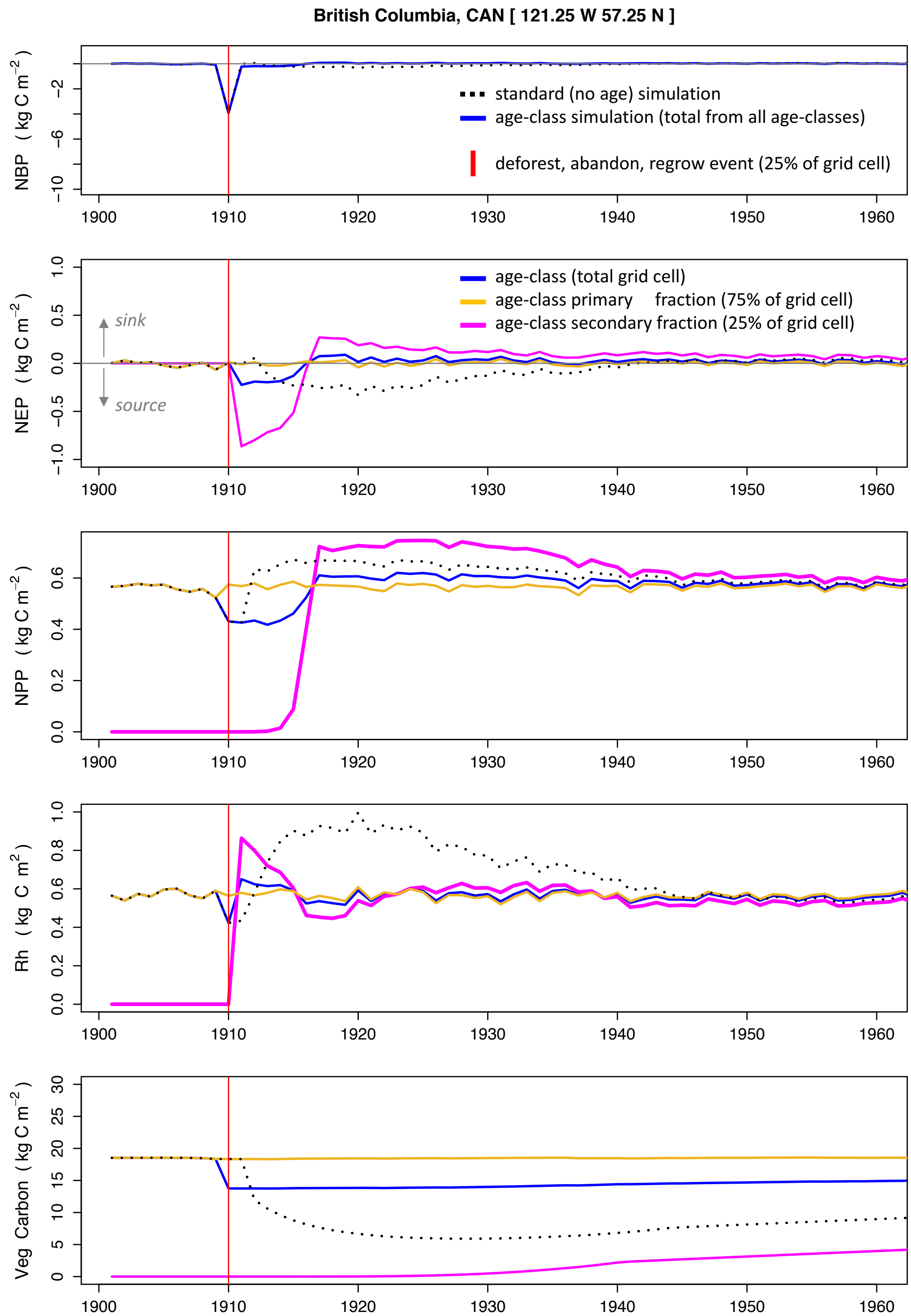


**Figure 4.5. A time-series comparison between the standard LPJ simulation ($S_{noage\_event}$) and the age-class approach ($S_{age\_event}$) in an idealized single-cell simulation of a deforestation, abandonment, and subsequent regrow event. x-axis is the simulation year. See Table 4.2 for simulation details.**

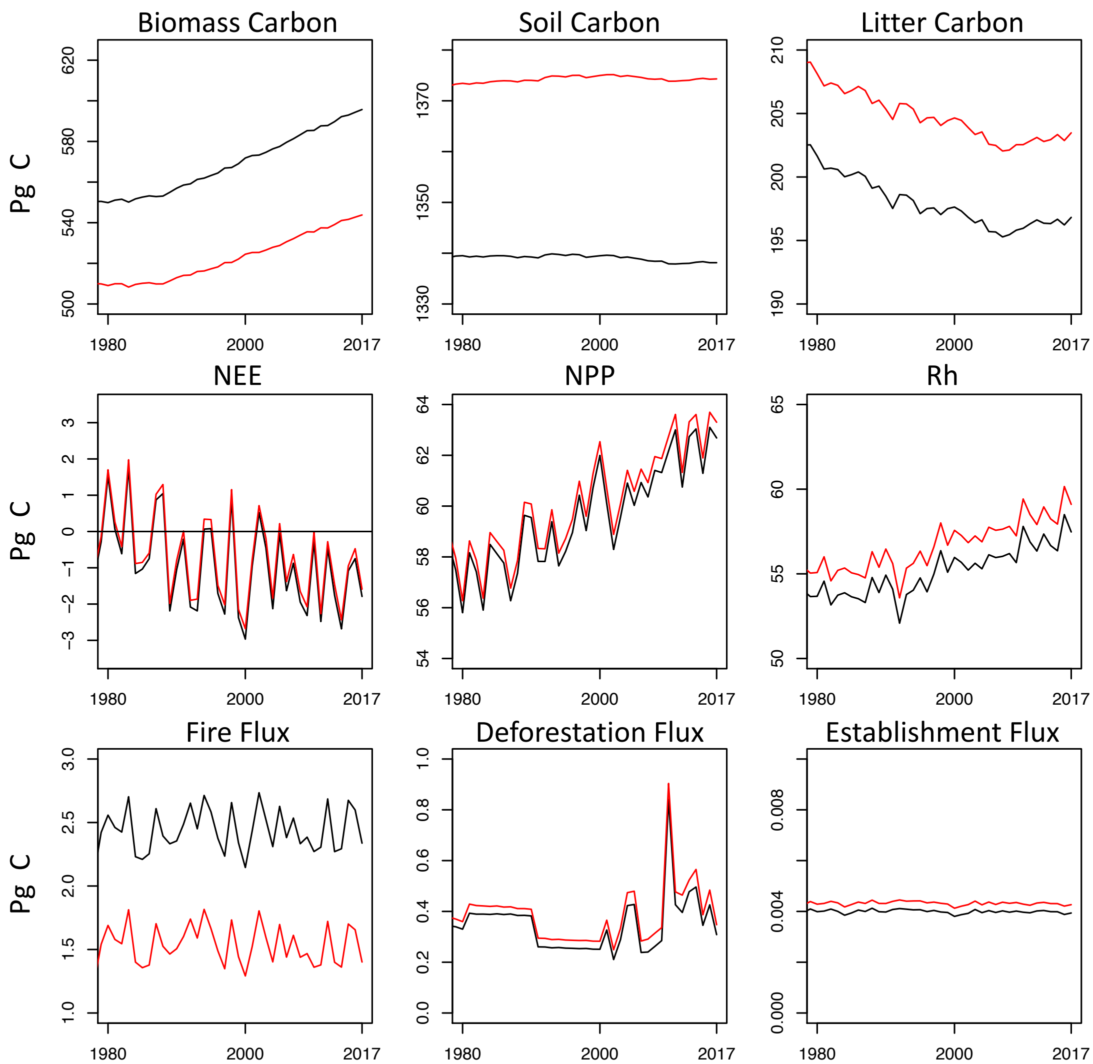


**Figure 4.6. Time-series of global carbon stocks and fluxes from LPJ simulation *without* age-classes (black lines) compared against simulations *with* age-classes (red).**

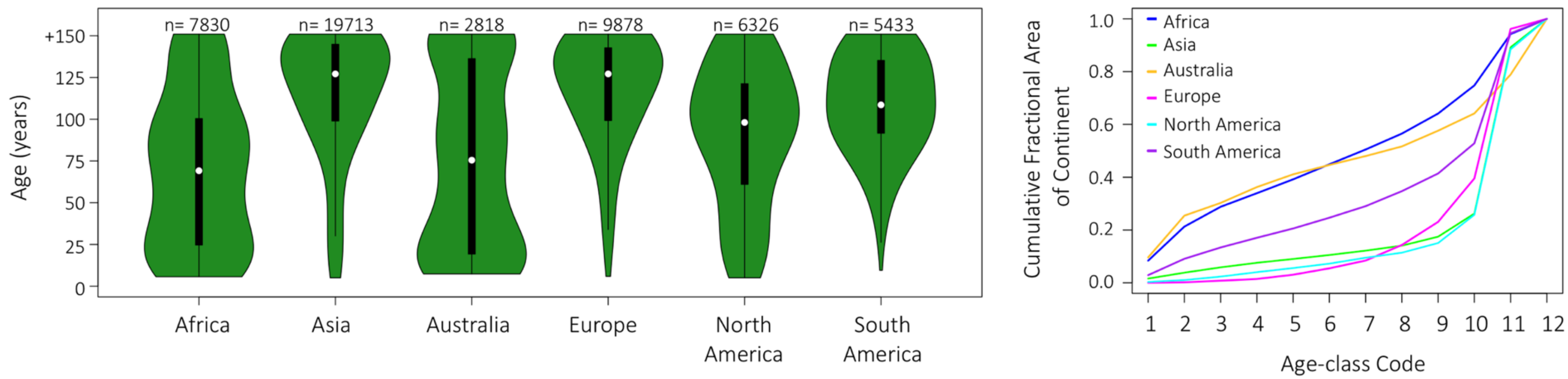


**Figure 4.7. Age-class distributions by Continent. (left) Violin plots of Ecosystem Age by continent averaged over 2000-2010, based on LPJ simulations. Violin plots show the distribution of data points (green), interquartile range (black box) and the median value (white circle). The number of vegetated 0.5° grid-cells in each continent are above plot. (right) Cumulative fractional area in continent by age-classes. Age-class codes, lowest (youngest) to greatest (oldest), correspond to the *10-yr-equalbin* age-class setup (Table 4.1).**

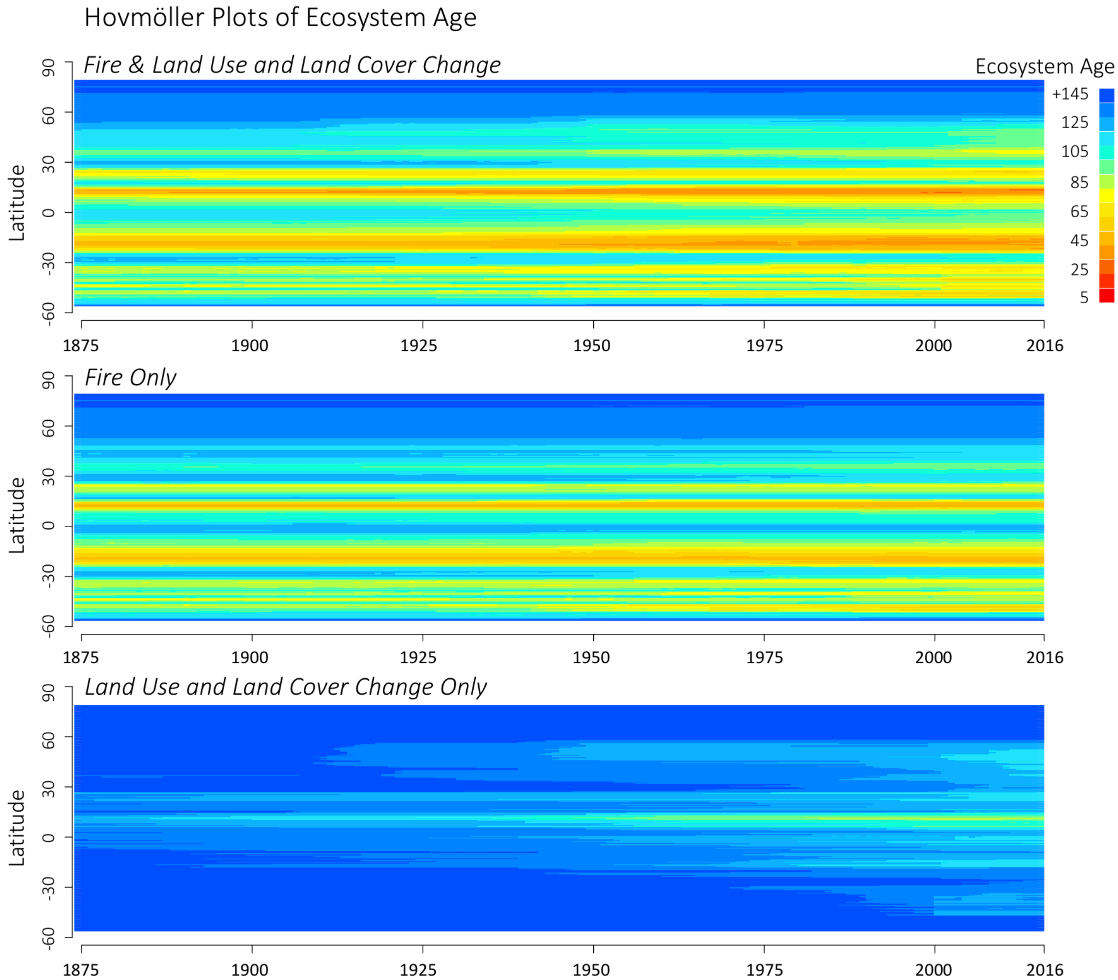


**Figure 4.8. Zonal Ecosystem Age versus year based on LPJ simulations using full forcing (top), only fire (middle), or only land use and land cover change (only).**

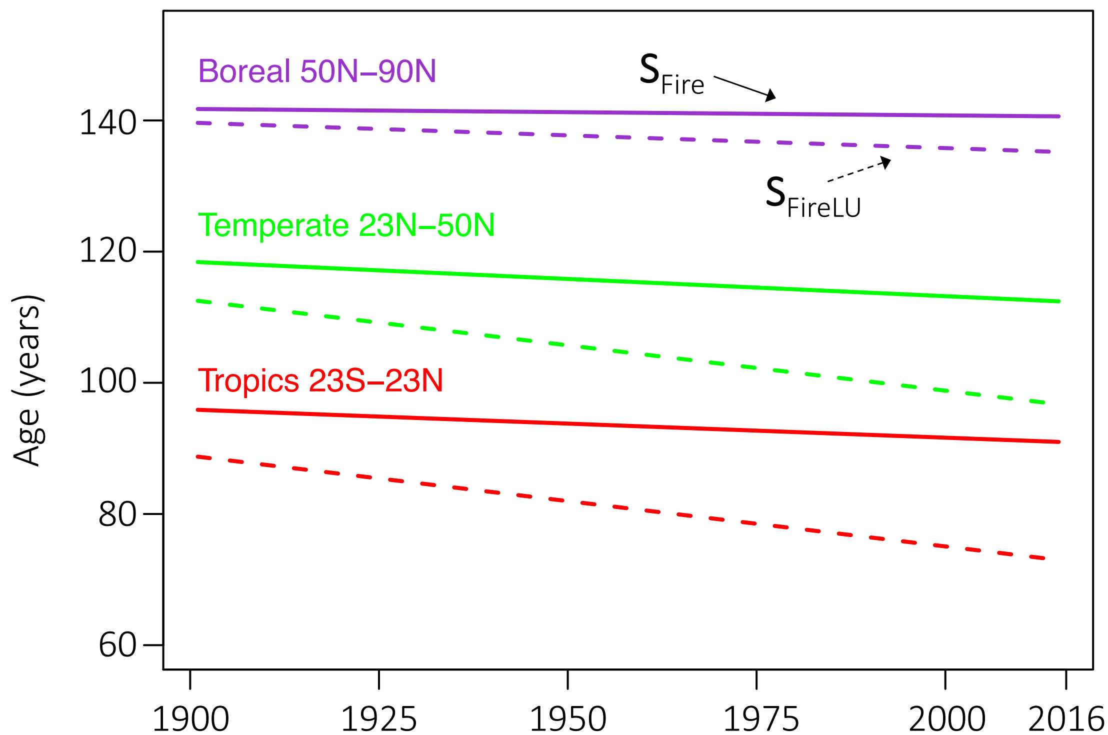


**Figure 4.9. Trend in Ecosystem Age by zonal band for LPJ simulation with only Fire ($S_{Fire}$, solid lines) and with both Fire and LUCLM ($S_{FireLU}$, dashed lines). Fire causes zonal bands to differ in ecosystem age by ~23 years, and decreases the average age by 0.009 to 0.054/yr. LUCLM decreased ecosystem age at rates up to 3-times the rate of fire, from 0.038/yr in Boreal zones to 0.138/yr in Temperate and Tropical zones.**

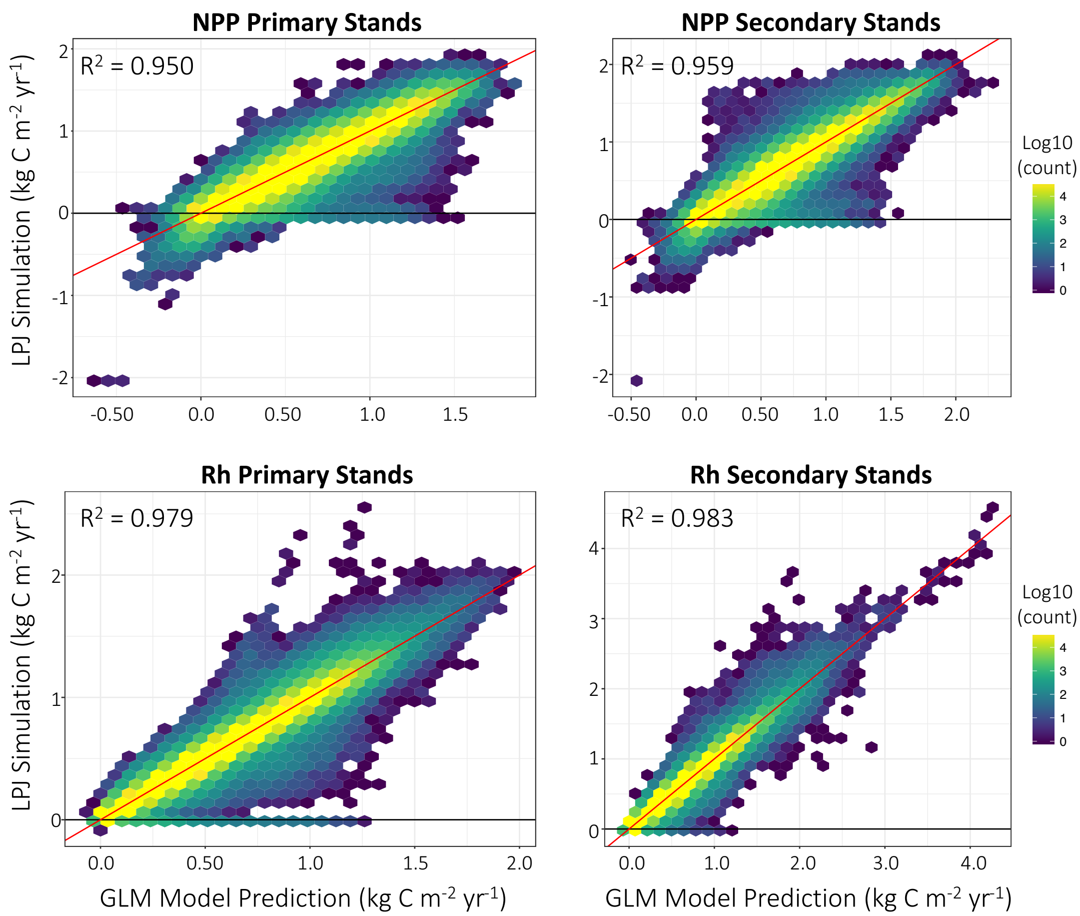


**Figure 4.10. Annual fluxes (NPP, Rh) (2000-2017) from LPJ Simulations versus Predictions of LPJ Fluxes based on a Generalized Linear Model (Flux = Precipitation + Temperature + Age-class); coefficients were allowed to vary by grid-cell, in essence, reducing the effect of variation in plant composition, soil texture and hydrology. Coloring is by density of grid-cells on a log scale; diagonal red line is the 1:1 correspondence line. The simplified statistical model is can simplify the dynamics in the global vegetation model, with coefficients from the GLM helping to determine the relative importance of a small set of predictors.**

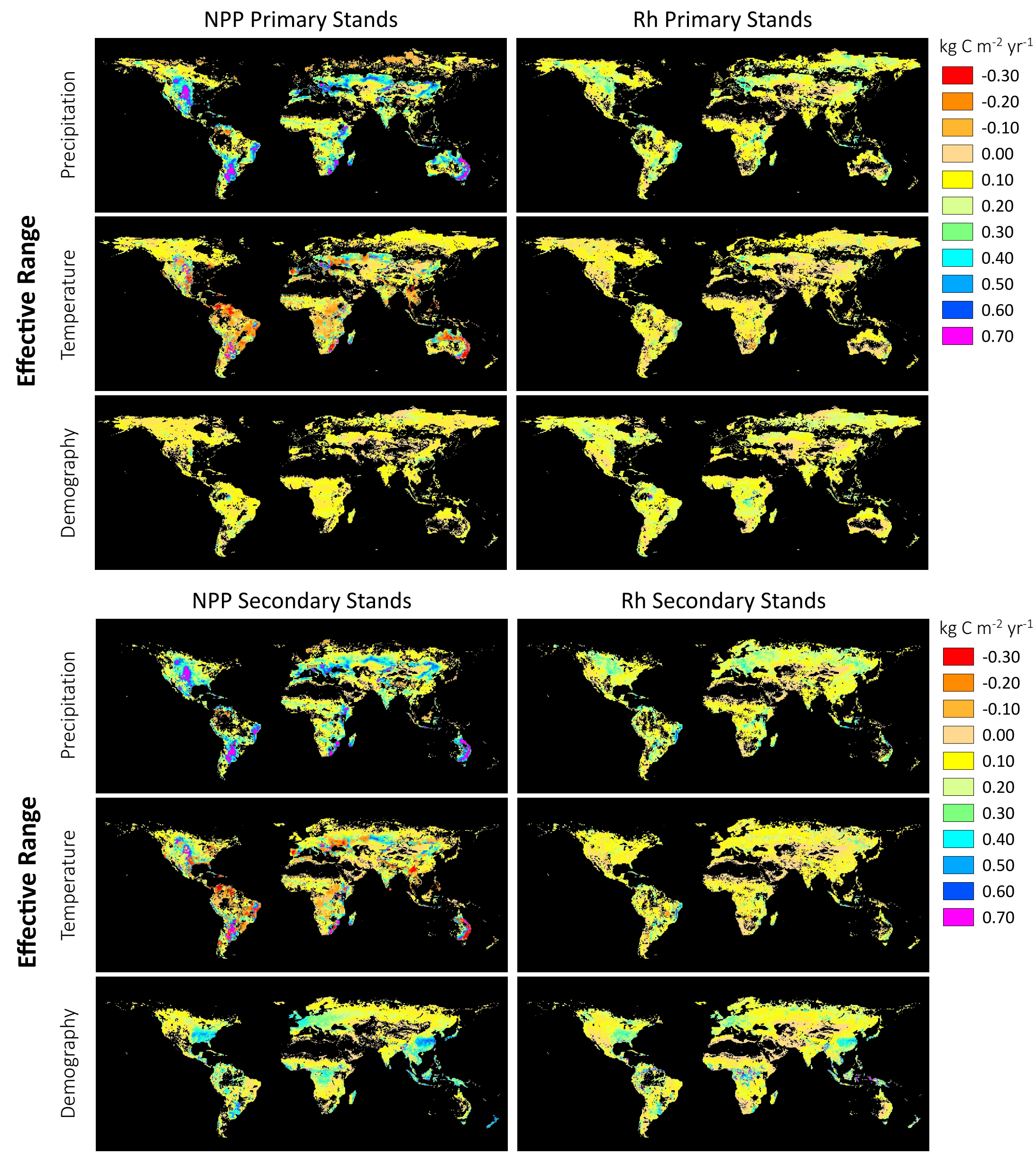


**Figure 4.11. Global maps of the Effective Range of the Predictors (precipitation, temperature, demography) on LPJ Fluxes (NPP, Rh); black is zero values or no-data. The Effective Range of the predictor is calculated as the grid-cell-specific beta (ß) coefficient multiplied by the observed range of the predictor variable for the grid-cell, for years 2000-2017. Units are on the scale of the predicted flux (kg C m$^{-2}$ yr$^{-1}$). In these maps, an emphasis is placed on the effective range of the predictor rather than the absolute value of the coefficient, although these too can be mapped for forecasting purposes. See *Sect 3.3 Climate Sensitivity* for methodological details.**

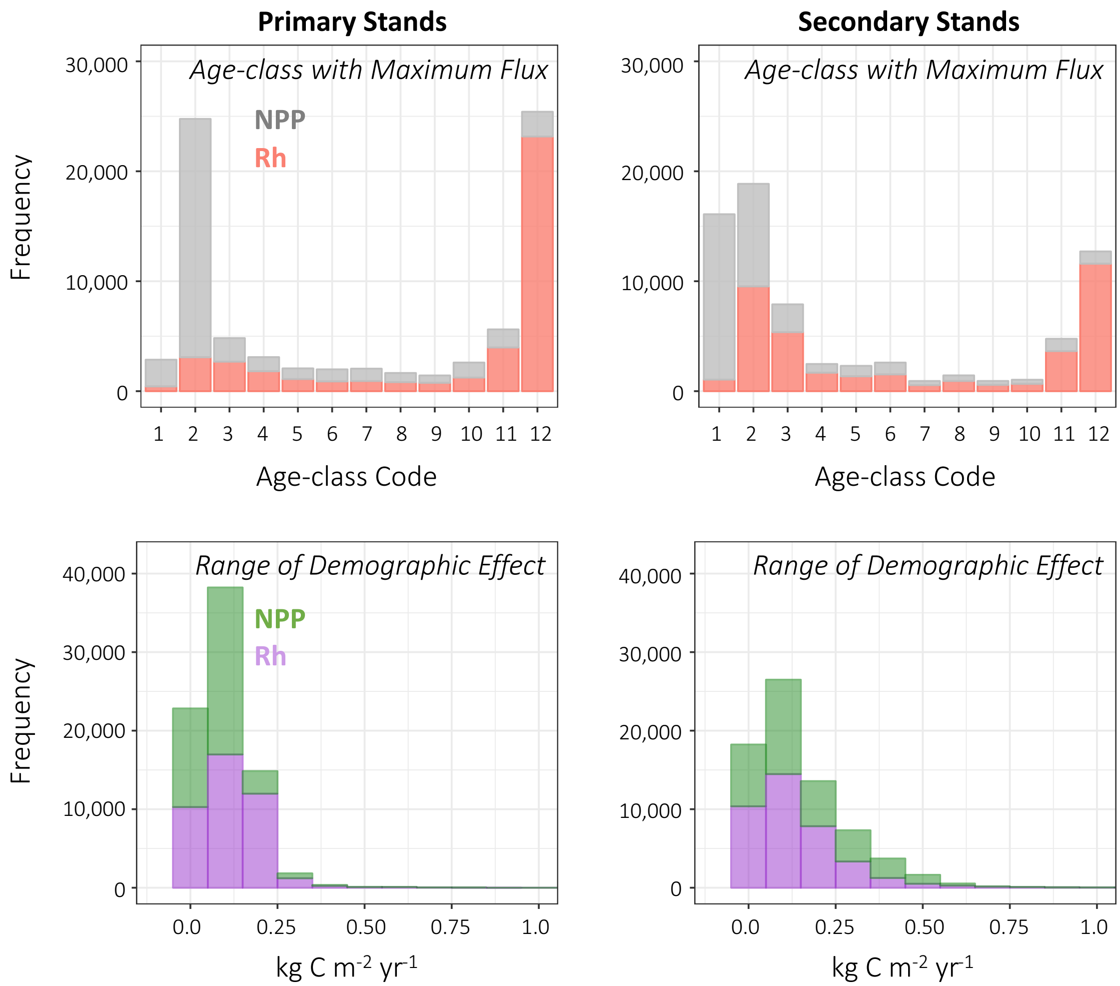


**Figure 4.12. Stacked frequency plots for NPP, Rh on Primary and Secondary stands. (top row) Global frequency of age-classes with the largest flux (NPP, Rh), relative to other age-classes in the grid-cell. Age-class codes, lowest (youngest) to greatest (oldest), correspond to the *10-yr-equalbin* age-class setup (Table 4.1). (bottom row) Global frequency of the range of the demographic effect on fluxes, bin width is 0.10 kg C $m^{-2}$ $yr^{-1}$. An example interpretation, on Primary Stands, (top left) NPP is greatest in the second age-class and (bottom left) the demographic effect on NPP is < 0.25 kg C $m^{-2}$ $yr^{-1}$.**

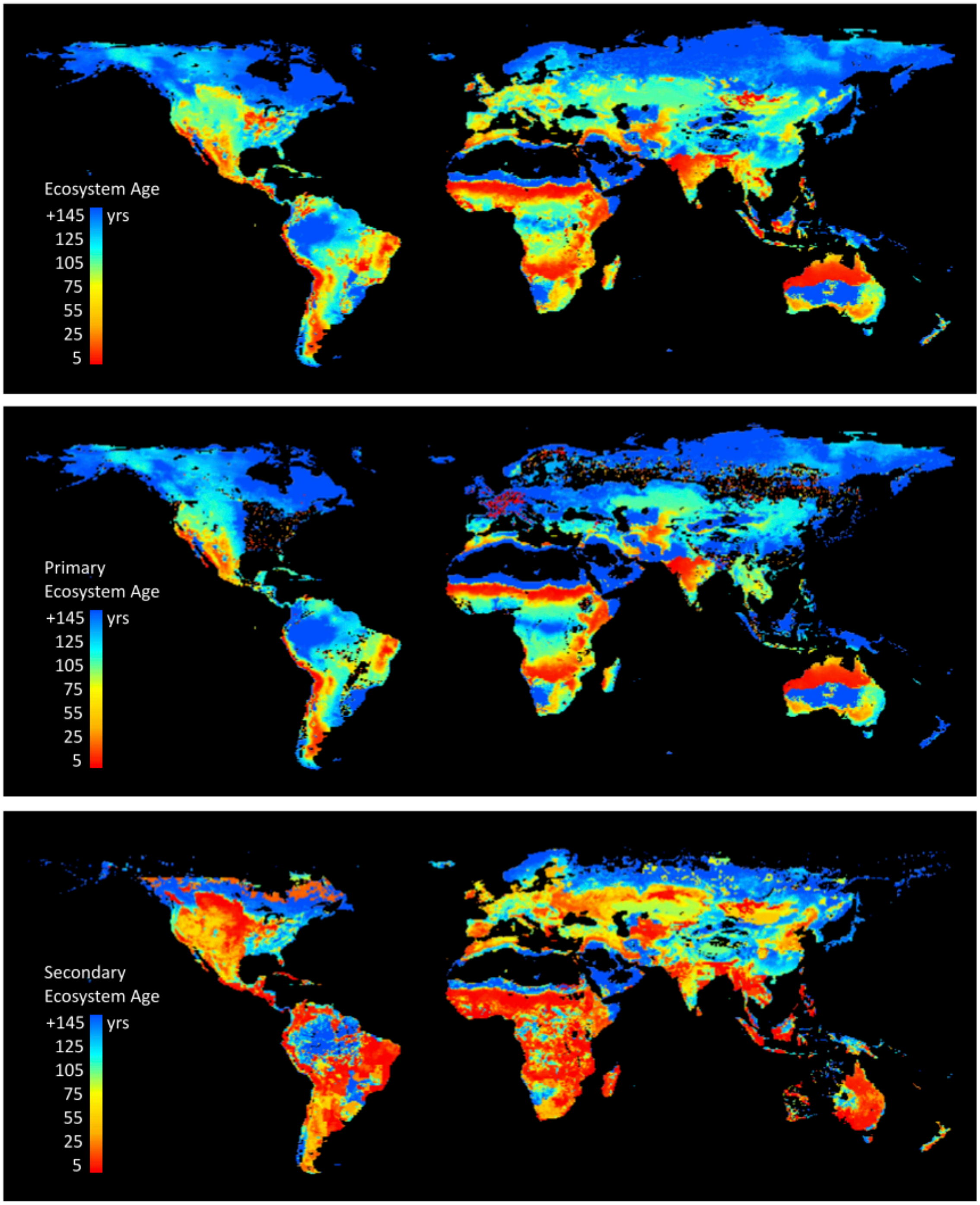


**Figure 4.13. LPJ simulated global distribution of Ecosystem Ages, defined as the time since disturbance by fire and/or land use change and land management (LUCLM) in year 2016. (top) Average age of the natural ecosystem, scaled to the area of natural lands within 0.5° grid-cells. (middle) Average age of Primary Ecosystems only, wherein only fire creates age structure, scaled to the area of primary lands. (bottom) Average age of Secondary Ecosystems only, wherein fire and LUCLM creates age structure, scaled to the area of secondary lands.**

**Supplementary Material –** Figures and Tables for "Ecosystem Age-class Dynamics in a Global Ecosystem Model"

**Table 4.SM1. LPJ Plant Functional Types (PFTs) phenology parameters and bioclimatic limits. Growing Degree Day (GDD) base is the temperature at which annual GDD sums begin. GDDmin is the minimum GDD required for establishment. GDDramp is the number of days required for full leaf out. Tmin and Tmax are the minimum and maximum annual temperatures for establishment, respectively. Trangemin is the minimum annual temperature range for establishment, and only relevant for the BoNS PFT.**

| Code | name | Habit | GDDbase | GDDmin | GDDramp | Tmin | Tmax | Trangemin |
|---|---|---|---|---|---|---|---|---|
| TrBE | Tropical Broadleaf Evergreen Tree | Evergreen | 0.0 | 0 | 1000 | 15.5 | 1000.0 | NA |
| TrBR | Tropical Broadleaf Raingreen Tree | Deciduous | 5.0 | 0 | 1000 | 15.5 | 1000.0 | NA |
| TeNE | Temperate Needleleaf Evergreen | Evergreen | 5.0 | 900 | 1000 | -2.0 | 20.0 | NA |
| TeBE | Temperate Broadleaf Evergreen | Evergreen | 5.0 | 1200 | 1000 | 3.0 | 18.8 | NA |
| TeBS | Temperate Broadleaf Summergreen | Deciduous | 5.0 | 1200 | 300 | -17.0 | 15.5 | NA |
| BoNE | Boreal Needleleaf Evergreen | Evergreen | 5.0 | 600 | 1000 | -32.5 | -2.0 | NA |
| BoBS | Boreal Broadleaf Summergreen | Deciduous | 5.0 | 350 | 200 | -1000.0 | -2.0 | NA |
| BoNS | Boreal Needleleaf Summergreen | Deciduous | 2.0 | 350 | 100 | -1000.0 | -2.0 | 43 |
| C3GR | C3 Perennial Grass | | 5.0 | 0 | 100 | -1000.0 | 15.5 | NA |
| C4GR | C4 Perennial Grass | | 5.0 | 0 | 100 | 15.5 | 1000.0 | NA |

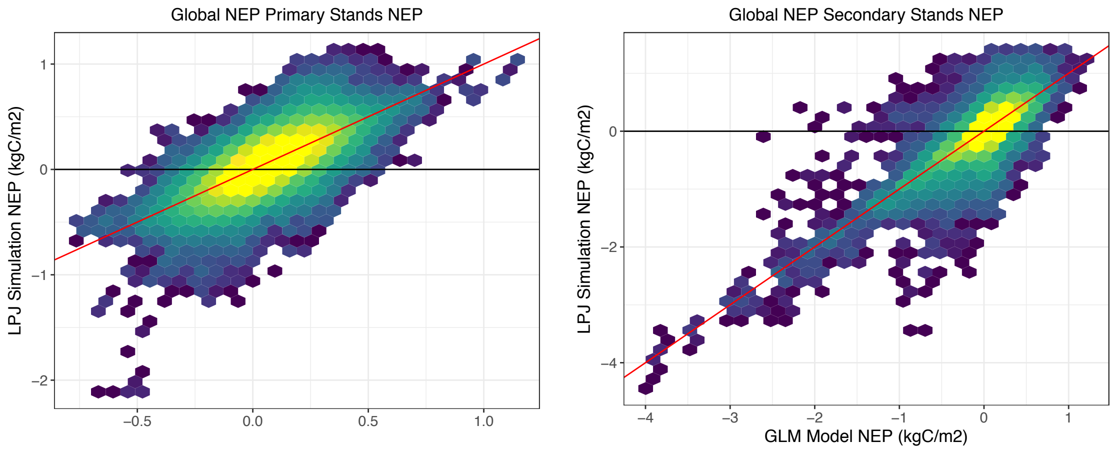


**Figure 4.SM1. Annual (2000-2017) NEP fluxes from LPJ Simulations versus Predictions of LPJ Fluxes based on a Generalized Linear Model (Flux = Precipitation + Temperature + Age-class); coefficients were allowed to vary by grid-cell, in essence, reducing the effect of variation in plant composition, soil texture and hydrology. Coloring is by density of grid-cells on a log scale; diagonal red line is the 1:1 correspondence line. For Primary Stands, $R^2$ = 0.60, and for Secondary Stands, $R^2$ = 0.65.**

# CHAPTER FIVE

# CONCLUSIONS

This research advances scientific understanding of the role of land use, land use change, and land management in the global carbon cycle. Southeast Asia, for instance, represents less than 5% of the vegetated land area on Earth, but this area was found to comprise up to 25% of global land use change emissions. Land conversion by deforestation does not appear to be abating in Southeast Asia as old-growth tropical forests are routinely transformed into oil palm plantations. Oil palms are part of a large diversity of agricultural crops to be used as food, animal feed, biofuel, or fiber, but which have a poor representation in global models. Oil palms may never fully offset carbon losses from deforestation, but they do they do represent a carbon sink in themselves. As the human population grows and the demand for food and fiber grows in tandem, a greater number of models will need to focus efforts on improving representation of a complex set of processes from agriculture and land management. These issues were only partly addressed in the research chapters.

The ability of global ecosystem models to reproduce global-scale atmospheric seasonal cycles is limited and there is not enough attention paid to simultaneously resolving both the seasonality of fluxes and the simulated long-term trend in $CO_2$. Land use change, for instance, caused an inter-annual variation in seasonality that was comparable to baseline levels – that is, in instances where land use change was absent. Yet the global modeling community has lent much focus to quantifying the effect of land use change at annual time scales because it is directly related to long-term trends. Should there be a concern if annual values are in-line with the general consensus even if seasonal cycles are not? An inherent requirement for reproducing the atmospheric signals is that the land-to-atmosphere fluxes are reasonable in magnitude, duration and timing in all land regions, or at the very least, in land regions with large vegetative areas that might disproportionately dominate the signal. This is an extreme level of proficiency that, simply, the models do not currently exhibit. There is obvious room for model improvement, but much work ahead.

In the last chapter, developments were presented to explicitly track and model forest age dynamics in global models. By and large, Fire was the main driver of age differences between Boreal (50N to 90N) and Tropical (23S to 23N) latitudes. Land use change was found to further decrease the average age of ecosystems by up to 23 years since 1860, The impact of land use change and land management on ecosystem age will increase as human modification of natural lands becomes even more widespread in the future. The demography module presented in this study has clear limitations, lacking a suite of disturbance processes that would otherwise shift the ecosystem age to younger states. It also represents age-classes as even-height stands, so lacks structural complexity and an understory that is more representative of real forests. There are numerous model improvements that can be made to integrate the demography module with long-standing forestry knowledge. Nevertheless, the demography model is state-of-the-art in global models and represents one step forward.

This conclusion is critical of global ecosystem model limitations, but only as a loving parent might be to a child. I see the supreme benefit to scientific understanding for which global models have consistently contributed throughout their inception. For as much as we praise and lean on models as a foundation for understanding Earth's ecosystems, we must also confront the models with a clear and open mind, always asking ourselves if model representation fits within the current state of knowledge. We ought to ask critical questions of models and reveal their limitations so that we can guide their future development in directions that we find most important.

*Alice: "Would you tell me, please, which way I ought to go from here?"*
*Cheshire Cat: "That depends a good deal on where you want to get to."*
*Alice: "I don't much care where –"*
*Cheshire Cat: "Then it doesn't matter which way you go."*

Alice and The Cheshire Cat, Alice in Wonderland by Lewis Carroll

# CUMULATIVE LITERATURE CITED


1. Achard, F., Beuchle, R., Mayaux, P., Stibig, H.-J., Bodart, C., Brink, A., Carboni, S., Desclée, B., Donnay, F., Eva, H. D., Lupi, A., Raši, R., Seliger, R., and Simonetti, D.: Determination of tropical deforestation rates and related carbon losses from 1990 to 2010. *Global Change Biology*, 20, 2540–54, 2014.

2. Ahlström, A., Xia, J., Arneth, A., Luo, Y., and Smith, B.: Importance of vegetation dynamics for future terrestrial carbon cycling. *Environmental Research Letters*, doi:10.1088/1748-9326/10/5/054019, 2015.

3. Ahlström, A., Raupach, M. R., Schurgers, G., Smith, B., Arneth, A., Jung, M., Reichstein, M., Canadell, J. G., Friedlingstein, P., Jain, A. K., Kato, E., Poulter, B., Sitch, S., Stocker, B. D., Viovy, N., Wang, Y. P., Wiltshire, A., Zaehle, S., and Zeng, N.: The dominant role of semi-arid ecosystems in the trend and variability of the land $CO_2$ sink. *Science*, 348, 895-898, doi:10.1126/science.aaa1668, 2015.

4. Anav, A., Friedlingstein, P., Beer, C., Ciais, P., Harper, A., Jones, C., Murray-Tortarolo, G., Papale, D., Parazoo, N. C., Peylin, P., Piao, S., Sitch, S., Viovy, N., Wiltshire, A., & Zhao, M.: Spatiotemporal patterns of terrestrial gross primary production – a review. Reviews of Geophysics, 53, 785-818. doi:10.1002/2015RG000483, 2015.

5. Arneth, A., Sitch, S., J. Pongratz, Stocker, B. D., Ciais, P., Poulter, B., Bayer, A. D., Bondeau, A., Calle, L., Chini, L. P., Gasser, T., Fader, M., Friedlingstein, P., Kato, E., Li, W., Lindeskog, M., Nabel, J. E. M. S., Pugh, T. A. M., Robertson, E., Viovy, N., Yue, C., & Zaehle, S.: Historical carbon dioxide emissions caused by land-use changes are possibly larger than assumed. Nature Geoscience, 10. doi:10.1038/NGEO2882, 2017.

6. Austin, K.G., Kasibhatla, P.S., Urban, D. L., Stolle, F., and Vincent, J.: Reconciling Oil Palm Expansion and Climate Change Mitigation in Kalimantan, Indonesia. *PLoS ONE* 10, e0127963, doi:10.1371/journal.pone.0127963, 2015.

7. Asner, G. P., Kellner, J. R., Kennedy-Bowdoin, T., Knapp, D. E., Anderson, C., and Martin, R. E.: Forest canopy gap distributions in the Southern Peruvian Amazon. *PLoS ONE*, 8, e60875, doi:10.1371/journal.pone.0060875, 2013.

8. Baccini, A., Goetz, S. J., Walker, W. S., Laporte, N. T., Sun, M., Sulla-Menashe, D., Hackler, J., Beck, P. S. A., Dubayah, R., Friedl, M. A., Samanta, S., and Houghton, R. A.: Estimated carbon dioxide emissions from tropical deforestation improved by carbon-density maps. *Nature Climate Change*, 2,182–185, 2012.

9. Bagley, J. E., Desai, A. R., Harding, K. J., Snyder, P. K. & Foley, J. A.: Drought and deforestation – Has land cover change influence recent precipitation extremes in the Amazon? *Journal of Climate*, 27, 345-361, doi:10.1175/JCLI-D-12-00369.1, 2014.

10. Belikov, D. A., Maksyutov, S., Ganshin, A., Zhuravlev, R., Deutscher, N. M., Wunch, D., Feist, D. G., Morino, I., Parker, R. J., Strong, K., Yoshida, Y., Bril, A., Oshchepkov, S., Boesch, H., Dubey, M. K., Griffith, D., Hewson, W., Kivi, R., Mendonca, J., Notholt, J., Schneider, M., Sussmann, R., Velazco, V. A., and Aoki, S.: Study of the footprints of short-term variation in $XCO_2$ observed by TCCON sites using NIES and FLEXPART atmospheric transport models. *Atmospheric Chemistry and Physics*, 17, 143-157, doi:10.5194/acp-17-143-2017, 2017.

11. Betts, A. K., Desjardins, R., Worth, D., and Cerkowniak, D.: Impact of land use change on the diurnal cycle climate of the Canadian Prairies. *Journal of Geophysical Research – Atmospheres,* 188, 996-12011, doi:10.1002/2013JD020717, 2013.

12. Bonan, G. B.: Forests and climate change – forcings, feedbacks, and the climate benefits of forests. *Science*, 320, 1444. doi:10.1126/science.1155121, 2008.

13. Box, E. O.: Plant functional types and climate at the global scale. *Journal of Vegetation Science*, 7, 309-320, 1996.

14. Calle, L., Canadell, J. G., Patra, P. K., Ciais, P., Ichii, K., Tian, H., Kondo, M., Piao, S., Arneth, A., Harper, A. B., Ito, A., Kato, E., Koven, C., Sitch, S., Stocker, B. D., Vivoy, N., Wiltshire, A., Zaehle, S., and Poulter, B.: Regional carbon fluxes from land use and land cover change in Asia, 1980-2009. *Environmental Research Letters,* 11, 074011, 2016.

15. Carlson, K. M., Curran, L. M., Ratnasari, D., Pittman, A. M., Soares-Filho, B. S., Asner, G. P., Trigg, S. N., Gaveau, D. A., Lawrence, D., and Rodrigues, H. O.: Committed carbon emissions, deforestation, and community land conversion from oil palm plantation expansion in West Kalimantan, Indonesia. *Proceedings of the National Academy of Sciences of the United States of America*, 109, 7559-7564, 2012.

16. Chen, C., Park, T., Wang, X., Piao, S., Xu, B., Chaturvedi, R. K., Fuchs, R., Brovkin, V., Ciais, P., Fensholt, R., Tømmervik, H., Bala, G., Zhu, Z., Nemani, R. R., and Myneni, R. B.: China and India lead in greening of the world through land-use management. *Nature Sustainability*, 2, 122-129, 2019.

17. Ciais, P., C. Sabine, G. Bala, L. Bopp, V. Brovkin, J. Canadell, A. Chhabra, R. DeFries, J. Galloway, M. Heimann, C. Jones, C. Le Quéré, R. B. Myneni, S. Piao, and P. Thornton. Carbon and other biogeochemical cycles, in: Climate Change 2013: The Physical Science Basis, edited by: Stocker, T. F., D. Qin, G. –K. Plattner, M. Tignore, S. K. Allen, J. Boschung, A. Nauels, Y. Xia, V. Bex, and P. M. Midgley. Cambridge University Press, Cambridge, 2013.

18. Ciais, P., Dolman, A. J., Bombelli, A., Duren, R., Peregon, A., Rayner, P. J., Miller, C., Gobron, N., Kinderman, G., Marland, G., Gruber, N., Chevallier, F., Andres, R. J., Balsamo, G., Bopp, L., Bréon, F.-M., Broquet, G., Dargaville, R., Battin, T. J., Borges, A., Bovensmann, H., Buchwitz, M., Butler, J., Canadell, J. G., Cook, R. B., DeFries, R., Engelen, R., Gurney, K. R., Heinze, C., Heimann, M., Held, A., Henry, M., Law, B., Luyssaert, S., Miller, J., Moriyama, T., Moulin, C., Myneni, R. B., Nussli, C., Obersteiner, M., Ojima, D., Pan, Y., Paris, J.-D., Piao, S. L., Poulter, B., Plummer, S., Quegan, S., Raymond, P., Reichstein, M., Rivier, L., Sabine, C., Schimel, D., Tarasova, O., Valentini, R., Wang, R., van der Werf, G., Wickland, D., Williams, M. & Zehner, C.: Current systematic carbon-cycle observations and the need for implementing a policy-relevant carbon observing system. *Biogeosciences*, 11, 3547-3602, doi:10.5194/bg-11-3547-2014, 2015.

19. Crisp, D., Fisher, B. M., O'Dell, C. O., Frankenberg, C., Basilio, R., Bösch, H., Brown, L. R., Castano, R., Conner, B., Deutscher, N. M., Eldering, A., Griffith, D., Gunson, M., Kuze, A., Mandrake, L., McDuffie, J., Messerschmidt, J., Miller, C. E., Morino, I., Natraj, V., Notholt, J., O'Brien, D. M., Oyafuso, F., Polonsky, I., Robinson, J., Salawitch, R., Sherlock, V., Smyth, M., Suto, H., Taylor, T. E., Thompson, D. R., Wennberg, P. O., Wunch, D., & Yung, Y. L.: The ACOS $CO_2$ retrieval algorithm – Part II – Global $XCO_2$ data characterization. *Atmospheric Measurement Techniques*, 5, 687-707. doi:10.5194/amt-5-687-2012, 2012.

20. Dale, V. H., Joyce, L. A., McNulty, S., Neilson, R. P., Ayres, M. P., Flannigan, M. D., Hanson, P. J., Irland, L. C., Lugo, A. E., Peterson, C. J., Simberloff, D., Swanson, F. J., Stocks, B. J., and Wotton, B. M.: Climate change and forest disturbance. *BioScience*, 51, 723-734, 2001.

21. Drake, J. E., Raetz, L. M., Davis, S. C., and DeLucia, E. H.: Hydraulic limitation not declining nitrogen availability causes the age-related photosynthetic decline in loblolly pine (*Pinus taeda* L.). *Plant, Cell and Environment*, 33, 1756-1766, doi:10.1111/j.1365-3040.2010.02180.x, 2010.

22. Drake, J. E., Davis, S. C., Raetz, L. M., and DeLucia, E. H.: Mechanisms of age-related changes in forest production: the influence of physiological and successional changes. *Global Change Biology*, 17, 1522-1535, doi:10.1111/j.1365-2486.2010.02342.x, 2011.

23. Earles, J. M., Yeh, S. ,and Skog, K. E.: Timing of carbon emissions from global forest clearance. *Nature Climate Change*, 2, 682-685, 2012.

24. EDGARv4.3. Emission Database for Global Atmospheric Research (EDGAR), release version 4.3. European Commission, Joint Research Centre (JRC)/ Netherlands Environmental Assessment Agency (PBL): 2011. http://edgar.jrc.ec.europa.eu

25. Ehret, U., and Zehe, E.: Series distance – an intuitive metric to quantify hydrograph similarity in terms of occurrence, amplitude and timing of hydrological events. *Hydrology and Earth Systems Science*, 15, 877-896, doi:10.5194/hess-15-877-2011, 2011.

26. Eyring, V., Bony, S., Meehl, G. A., Senior, C. A., Stevens, B., Stouffer, R. J., and Taylor, K. E.: Overview of the Coupled Model Intercomparison Project Phase 6 (CMIP6) experimental design and organization. *Geoscientific Model Development*, 9, 1937-1958, doi:10.5194/gmd-9-1937-2016, 2016.

27. Fang, J., Chen, A., Peng, C., Zhao, S., and Ci, L.: Changes in forest biomass carbon storage in China between 1949 and 1998. *Science*, 292, 2320–2322, 2001.

28. FAO-FRA 2015. Global Forest Resource Assessment 2015. Food and Agriculture Organization of the United Nations.

29. Farquhar, G. D., von Caemmerer, S., and Berry, J. A.: A biochemical model of photosynthetic $CO_2$ assimilation in leaves of $C_3$ plants. *Planta*, 149, 78-90, 1980.

30. Federici, S., Tubiello, F. N., Salvatore, M., Jacobs, H., and Schmidhuber, J.: New estimates of CO2 forest emissions and removals: 1990-2015. *Forest Ecology and Management*, 352, 89–98, 2015.

31. Fischer, R., Bohn, F., de Paula, M. D., Dislich, C., Groeneveld, J., Gutiérrez, A. G., Kazmierczak, M., Knapp, N., Lehmann, S., Paulick, S., Pütz, S., Rödig, E., Taubert, F., Köhler, P., and Huth, A.: Lessons learned from applying a forest gap model to understand ecosystem and carbon dynamics of complex tropical forests. *Ecological Modelling*, 326, 124-133, doi:10.1016/j.ecolmodel.2015.11.018, 2016.

32. Fisher, R. A., Koven, C. D., Anderegg, W. R. L., Christoffersen, B. O., Dietze, M. C., Farrior, C. E., Holm, J. A., Hurtt, G. C., Knox, R. G., Lawrence, P. J., Lichstein, J. W., Longo, M., Matheny, A. M., Medvigy, D., Muller-Landau, H. C., Powell, T. L., Serbin, S. P., Sato, H., Shuman, J. K., Smith, B., Trugman, A. T., Viskari, T., Verbeeck, H., Wang, E., Xu, C., Xu, X., Zhang, T., Moorcroft, P. R.: Vegetation demographics in Earth System Models – A review of progress and priorities. *Global Change Biology*, 24, 35-54, doi:10.1111/gcb.13910, 2018.

33. Fleishcher, E., Khashimov, I., Hölzel, N., and Klemm, O.: Carbon exchange fluxes over peatlands in Western Siberia – possible feedback between land-use change and climate change. *Science of the Total Environment*, doi:10.1016/j.scitotenv.2015.12.073, 2016.

34. Foley, J. A., Defries, R., Asner, G. P., Barford, C., Bonan, G., Carpenter, S. R., Chapin, F. S., Coe, M. T., Daily, G. C., Gibbs, H. K., Helkowski, J. H., Holloway, T., Howard, E. A., Kucharik, C. J., Monfreda, C., Patz, J. A., Prentice, I. C., Ramankutty, N., and Snyder, P. K.: Global consequences of land use. *Science*, 309, 570–4, 2005.

35. Forkel, M., Carvalhais, N., Schaphoff, S., von Bloh, W., Migliavacca, M., Thurner, M., and Thonicke, K.: Identifying environmental controls on vegetation greenness phenology through model-data integration. *Biogeosciences*, 11, 7025-7050. doi:10.5194/bg-11-7025-2014, 2014.

36. Friedlingstein, P., Cox, P., Betts, R., Bopp, L., von Bloh, W., Brovkin, V., Cadule, Pl, Doney, S., Eby, M., Fung, I., Bala, G., John, J., Jones, C., Joos, F., Kato, T., Kawamiya, M., Knorr, W., Lindsay, K., Matthews, H. D., Raddatz, T., Rayner, P., Reick, C., Roeckner, E., Schnitzler, K.-G., Schnur, R., Strassmann, K., Weaver, A. J., Yoshikawa, C., and Zeng, N.: Climate-carbon cycle feedback analysis: Results from the $C^4$MIP Model Intercomparison. *Journal of Climate*, 19, 3337-3353, 2006.

37. Friedlingstein, P., Houghton, R. A., Marland, G., Hackler, J., Boden, T. A., Conway, T. J., Canadell, J. G., Raupach, M. R., Ciais, P., Le Quéré, C.: Update on CO2 emissions. *Nature Geoscience*, 3, 811-812. doi:10.1038/ngeo1022, 2010.

38. Friend, A. D., Lucht, W., Rademacher, T. T., Keribin, R., Betts, R., Cadule, P., Ciais, P., Clark, D. B., Dankers, R., Falloon, P. D., Ito, A., Kahana, R., Kleidon, A., Lomas, M. R., Nishina, K., Ostberg, S., Pavlick, R., Peylin, P., Schaphoff, S., Vuichard, N., Warszawski, Wiltshire, A., and Woodward, F. I.: Carbon residence time dominates uncertainty in terrestrial vegetation responses to future climate and atmospheric $CO_2$. *Proceedings of the National Academies of Science of the United States of America*, 111, 3280-3285, doi:10.1073/pnas.1222477110, 2014.

39. Frolking, S., Palace, M. W., Clark, D. B., Chambers, J. Q., Shugart, H. H., and Hurtt, G. C.: Forest disturbance and recovery: A general review in the context of spaceborne remote sensing of impacts on aboveground biomass and canopy structure. *Journal of Geophysical Research,* 114, G00E02, doi:10.1029/2008JG000911, 2009.

40. Fu, Z., Dong, J., Zhou, Y., Stoy, P. C., and Niu, S.: Long term trend and interannual variability of land carbon uptake – the attribution and processes. *Environmental*

*Research Letters*, 12, 014018, doi:10.1088/1748-9326/aa5685, 2017.

41. Gaveau, D. L. A., Sloan, S., Molidena, E., Yaen, H., Sheil, D., Abram, N. K., Ancrenaz, M., Nasi, R., Quinones, M., Wielaard, N., and Meijaard, E.: Four decades of forest persistence, clearance and logging on Borneo. *PLoS ONE,* 9, e101654. doi:10.1371/journal.pone.0101654, 2014.

42. Gitz, V., and Ciais, P.: Amplifying effects of land-use change on future atmospheric $CO_2$ levels. *Global Biogeochemical Cycles,* 17, 1024, doi:10.1029/2002GB001963, 2003.

43. Glecker, P. J., Taylor, K. E., and Doutriaux, C.: Performance metrics for climate models. *Journal of Geophysical Research - Atmospheres*, 113, D06104, doi:10.1029/2007/JD008972, 2008.

44. Goldewijk, K. K.: Estimating global land use change over the past 300 years: The HYDE Database. *Global Biogeochemical Cycles*, 15, 417–433, 2001.

45. Goldewijk, K. K., Beusen, A., van Drecht, G., and de Vos, M.: The HYDE 3.1 spatially explicit database of human-induced global land-use change over the past 12,000 years. *Global Ecology and Biogeography*, 20, 73-86, doi:10.1111/j.1466-8238.2010.00587.x, 2011.

46. Gray, J. M., Frolking, S., Kort, E. A., Ray, D. K., Kucharik, C. J., Ramankutty, N., and Friedl, M. A.: Direct human influence on atmospheric CO2 seasonality from increased cropland productivity. *Nature*, 515, 398-401, doi:10.1038/nature13957, 2014.

47. Guerlet, S., Butz, A., Schepers, D., Basu, S., Hasekamp, O. P., Kuze, A., Yokota, T., Blavier, J. F., Deutscher, N. M., Grif- fith, D. W. T., Hase, F., Kyro, E., Morino, I., Sherlock, V., Suss- mann, R., Galli, A., and Aben, I.: Impact of aerosol and thin cirrus on retrieving and validating $XCO_2$ from GOSAT shortwave infrared measurements. *Journal Geophysical Research - Atmospheres*, 118, 4887– 4905, doi:10.1002/jgrd.50332, 2013.

48. Hammerling, D. M., Kawa, S. R., Schaefer, K., Doney, S., and Michalak, A. M.: Detectability of $CO_2$ flux signals by a space-based lidar mission. *Journal of Geophysical Research – Atmospheres*, 120, 1794–1807, doi:10.1002/ 2014JD022483, 2015.

49. Hansen, M. C., Potapov, P. V., Moore, R., Hancher, M., Turubanova, S. A., Tyukavina, A., Thau, D., Stehman, S. V., Goetz, S. J., Loveland, T. R., Kommareddy, A., Egorov, A., Chini, L., Justice, C. O., and Townshend, J. R. G.:

High-resolution global maps of 21st-century forest cover change. *Science*, 342, 850–3, 2013.

50. Hantson, S., Arneth, A., Harrison, S. P., Kelley, D. I., Prentice, I. C., Rabin, S. S., Archibald, S., Mouillot, F., Arnold, S. R., Artaxo, P., Bachelet, D., Ciais, P., Forrest, M., Friedlingstein, P., Hickler, T., Kaplan, J. O., Kloster, S., Knorr, W., Lasslop, G., Li, F., Mangeon, S., Melton, J. R., Meyn, A., Sitch, S., Spessa, A., van der Werf, G. R., Voulgarakis, A., and Yue, C.: The status and challenge of global fire modelling. *Biogeosciences*, 13, 335903375, doi:10.5194/bg-13-3359-2016, 2016.

51. Harris, N., Brown, S., Hagen, S. C., Baccini, A., and Houghton, R. A.: Progress toward a consensus on carbon emissions from tropical deforestation. *Policy Brief* for Winrock International, WHOI, and the Meridian Institute, 2012a.

52. Harris, N. L., Brown, S., Hagen, S. C., Saatchi, S. S., Petrova, S., Salas, W., Hansen, M. C., Potapov, P. V., and Lotsch, A.: Baseline Map of Carbon Emissions from Deforestation in Tropical Regions. *Science*, 336, 1573, doi:10.1126/science.1217962, 2012b.

53. Haverd, V., Smith, B., Nieradzik, L. P., and Briggs, P. R.: A stand-alone tree demography and landscape structure module for Earth system models: integration with inventory data from temperate and boreal forests. *Biogeosciences*, 11, 4039-4055, doi:10.5194/bg-11-4039-2014, 2014.

54. Haxeltine, A., and Prentice, I. C.: A general model for the light-use efficiency of primary production. *Functional Ecology*, 10, 551-561, 1996.

55. Hooijer, A., Silvius, M., Wösten, H., and Page, S.: PEAT-CO2, Assessment of CO2 emissions from drained peatlands in SE Asia. *Delft Hydraulics report* Q3943/2006, 36p, http://peat-co2.deltares.nl, 2006.

56. Hooijer, A., Page, S., Canadell, J. G., Silvius, M., Kwadijk, J., Wösten, H., and Jauhiainen, J.: Current and future CO2 emissions from drained peatlands in Southeast Asia, *Biogeosciences*, 7, 1505–1514, 2010.

57. Houghton, R. A.: The annual net flux of carbon to the atmosphere from changes in land use 1850-1990. *Tellus B*, 51B, 298-313, 1999.

58. Houghton, R. A.: Revised estimates of the annual net flux of carbon to the atmosphere from changes in land use and land management 1850-2000. *Tellus* B, 378-390, 2003.

59. Houghton, R. A.: How well do we know the flux of CO2 from land-use change? *Tellus* B, 337-351, 2010.

60. Houghton, R. A., House, J. I., Pongratz, J., van Der Werf, G. R., Defries, R. S., Hansen, M. C., Le Quéré, C., and Ramankutty, N.: Carbon emissions from land use and land-cover change. *Biogeosciences*, 9, 5125–5142, 2012.

61. Huang, Y., Lu, X., Shi, Z., Lawrence, D., Koven, C. D., Xia, J., Du, Z., Kluzek, E., and Luo, Y.: Matrix approach to land carbon cycle modeling: A case study with the Community Land Model. *Global Change Biology*, 24, 1394-1404, doi:10.1111/gcb.13948, 2018.

62. Hurtt, G. C., Frolking, S., Fearon, M. G., Moore, B., Shevliakova, E., Malyshev, S., Pacala, S. W., and Houghton, R. A.: The underpinnings of land-use history: three centuries of global gridded land-use transitions, wood-harvest activity, and resulting secondary lands. *Global Change Biology*, 12, 1208–1229, 2006.

63. Hurtt, G. C., Chini, L. P., Frolking, S., Betts, R. A., Feddema, J., Fischer, G., Fisk, J. P., Hibbard, K., Houghton, R. A., Janetos, A., Jones, C. D., Kindermann, G., Kinoshita, T., Goldewijk, K. K., Riahi, K., Shevliakova, E., Smith, S., Stehfest, E., Thomson, A., Thornton, P., van Vuuren, D. P., and Wang, Y. P.: Harmonization of land-use scenarios for the period 1500-2100: 600 years of global gridded annual land-use transitions, wood harvest, and resulting secondary lands. *Climatic Change*, 109, 117–161, 2011.

64. Hurtt G., Chini, L., Sahajpal, R., and Frolking, S.: Harmonization of global land-use change and management for the period 850-2100, version 2. Available at luh.umd.edu/data.shtml, 2017.

65. Jones, C. D., and Cox, P. M.: Modeling the volcanic signal in the atmospheric $CO_2$ record. *Global Biogeochemical Cycles*, 15, 452-465, 2001.

66. Kato, E., Kinoshita, T., Ito, A., Kawamiya, M., and Yamagata, Y.: Evaluation of spatially explicit emission scenario of land-use change and biomass burning using a process-based biogeochemical model. *Journal of Land Use Science*, 8, 104-122, doi:10.1080/1747423X.2011.628705, 2013.

67. Keeling, C. D., Whorf, T. P., Wahlen, M., and van der Plicht, J.: Interannual extremes in the rate of rise of atmospheric carbon dioxide since 1980. *Nature*, 375, 666-670, 1995.

68. Keim, B. D., Muller, R. A., and Stone, G. W.: Spatiotemporal patterns and return periods of tropical storm and hurricane strikes from Texas to Maine. *Journal of Climate*, 20, 3498-3509, doi:10.1175/JCLI4187.1, 2007.

*69.* Kim, D.H., Sexton, J. O., and Townshend, J. R.: Accelerated Deforestation in the Humid Tropics from the 1990s to the 2000s. *Geophysical Research Letters*, 42, 3495–3501, doi:10.1002/2014GL062777, 2015.

70. Kirschke, S., Bousquet, P., Ciais, P., Saunois, M., Canadell, J. G., Dlugokencky, E. J., Bergamaschi, P., Bergmann, D., Blake, D. R., Bruhwiler, L., Cameron-Smith, P., Castaldi, S., Chevallier, F., Feng, L., Fraser, A., Heimann, M., Hodson, E. L., Houweling, S., Josse, B., Fraser, P. J., Krummel, P. B., Lamarque, J.-F., Langenfelds, R. L., Le Quéré, C., Naik, V., O'Doherty, S., Palmer, P. I., Pison, I., Plummer, D., Poulter, B., Prinn, R. G., Rigby, M., Ringeval, B., Santini, M., Schmidt, M., Shindell, D. T., Simpson, I. J., Spahni, R., Steele, L. P., Strode, S. A., Sudo, K., Szopa, S., van der Werf, G. R., Voulgarakis, A., van Weele, M., Weiss, R. F., Williams, J. E., and Zeng, G.: Three decades of global methane sources and sinks. *Nature Geoscience*, 6, 813–823, 2013.

71. Kondo, M., Ichii, K., Patra, P. K., Poulter, B., Calle, L., Koven, C., Pugh, T. A. M., Kato, E., Harper, A., Zaehle, S., and Wiltshire, A.: Plant regrowth as a driver of recent enhancement of terrestrial CO2 uptake. *Geophysical Research Letters*, 45, 4820-4830, doi:10.1029/2018GL077633, 2018.

72. Krinner, G., Viovy, N., de Noblet-Ducoudré, N., Ogeé, J., Polcher, J., Friedlingstein, P., Ciais, P., Sitch, S., and Prentice, I. C.: A dynamic global vegetation model for studies of the coupled atmosphere–biosphere system. *Global Biogeochemical Cycles*, 19, GB1015. doi:10.1029/2003GB002199, 2005.

73. Langner, A., Achard, F., and Grassi, G.: Can recent pan-tropical biomass maps be used to derive alternative Tier 1 values for reporting REDD+ activities under UNFCCC? *Environmental Research Letters*, 9, 124008, 2014.

74. Lawrence, D. M., Oleson, K. W., Flanner, M. G., Thornton, P. E., Swenson, S. C., Lawrence, P. J., Zeng, X., Yang, Z. L., Levis, S., Sakaguchi, K., Bonan, G. B., & Slater, A. G.: Parameterization improvements and functional and structural advances in version 4 of the Community Land Model. Journal of Advances in Modeling Earth Systems, 3, M03001. doi:10.1029/2011MS000045, 2011.

75. Lawrence, D.M., Fisher, R.A., Koven, C.D., Oleson, K.W., Swenson, S.C., Vertenstein, M., Andre, B., Bonan, G., Ghimire, B., van Kampenhout, L., Kennedy, D., Kluzek, E., Knox, R., Lawrence, P. J., Li, F., Li, H., Lombardozzi, D., Lu, Y., Perket, J., Riley, W.J. Sacks, W.J., Shi, M., Wieder, W.R., Xu, C., Ali, A., Badger, A., Bisht, G., Broxton, P., Brunke, M., Buzan, J., Clark, M., Craig, A., Dahlin, K., Drewniak, B., Fisher, J. B., Flanner, M., Gentine, P., Lenaerts, J., Levis, S., Leung, L. R., Lipscomb, W. H., Pelletier, J. D., T., Ricciuto, D. M., Sanderson, B. M., Shuman, J., Slater, A., Subin, Z., Tang, J., Tawfik, A., Thomas, R. Q., Tilmes, S.,

Vitt, F., and Zeng, X.: Technical description of version 5.0 of the Community Land Model (CLM). The National Center for Atmospheric Research, 2019.

76. Le Quéré, C., Andrew, R. M., Peters, G. P., Ciais, P., Friedlingstein, P., Jones, S., Sitch, S., Tans, P., Arneth, A., Boden, T. A., Bopp, L., Bozec, Y., Canadell, J. G., Chini, L. P., Chevallier, F., Cosca, C. E., Harris, I., Hoppema, M., Houghton, R. A., House, J. I., Jain, A. K., Johannessen, T., Kato, E., Keeling, R. F., Kitidis, V., Goldewijk, K. K., Koven, C., Landa, C. S., Landschützer, P., Lenton, A., Lima, I. D., Marland, G., Mathis, J. T., Metzl, N., Nojiri, Y., Olsen, A., Ono, T., Peng, S., Peters, W., Pfeil, B., Poulter, B., Raupach, M. R., Regnier, P., Rödenbeck, C., Saito, S., Salisbury, J. E., Schuster, U., Schwinger, J., Séférian, R., Segschneider, J., Steinho, T., Stocker, B. D., Sutton, A. J., Takahashi, T. Tilbrook, B., van der Werf, G. R., Viovy, N., Wang, Y.–P., Wanninkhof, R., Wiltshire, A., and Zeng, N.: Global carbon budget 2014. *Earth System Science Data*, 7, 47–85, doi:10.5194/essd-7-47-2015, 2015.

77. Le Quéré, C., Andrew, R. M., Friedlingstein, P., Sitch, S., Pongratz, J., Manning, A. C., Korsbakken, J. I., Peters, G. P., Canadell, J. G., Jackson, R. B., Boden, T. A., Tans, P. P., Andrews, O. D., Arora, V. K., Bakker, D. C. E., Barbero, L., Becker, M., Betts, R. A., Bopp, L., Chevallier, F., Chini, L. P., Ciais, P., Cosca, C. E., Cross, J., Currie, K., Gasser, T., Harris, I., Hauck, J., Haverd, V., Houghton, R. A., Hunt, C. W., Hurtt, G. C., Ilyina, T., Jain, A. K., Kato, E., Kautz, M., Keeling, R. F., Goldewijk, K. K., Körtzinger, Landschützer, P., Lefèvre, N., Lenton, A., Lienert, S., Lima, I., Lombardozzi, D., Metzl, N., Millero, F., Monteiro, P. M. S., Munro, D. R., Nabel, J. E. M. S., Nakaoka, S., Nojiri, Y., Padin, X. A., Peregon, A., Pfeil, B., Pierrot, D., Poulter, B., Rehder, G., Reimer, J., Rödenbeck, C., Schwinger, J., Séférian, R., Skjelvan, I., Stocker, B. D., Tian, H., Tilbrook, B., Tubiello, F. N., van der Laan-Luijkx, I. T., van der Werf, G. R., van Heuven, S., Viovy, N., Vuichard, N., Walker, A. P., Watson, A. J., Wiltshire, A. J., Zaehle, S. & Zhu, D.: Global Carbon Budget, Earth System Science Data, 10, 405-448, doi:10.5194/essd-10-405-2018, 2018.

78. Li, P., Zhu, J., Hu, H., Guo, Z., Pan, Y., Birdsey, R., and Fang, J.: The relative contributions of forest growth and areal expansion to forest biomass carbon sinks in China. *Biogeosciences Discussions*, 12, 9587–9612, 2015.

79. Lindqvist, H., O'Dell, C. W., Basu, S., Boesch, H., Chevallier, F., Deutscher, N., Feng, L., Fisher, B., Hase, F., Inoue, M., Kivi, R., Morino, I., Palmer, P. I., Parker, R., Schneider, M., Sussmann, R., and Yoshida, Y.: Does GOSAT capture the true seasonal cycle of carbon dioxide? *Atmospheric Chemistry and Physics*, 15, 13023–13040, doi:10.5194/acp-15-13023-2015, 2015.

80. Liptak, J., Keppel-Aleks, G., and Lindsay, K.: Drivers of multi-century trends in the atmospheric $CO_2$ mean annual cycle in a prognostic ESM. *Biogeosciences*, 14,

1383-1401, doi:10.5194/bg-14-1383-2017, 2017.

81. Liu, M., and Tian, H. Q.: China's land-cover and land-use change from 1700 to 2005: estimations from high-resolution satellite data and historical archives. *Global Biogeochemical Cycles*, 24, GB3003, doi:10.1029/2009GB003687, 2010.

82. Liu, Y. Y., van Dijk, A. I. J. M., de Jeu, R. A. M., Canadell, J. G., McCabe, M. F., Evans, J. P., and Wang, G.: Recent reversal in loss of global terrestrial biomass. *Nature Climate Change*, 5, 470–474, 2015.

83. Liu, Z., Guan, D., Wei, W., Davis, S. J., Ciais, P., Bai, J., Peng, S., Zhang, Q., Hubacek, K., Marland, G., et al.: Reduced carbon emission estimates from fossil fuel combustion and cement production in China. *Nature*, 524, 335–338, 2015.

84. Loarie, S. R., Asner, G. P., and Field, C. B.: Boosted carbon emissions from Amazon deforestation. *Geophysical Research Letters*, 36, L14810, 2009.

85. Margono, B. A., Potapov, P. V., Turubanova, S., Stolle, F., and Hansen, M. C.: Primary forest cover loss in Indonesia over 2000-2012. *Nature Climate Change*, 4, 730-735, 2014.

86. McGuire, A. D., Sitch, S., Clein, J. S., Dargaville, R., Esser, G., Foley, J., Heimann, M., Joos, F., Kaplan, J., Kicklighter, D. W., Meier, R. A., Melillo, J. M., Moore III, B., Prentice, I. C., Ramankutty, N., Reichenau, T., Schloss, A., Tian, H., Williams, L. J., and Wittenberg, U.: Carbon balance of the terrestrial biosphere in the twentieth century: Analyses of $CO_2$, climate and land use effects with four process-based ecosystem models. *Global Biogeochemical Cycles*, 15, 183-206, 2001.

87. Medvigy, D., Wofsy, S. C., Munger, J. W., Hollinger, D. Y., and Moorcroft, P. R.: Mechanistic scaling of ecosystem function and dynamics in space and time: Ecosystem Demography model version 2. *Journal of Geophysical Research*, 114, G01002, doi:10.1029/2008JG000812, 2009.

88. Meittinen, J., Shi, C., and Liew, C. S.: Influence of peatland and land cover distribution on fire regimes in insular Southeast Asia. *Regional Environmental Change,* 11, 191-201, 2011.

89. Miettinen, J., Shi, C., and Liew, S. C.: Land cover distribution in the peatlands of Peninsular Malaysia, Sumatra, and Borneo in 2015 with changes since 1990. *Global Ecology and Conservation,* 6, 67-78, 2016.

90. Miller, A. D., Dietze, M. C., DeLucia, E. H., and Anderson-Teixeira, K. J.: Alteration of forest succession and carbon cycling under elevated $CO_2$. *Global Change Biology*, 22, 351-363, doi:10.1111/gcb.13077, 2016.

91. Nakazawa, T., Ishizawa, M., Higuchi, K., and Trivett, N. B. A.: Two curve fitting methods applied to CO2 flask data. *Environmetrics*, 8, 197-218, 1997.

92. Nachtergaele, F., Van Velthuizen, H., Verelst, L., Batjes, N., Dijkshoorn, K., Van Engelen, V., Fischer, G., Jones, A., Montanarella, L., and Petri, M.: Harmonized world soil database, FAO, Rome, Italy and IIASA, Laxenburg, Austria, 2008.

93. O'Dell, C. W., Conner, B., Bösch, H., O'Brien, D. O., Frankenberg, C., Castano, R., Christi, M., Crisp, D., Eldering, A., Fisher, B., Gunson, M., McDuffie, J., Miller, C. E., Natraj, V., Oyafuso, F., Polonsky, I., Smyth, M., Taylor, T., Toon, G. C., Wennberg, P. O., and Wunch, D.: The ACOS $CO_2$ retrieval algorithm – Part 1 – Description and validation against synthetic observations. *Atmospheric Measurement Techniques*, 5, 99-121, doi:10.5194/amt-5-99-2012, 2012.

94. Odum, E. P.: The strategy of ecosystem development. *Science* 164:262-270, 1969.

95. Olsen, S. C. and Randerson, J. T.: Differences between surface and column atmospheric $CO_2$ and implications for carbon cycle research. *Journal of Geophysical Research,* 109, D02301, doi:10.1029/2003JD003968, 2004.

96. Page, S. E., Siegert, F., Rieley, J. O., Boeheim, H. D. V., Jaya, A., and Limin, S.: The amount of carbon released from peat and forest firest in Indonesia during 1997. *Nature*, 420, 61-65, 2002.

97. Pan, Y., Chen, J. M., Birdsey, R., McCullough, K., He, L, and Deng, F.: Age structure and disturbance legacy of North American forests. *Biogeosciences*, 8, 715-732, doi:10.5194/bg-8-715-2011, 2011.

98. Pan, Y., R. A. Birdsey, J. Fang, R. Houghton, P. E. Kauppi, W. A. Kurz, O. L. Phillips, A. Shvidenko, S. L. Lewis, J. G. Canadell, P. Ciais, R. B. Jackson, S. W. Pacala, A. D. McGuire, S. Piao, A. Rautiainen, S. Sitch, and D. Hayes. 2011. A large and persistent carbon sink in the world's forests. *Science* 333:988–993.

99. Parazoo, N. C., Commane, R., Wofsy, S. C., Koven, C. D., Sweeney, C., Lawrence, D. M., Lindaas, J., Chang, R. Y.-W., and Miller C. E.: Detecting regional patterns of changing $CO_2$ flux in Alaska. *Proceedings of the National Academies of Science of the United States of America*, 113, 7733-7738, doi:10.1073/pnas.1601085113, 2016.

100. Patra, P. K., Ishizawa, M., Maksyutov, S., Nakazawa, T., and Inoue, G.: Role of biomass burning and climate anomalies for land-atmosphere carbon fluxes based on inverse modeling of atmospheric CO2. *Global Biogeochemical Cycles*, 19, 1–10, 2005.

101. Patra, P. K., Takigawa, M., Dutton, G. S., Uhse, K., Ishijima, K., Lintner, B. R., Miyazaki, K., and Elkins, J. W.: Transport mechanisms for synoptic, seasonal and interannual SF6 variations and 'age' of air in troposphere. *Atmospheric Chemistry and Physics*, 9, 1209-1225, 2009.

102. Peng, S., Ciais, P., Chevallier, F., Peylin, P., Cadule, P., Sitch, S., Piao, S., Ahlström, A., Huntingford, C., Levy, P., Li, X., Liu, Y., Lomas, M., Pouler, B., Viovy, N., Wang, T., Wang, X., Zaehle, S., Zeng, N., Zhao, F., and Zhao, H.: Benchmarking the seasonal cycle of CO2 fluxes simulated by terrestrial ecosystem models. *Global Biogeochemical Cycles*, 29, 46-64. doi:10.1002/2014GB004931, 2015.

103. Piao, S., Fang, J., Ciais, P., Peylin, P., Huang, Y., Sitch, S., and Wang, T.: The carbon balance of terrestrial ecosystems in China. *Nature*, 458, 1009–1013, 2009.

104. Piao, S., Ito, A., Li, S. G., Huang, Y., Ciais, P., Wang, X. H., Peng, S. S., Nan, H. J., Zhao, C., Ahlström, A., Andres, R. J., Chevallier, F., Fang, J. Y., Hartmann, J., Huntingford, C., Jeong, S., Levis, S., Levy, P. E., Li, J. S., Lomas, M. R., Mao, J. F., Mayorga, E., Mohammat, A., Muraoka, H., Peng, C. H., Peylin, P., Poulter, B., Shen, Z. H., Shi, X., Sitch, S., Tao, S., Tian, H. Q., Wu, X. P., Xu, M., Yu, G. R., Viovy, N., Zaehle, S., Zeng, N., and Zhu, B.: The carbon budget of terrestrial ecosystems in East Asia over the last two decades. *Biogeosciences*, 9, 3571–3586, 2012.

105. Pickers, P. A., and Manning, A. C.: Investigating bias in the application of curve fitting programs to atmospheric time series. *Atmospheric Measurement Techniques*, 8, 1469-1489, doi, 10.5194/amt-8-1469-2015, 2015.

106. Pimm, S. L.: The complexity and stability of ecosystems. *Nature*, 307, 321-326, 1984.

107. Pongratz, J., Reick, C. H., Houghton, R. A., and House, J. I.: Terminology as a key uncertainty in net land use and land cover change carbon flux estimates. *Earth System Dynamics*, 5, 177–195, 2014.

108. Potter, C., Tan, P.-N., Steinbach, M., Klooster, S., Kumar, V., Myneni, R., and Genovese, V.: Major disturbance events in terrestrial ecosystems detected using global satellite data sets. *Global Change Biology*, 9, 1005-1021, 2003.

109. Poulter, B., Ciais, P., Hodsen, E., Lischke, H., Maignan, F., Plummer, S., and Zimmermann, N. E.: Plant functional type mapping for earth system models. *Geoscientific Model Development*, 4, 993-1010. doi:10.5194/gmd-4-993-2011, 2011.

110. Poulter, B., Frank, D., Ciais, P., Myneni, R. B., Andela, N., Bi, J., Broquet, G., Canadell, J. G., Chevallier, F., Liu, Y. Y., Running, S. W., Sitch, S., and van der Werf, G. R.: Contribution of semi-arid ecosystems to interannual variability of the global carbon cycle. *Nature*, 509, 600-603, doi:10.1038/nature13376, 2014.

111. Prentice, I. C., Kelley, D. I., Foster, P. N., Friedlingstein, P., Harrison, S. P., and Bartlein, P. J.: Modeling fire and the terrestrial carbon balance. *Global Biogeochem Cycles*, 25, GB3005–GB3005, 2011.

112. Pretzsch, H., and Biber, P.: A re-evaluation of Reineke's Rule and stand density index. *Forest Science*, 51, 304-320, 2005.

113. Pretzsch, H., Grote, R., Reineking, B., Rötzer, TH., and Seifert, ST.: Models for Forest Ecosystem Mangement: A European Perspective. *Annals of Botany*, 101, 1065-87, doi:10.1093/aob/mcm246, 2008.

114. Pugh, T. A. M., Müller, C., Arneth, A., Haverd, V., and Smith, B.: Key knowledge and data gaps in modelling the influence of $CO_2$ concentration on the terrestrial carbon sink. *Journal of Plant Physiology*, 203, 3-15, 2016.

115. Pugh, T. A. M., Lineskog, M., Smith, B., Poulter, B., Arneth, A., Haverd, V., and Calle, L.: Role of forest regrowth in global carbon sink dynamics. *Proceedings of the National Academies of Science of the United States of America*, doi:10.1073/pnas.1810512116, 2019.

116. Pütz, S., Groeneveld, J., Alves, L. F., Metzger, J. P., and Huth, A.: Fragmentation drives tropical forest fragments to early successional states: A modelling study for Brazilian Atlantic forests. *Ecological Modelling*, 222, 1986-1997, doi:10.1016/j.ecolmodel.2011.03.038, 2011.

117. Pütz, S., Groeneveld, J., Henle, K., Knogge, C., Martensen, A. C., Metz, M., Metzger, J. P., Ribeiro, M. C., de Paula, M. D., and Huth, A.: Long-term carbon loss in fragmented Neotropical forests. *Nature communications,* 5, 5037. doi:10.1038/ncomms6037, 2014.

118. R Development Core Team. R: A language and environment for statistical computing. R Foundation for Statistical Computing, Vienna, Austria. ISBN 3-900051-07-0, URL http://www.R-project.org., 2008.

119. Randerson, J. T., Thompson, M. V., Conway, T. J., Fung, I. Y., and Field, C. B.: The contribution of terrestrial sources and sinks to trends in the seasonal cycle of atmospheric carbon dioxide. *Global Biogeochemical Cycles*, 11, 535-560, 1997.

120. Reichstein, M., Bahn, M., Ciais, P., Frank, D., Mahecha, M. D., Seneviratne, S. I., Zscheischler, J., Beer, C., Buchmann, N., Frank, D. C., Papale, D., Rammig, A., Smith, P., Thonicke, K., van der Velde, M., Vicca, S., Walz, A., and Wattenbach, M.: Climate extremes and the carbon cycle. *Nature*, 500, 287-295, doi:10.1038/nature12350, 2013.

121. Richardson, A. D., Anderson, R. S., Arain, M. A., Barr, A. G., Bohrer, G., Chen, G., Chen, J. M., Ciais, P., Davis, K. J., Desai, A. R., Dietze, M. C., Dragnoi, D., Garrity, S. R., Gough, C. M., Grant, R., Hollinger, D. Y., Margolis, H. A., McCaughey, H., Migliavacca, M., Monson, R. K., Munger, J. W., Poulter, B., Raczka, B. M., Ricciuto, D. M., Sahoo, A. K., Schaefer, K., Tian, H., Vargas, R., Verbeeck, H., Xiao, J., and Xue, Y.: Terrestrial biosphere models need better representation of vegetation phenology – results from the North American Carbon Program site synthesis. *Global Change Biology*, 18, 566-584, doi:10.1111/j.1365-2486.2011.02562.x, 2012.

122. Rosa, I. M. D., Ahmed, S. E., and Ewers, R. M.: The transparency, reliability and utility of tropical rainforest land-use and land-cover change models. *Global Change Biology,* 20, 1707-1722, 2014.

123. Ruesch, A., and Gibbs, H. K.: New IPCC Tier-1 Global Biomass Carbon Map For the Year 2000. Available online from the Carbon Dioxide Information Analysis Center [http://cdiac.ornl.gov*]*, Oak Ridge National Laboratory, Oak Ridge, Tennessee, 2008.

124. Ryan, M. G., Binkley, D., Fownes, J. H., Giardina, C. P., and Senock, R. S.: An experimental test of the causes of forest growth decline with stand age. *Ecological Monographs*, 74, 393-414, 2004.

125. Saatchi, S. S., Harris, N. L., Brown, S., Lefsky, M., Mitchard, E. T. A., Salas, W., Zutta, B. R., Buermann, W., Lewis, S. L., Hagen, S., Petrova, S., White, L., Silman, M., and Morel, A.: Benchmark map of forest carbon stocks in tropical regions across three continents. *Proceedings of the National Academy of Sciences of the United States of America*, 108, 9899–9904, 2011.

126. Saeki, T., and Patra, P. K.: Implications of overestimated anthropogenic $CO_2$ emissions on East Asian and global land $CO_2$ flux inversion. *Geoscience Letters,* 4, 9, doi:10.1186/s40562-017-0074-7, 2017.

127. Saito, R., Patra, P. K., Deutscher, N., Wunch, D., Ishijima, K., Sherlock, V., Blumenstock, T., Dohe, S., Griffith, D., Hase, F., Heikkinen, P., Kyro, E., Macatangay, R., Mendonca, J., Messerschmidt, J., Morino, I., Notholt, J., Rettinger, M., Strong, K., Sussmann, R., and Warneke, T.: Technical Note – Latitude-time variations of atmospheric column-average dry air mole fractions of CO2, CH4,

N2O. *Atmospheric Chemistry and Physics*, 12, 7767-7777, doi:10.5194/acp-12-7767-2012, 2012.

128. Schneising, O., Reuter, M., Buchwitz, M., Heymann, J., Bovensmann, H., and Burrows, J. P.: Terrestrial carbon sink observed from space – variation of growth rates and seasonal cycle amplitudes in response to interannual surface temperature variability. *Atmospheric Chemistry and Physics*, 14, 133-141, doi:10.5194/acp-14-133-2014, 2014.

129. Shevliakova, E., Pacala, S. W., Malyshev, S., Hurtt, G. C., Milly, P. C. D., Caspersen, J. P., Sentman, L. T., Fisk, J. P., Wirth, C., and Crevoisier, C.: Carbon cycling under 300 years of land use change: importance of the secondary vegetation sink. *Global Biogeochemical Cycles*, 23, GB2022, 2009.

130. Sitch, S., Smith, B., Prentice, I. C., Arneth, A., Bondeau, A., Cramer, W., Kaplan, J. O., Levis, S., Lucht, W., Sykes, M. T., Thonicke, K., and Venevsky, S.: Evaluation of ecosystem dynamics, plant geography and terrestrial carbon cycling in the LPJ dynamic global vegetation model. *Global Change Biology*, 9, 161–185, 2003.

131. S. Sitch, Friedlingstein, P., Gruber, N., Jones, S. D., Murray-Tortarolo, G., Ahlström, A., Doney, S. C., Graven, H., Heinze, C., Huntingford, C., Levis, S., Levy, P. E., Lomas, M., Poulter, B., Viovy, N., Zaehle, S., Zeng, N., Arneth, A., Bonan, G., Bopp, L., Canadell, J. G., Chevallier, F., Ciais, P., Ellis, R., Gloor, M., Peylin, P., Piao, S. L., Le Quéré, C., Smith, B., Zhu, Z., and Myneni, R.: Recent trends and drivers of regional sources and sinks of carbon dioxide. *Biogeosciences*, 12, 653-679, 2015.

132. Smith, B., Prentice, I. C., amd Sykes, M. T.: Representation of vegetation dynamics in the modelling of terrestrial ecosystems: comparing two contrasting approaches within European climate space. *Global Ecology and Biogeography*, 10, 621–638, 2001.

133. Song, X.-P., Huang, C., Saatchi, S. S., Hansen, M. C., and Townshend, J. R.: Annual Carbon Emissions from Deforestation in the Amazon Basin between 2000 and 2010. *PLoS ONE* , 10, e0126754. doi:10.1371/journal.pone.0126754, 2015.

134. Stephenson, N. L., Das., A. J., Condit, R., Russo, S. E., Baker, P. J., Beckman, N. G., Coomes, D. A., Lines, E. R., Morris, W. K., Rüger, N., Alvarez, E., Blundo, C., Bunyavejchewin, S., Chuyong, G., Davies, S. J., Duque, A., Ewango, C. N., Flores, O., Franklin, J. F., Grau, H. R., Hao, Z., Harmon, M. E., Hubbell, S. P., Kenfack, D., Lin, Y., Makana, J.-R., Malizia, A., Malizia, L. R., Pabst, R. J., Pongpattananurak, N., Su, S.-H., Sun, I-F., Tan, S., Thomas, D., van Mantgem, P. J., Wang, X., Wiser, S. K., and Zavala, M. A.: Rate of tree carbon accumulation increases continuously with tree size. *Nature*, 507, 90-93, doi:10.1038/nature12914,

2014.

135. Stibig, H.-J., Achard, F., Carboni, S., Raši, R., and Miettinen, J.: Change in tropical forest cover of Southeast Asia from 1990 to 2010. *Biogeosciences*, 11, 247-258, 2014.

136. Stocker, B. D., Feissli, F., Strassmann, K. M., Spahni, R., and Joos, F.: Past and future carbon fluxes from land use change, shifting cultivation and wood harvest. *Tellus B*, 66, 23188, doi:10.3402/tellusb.v66.23188, 2014.

137. Sweeney, C., Karion, A., Wolter, S., Newberger, T., Guenther, D., Higgs, J. A., Andrews, A. E., Lang, P. M., Neff, D., Dlugokencky, E., Miller, J. B., Montzka, S. A., Miller, B. R., Masarie, K. A., Biraud, S. C., Novelli, P. C., Crotwell, M., Crotwell, A. M., Thoning, K., and Tans, P. P.: Seasonal climatology of $CO_2$ across North America from aircraft measurements in the NOAA/ESRL Global Greenhouse Gas Reference Network. *Journal of Geophysical Research – Atmospheres*, 120, 5155–5190, doi:10.1002/ 2014JD022591, 2015.

138. Tao, B., Tian, H., Chen, G., Ren, W., Lu, C., Alley, K.D., Xu, X., Liu, M., Pan, S., and Virji, H.: Terrestrial carbon balance in tropical Asia: contribution from cropland expansion and land management. *Global and Planetary Change,* 100, 85-98, doi:10.1016/j.gloplacha.2012.09.006, 2013.

139. Taylor, K. E.: Summarizing multiple aspects of model performance in a single diagram. *Journal of Geophysical Research - Atmospheres*, 106, 7183-7192, 2001.

140. Thonicke, K., Venevsky, S., Sitch, S., and Cramer, W.: The role of fire disturbance for global vegetation dynamics: coupling fire into a Dynamic Global Vegetation Model. *Global Ecology & Biogeography*, 10, 661-677, 2001.

141. Thoning, K. W., Tans, P. P., and Komhyr, W. D.: Atmospheric carbon dioxide at Mauna Loa Observatory, 2. Analysis of the NOAA CMCC data, 1974-1985. *Journal of Geophysical Research*, 94, 8549-8565, 1989.

142. Tian, H., Banger, K., Tao, B., and Dadhwal, V. K.: History of land use in India during 1880-2010: Large-scale land transformation reconstructed from satellite data and historical achieves. *Global and Planetary Change*, 121, 76-88, 2014.

143. Tilman, D., and Downing, J. A.: Biodiversity and stability in grasslands. *Nature*, 367, 363-365, 1994.

144. Turner, M. G.: Disturbance and landscape dynamics in a changing world. *Ecology*, 91, 2833-2849, 2010.

145. van der Werf, G. R., Randerson, J. T., Giglio, L., Collatz, G. J., Kasibhatla, P. S., and Arellano, A. F.: Interannual variability of global biomass burning emissions from 1997 to 2004. *Atmospheric Chemistry and Physics*, 6, 3423–3441.

146. van der Werf, G. R., Dempewolf, J., Trigg, S. N., Randerson, J. T., Kasibhatla, P. S., Gigio, L., Murdiyarso, D., Peters, W., Morton, D. C., Collatz, G. J., Dolman, A. J., and DeFries, R. S.: Climate regulation of fire emissions and deforestation in equatorial Asia. *Proceedings of the National Academy of Sciences of the United States of America,* 105, 20350–20355, 2008.

147. van der Werf, G. R., Randerson, J. T., Giglio, L., Collatz, G. J., Mu, M., Kasibhatla, P. S., Morton, D. C., DeFries, R. S., Jin, Y., and van Leeuwen, T. T.: Global fire emissions and the contribution of deforestation, savanna, forest, agricultural, and peat fires (1997–2009). *Atmospheric Chemistry and Physics*, 10, 11707–11735, *2010.*

148. van der Werf, G. R., Randerson, J. T., Giglio, L., van Leeuwen, T. T., Chen, Y., Rogers, B. R., Mu, M., van Marle, M. J. E., Morton, D. C., Collatz, G. J., Yokelson, R. J., and Kasibhatla, P. S.: Global fire emissions estimates during 1997-2016. *Earth System Science Data*, 9, 697-720, doi:10.5194/essd-9-697-2017, 2017.

149. Wilkenskjeld, S., Kloster, S., Pongratz, J., Raddatz, T., and Reick, C.: Comparing the influence of net and gross anthropogenic land use and land cover changes on the carbon cycle in the MPI-ESM. *Biogeosciences Discussions*, 11, 5443–5469, 2014.

150. Williams, C A., Gu, H., MacLean, R., Masek, J. G., and Collatz, G. J.: Disturbance and the carbon balance of US forests: A quantitative review of impacts from harvests, fires, insects, and droughts. *Global and Planetary Change*, 143, 66-80, doi:10.1016/j.gloplacha.2016.06.002, 2016.

151. Wunch, D., Wennberg, P. O., Toon, G. C., Connor, B. J., Fisher, B., Osterman, G. B., Frankenberg, C., Mandrake, L., O'Dell, C., Ahonen, P., Biraud, S. C., Castano, R., Cressie, N., Crisp, D., Deutscher, N. M., Eldering, A., Fisher, M. L., Griffith, D. W. T., Gunson, M., Heikkinen, P., Keppel-Aleks, G., Kyro, E., Lindenmaier, R., Macatangay, R., Mendonca, J., Messerschmidt, J., Miller, C. E., Morino, I., Notholt, J., Oyafuso, F. A., Rettinger, M. A., Robinson, J., Roehl, C. M., Salawitch, R. J., Sherlock, V., Strong, K., Sussmann, R., Tanaka, T., Thompson, D. R., Uchino, O., Warneke, T., and Wofsy, S. C.: A method for evaluating bias in global measurements of CO2 total columns from space. *Atmospheric Chemistry and Physics*, 11, 12317-12337, 2011.

152. Xia, J., Luo, Y., Wang, Y.-P., and Hararuk, O.: Traceable components of terrestrial carbon storage capacity in biogeochemical models. *Global Change Biology*, 19, 2104–16, 2013.

153. Xia, J., Niu, S., Ciais, P., Janssens, I. A., Chen, J., Ammann, C., Arain, A., Blanken, P. D., Cescatti, A., Bonal, D., Buchmann, N., Curtis, P. S., Chen, S., Dong, J., Flanagan, L. B., Frankenberg, C., Georgiadis, T., Gough, C. M., Hui, D., Kiely, G., Li, J., Lund, M., Magliulo, V., Marcolla, B., Merbold, L., Montagnani, L, Moors, E. J., Olesen, J. E., Piao, S., Raschi, A., Roupsard, O., Suyker, A. E., Urbaniak, M., Vaccari, F. P., Varlagin, A., Vesala, T., Wilkinson, M., Weng, E., Wohlfahrt, G., Yan, L., and Luo, Y.: Joint control of terrestrial gross primary production by plant phenology and physiology. *Proceedings of the National Academies of Science of the United States of America,* 112, 2788-2793, doi:10.1073/pnas.1413090112, 2015.

154. Yang, X., Richardson, T. K., and Jain, A. K.: Contributions of secondary forest and nitrogen dynamics to terrestrial carbon uptake. *Biogeosciences*, 7, 3041–3050, 2010.

155. Yoshida, Y., Ota, Y., Eguchi, N., Kikuchi, N., Nobuta, K., Tran, H., Morino, I., and Yokota, T.: Retrieval algorithm for $CO_2$ and $CH_4$ column abundances from short-wavelength infrared spectral observations by the greenhouse gases observing satellite. *Atmospheric Measurement and Techniques*, 4, 717–734, doi:10.5194/amt-4-717-2011, 2011.

156. Yue, C., Ciais, P., Luyssaert, S., Li, W., McGrath, M. J., Chang, J., and Peng, S.: Representing anthropogenic gross land use change, wood harvest and forest age dynamics in a global vegetation model ORCHIDEE-MICT v8.4.2. *Geoscientific Model Development*, 11, 409–428, doi:10.5194/gmd-11-409-2018, 2018.

157. Zaehle, S., and Friend, A. D.: Carbon and nitrogen cycle dynamics in the O-CN land surface model: 1. Model description, site-scale evaluation, and sensitivity to parameter estimates. *Global Biogeochemical Cycles*, 24, GB1005. doi:10.1029/2009GB003521, 2010.

158. Zeng, N., Zhao, F., Collatz, G. J., Kalnay, E., Salawitch, R. J., West, T. O., and Guanter, L.: Agricultural green revolution as a driver of inreasing atmospheric CO2 seasonal amplitude. *Nature*, 515, 394-397, doi:10.1038/nature13893, 2014.